THE UNIVERSITY *of* EDINBURGH

New Tools Reveal Interaction Determinants and Post-mitotic Function of Crucial Microtubule Regulators

Karolina Leśniewska

Presented for the Degree of Doctor of Philosophy

The University of Edinburgh

August 2013

Declaration

I declare that the work presented in this thesis is of my own, except where otherwise stated.

Karolina Leśniewska

August 2013

Acknowledgements

This work was supported by BBSRC, SULSA and Wellcome Trust, whom I want to thank for making my studies possible.

I would like to thank my thesis supervisor, Hiro Ohkura, for all the help I received over the course of my PhD. The scientific guidance, inspirational discussions and encouragement made my project a fascinating story. The time spent in your lab was not only a science lesson but also a valuable life experience. Most of all, I am grateful for your patience.

I also thank Emma Warbrick for sharing new ideas and giving feedback on my work.

I would like to thank all the lab members for making the past four years so enjoyable. It was so much fun to work with you, not to mention the tea breaks!

Thank you also to my parents, Wanda and Mieczysław, for looking on the bright side of life, it always made me optimistic and appreciative.

The biggest thank you goes to my husband Bogdan. Your support was invaluable.

Abstract

Microtubules are a major constituent of the cytoskeleton in all eukaryotic cells. They are essential for cell morphogenesis and motility. Specifically in the dividing cells, microtubules form the spindle which segregates chromosomes. Microtubule plus ends constantly switch between phases of growth and shrinkage which is necessary for microtubule reorganization and thus their function. Importantly, microtubule dynamics are highly regulated by microtubule-associated proteins (MAPs).

EB1 and Mini spindles (Msps) are unique amongst MAPs because they bind and track growing microtubule plus ends autonomously. Although essential for cell division and thus highly expressed in dividing cells, EB1 and Msps are also abundant in differentiated cells. However, to identify post-mitotic roles of proteins essential for cell division, particularly in context of a multicellular organism, is a challenge requiring new tools which I aimed to develop in my project.

Since EB1 acts by recruiting MAPs to the microtubule plus ends, I generated short peptides which bind to Drosophila EB1 to block interactions with these MAPs. I showed that an EB1-MAP interaction was disturbed in Drosophila S2 cultured cells and expressing these peptides in developing Drosophila reduced fly viability. Further screening and analysis of peptides interacting with fly EB1 and its human homologues uncovered sequence determinants promoting strong binding and specificity. To uncover Msps function, I generated a *msps* temperature sensitive mutant and found that Msps is essential for neuromuscular function in developing Drosophila.

This study showed that the regulation of microtubule dynamics has crucial functions at the whole organism level. These new tools allow the roles of microtubule regulation to be dissected in developing organisms.

Thesis contents

Figures

Abbreviations

3-AT	3-Amino-1,2,4-triazole
AD	activation domain
AG-2	anterior gradient-2
ALT	alanine aminotransferase
ANK	Ankyrin
APC	Adenomatous polyposis coli
BD	DNA-binding domain
CAP-Gly	cytoskeleton-associated protein-glycine-rich
Cdk2	cyclin dependent kinase 2
CH	calponin homology
CLASP2	cytoplasmic linker-associated protein 2
CLIPs	cytoplasmic linker proteins
ConA	Concanavalin A
DMSO	Dimethyl sulfoxide
D-TACC	Drosophila transforming acidic coiled-coil-containing
E. coli	*Escherichia coli*
EB1	End binding 1
EBH	EB homology
EEY/F	Glu-Glu-Tyr/Phe
ELISA	enzyme-linked immunosorbent assay
FBS	Foetal Bovine Serum heat inactivated
GCP	γ-tubulin complex protein
GFP	green fluorescent protein
GKNDG	Gly-Lys-Asn-Asp-Gly
GMPCPP	guanylyl (α,β) methylenediphosphonate
HEAT	Huntingtin, elongation factor 3 (EF3), protein phosphatase 2A (PP2A), and the yeast kinase TOR1
HPA-1a	human platelet antigen antibodies
HPV	human papillomavirus
ICD	intracellular domain
IPTG	isopropyl β-D-1-thiogalactopyranoside
ITC	isothermal titration calorimetry
k-fibers	kinetochore fibers
MACF	microtubule-actin crosslinking factor
MAPs	microtubule associated proteins
MCAK	mitotic centromere-associated protein
mRFP	monomeric red fluorescent protein
Msps	Mini spindles
MT1-MMP	Membrane-Type 1 Matrix Matalloproteinase
MTOCs	microtubule organising centres

NAIT	neonatal alloimmune thrombocytopenia
Ncd	Non-claret disjunctional
NLS	nuclear localisation signal
ONP	o-nitrophenol
ONPG	o-nitrophenyl-β-D-galactoside
PCNA	proliferating cell nuclear antigen
PCR	polymerase chain reaction
Rb	retinoblastoma
S. cerevisiae	*Saccharomyces cerevisiae*
S. pombe	*Schizosaccharomyces pombe*
SGSG	Ser-Gly-Ser-Gly
SNase	staphylcoccal nuclease
STM	Stefin A triple mutant
SxIP	Ser-any amino acid-Ile-Pro
TOG	Tumor Overexpressed Gene
TrxA	Thioredoxin
UAS	upstream activating sequence
XMAP215	Xenopus microtubule assembly protein
Y2H	yeast two-hybrid
YMM	yeast minimum media
β-cat	β-catenin
γ-TuRC	γ-tubulin ring complex
γ-TuSCs	γ-tubulin small complexes

CHAPTER 1

Introduction

1.1. The microtubules cytoskeleton

Microtubules were observed in 1950s owing to first electron microscopy images which revealed long structures inside the cells called at the time canaliculi, endoplasmic reticulum or filamentous elements (Wells, 2005). They were first not given much attention and omitted by many researchers up until 1963 when, independently by Slautterback as well as Ledbetter and Porter, they were named "microtubules" and described as cylindrical cellular structures composed of globular subunits (Bryan, 1974; Wells, 2005). The first observations of microtubules in the interphase and the mitotic cells were confirmed by other research groups and the great importance of these structures was soon recognised.

Microtubules are an essential element of a eukaryotic cell cytoskeleton, required for many cellular processes. They are central to chromosome segregation in mitotic and meiotic cell division, cell motility and polarity, organisation of an intracellular structure as well as cytoplasmic movement of organelles and proteins. Architecture of microtubule network undergoes dynamic changes and depends on an activity which is performed by microtubules.

1.1.1. Structure of microtubules

Tubulins make a large protein family, so far α-, β-, γ-, δ-, ε-, ζ and η-tubulin have been identified, of which α- and β-tubulin are most studied since they are the building blocks of microtubules (McKean et al, 2001; Teixido-Travesa et al, 2012). Amino acid sequence analysis reveals that similarity within α-tubulins or β-tubulins from different species is very high (Tuszynski et al, 2006). Microtubules are filamentous, hollow tube-like structures built of tubulin subunits (Figure 1.1). The subunits are heterodimers of α- and β-tubulin monomers, each of 55 kDa. Folding of the α- and β-tubulin is highly regulated, multistep process leading to formation of a very stable αβ-tubulin subunit (Lewis et al, 1997). First assisted by cytosolic chaperonin c-cpn, the folding is then facilitated by interaction with cofactors, A in case of α-tubulin and cofactor B facilitating β-tubulin folding (Lewis et al, 1997). The αβ-tubulin heterodimers polymerise by making interactions between their ends in a head to tail manner forming a longitudinal structure called "protofilament" (Figure 1.1). The αβ-tubulin heterodimer repeats in a protofilament every 8 nm and

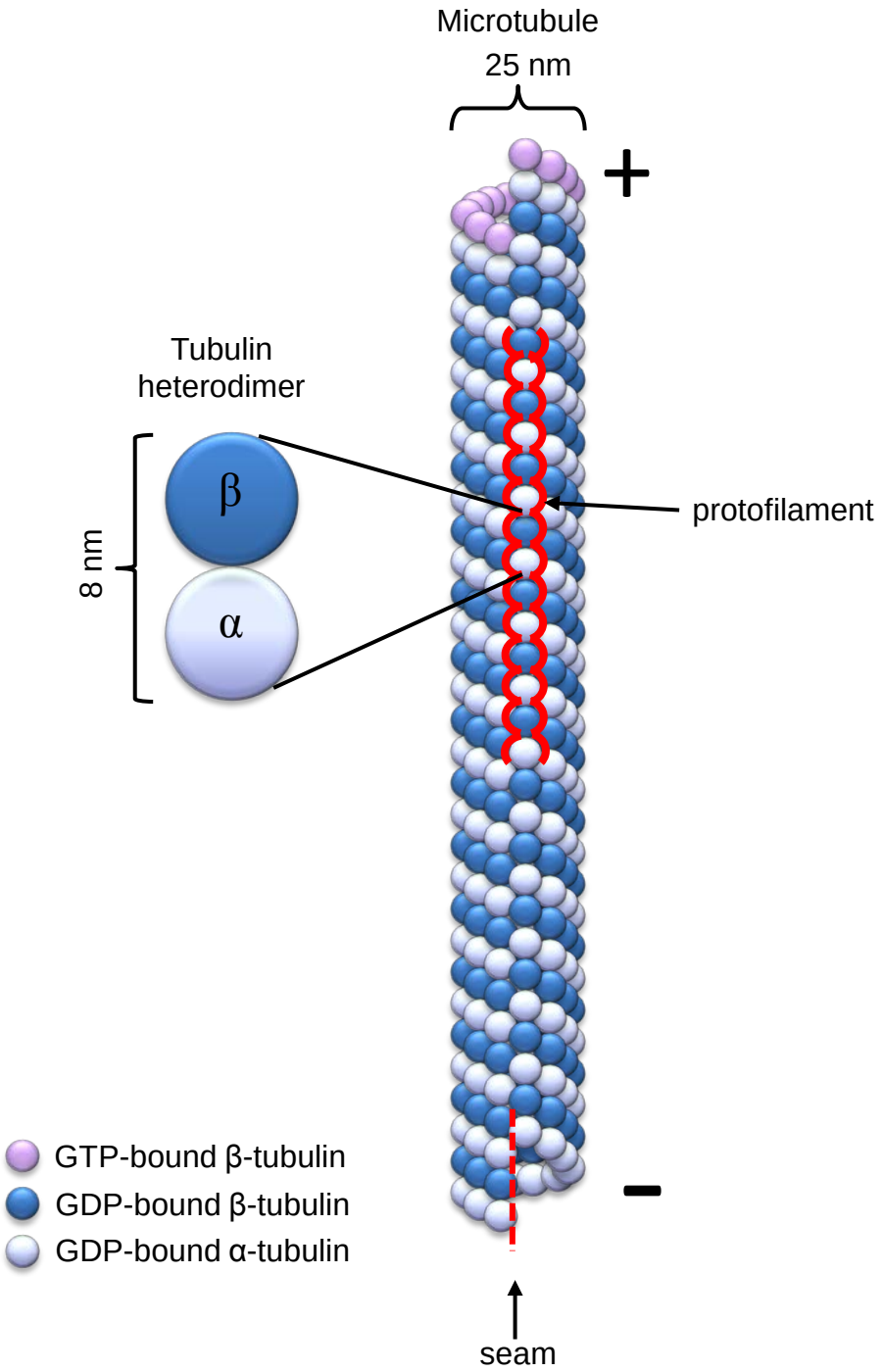

Figure 1.1 Structure of a microtubule
Microtubules are filamentous, hollow tubes built of αβ-tubulin heterodimers. These heterodimers polymerise by making interactions between α and β tubulin, giving microtubules polarity. The αβ-tubulin subunits repeat in a microtubule every 8 nm forming protofilaments which associate side by side and are staggered, making microtubule to adopt a helical structure. The helix spans three tubulin monomers with each turn which gives rise to a discontinuity in α-α-tubulin or β-β-tubulin contacts from the neighbouring protofilaments, called a “seam”. The more dynamic end where β tubulin is exposed is called a “plus” end and the other, less dynamic end is called a “minus” end.

each of the heterodimers makes sideways contacts with the subunits from adjacent protofilaments (Tuszynski et al, 2006). The side by side association of protofilaments forms a cylindrical structure, 24 nm in diameter, a microtubule (Figure 1.1). However, protofilaments are staggered by ~0.9 nm, thus making microtubule to adopt a helical structure (Mandelkow et al, 1986). The helix spans three tubulin monomers with each turn, which is called a 3-start helix (Erickson & Stoffler, 1996). While the lateral contacts of the protofilaments arise between either α-α-tubulin or β-β-tubulin, due to the 3-start helix a discontinuity arises along the microtubule, called a "seam", which results in a lateral contact being made between α- and β-tubulin (Figure 1.1) (Erickson & Stoffler, 1996).

Microtubules are generally assembled from 13 protofilaments in the *in vivo* conditions but there are exceptions such as an 11 or 15-protofilament microtubules in neurones of a nematode (Lodish et al, 2007). *In vitro*, microtubules have also been shown to vary in a number of protofilaments with 14-protofilament microtubules being the most common (Chrétien et al, 1992; Desai & Mitchison, 1997). Atop of the basic singlet structure, microtubules can form doublet and triplet structures by joining two and three microtubules laterally. While doublet microtubules are present in cilia and flagella, triplet microtubules are characteristic of centrioles and basal bodies (Esparza et al, 2013; Lodish et al, 2007; Piasecki & Silflow, 2009). There are 13 protofilaments in one of the microtubules and 10 protofilaments in the adjacent microtubule of these compound microtubules (Lodish et al, 2007).

1.1.2. Dynamics of microtubules

Due to the α- to β-tubulin binding of the heterodimers forming a microtubule, microtubules have a polarity. Hence, the plus end of the polymer is where the β-tubulin is exposed and the minus end exposes α-tubulin. In the mitotic and meiotic spindle, the minus ends of microtubules are anchored in the centrosome and the plus ends are mainly associated with the spindle mid-zone. Microtubules are less dynamic at the minus ends than at the plus ends. Polymerisation of microtubules at the minus ends is very slow and it is observed *in vitro* while in cells and *in vivo* the minus end is usually stabilised by a cap or it depolymerises (Jiang & Akhmanova, 2011). Contrarily, microtubules can both grow and shrink at the plus ends.

The kinetics of microtubule plus and microtubule minus ends differ from each other. When concentration of tubulin dimer is above the critical level, a microtubule end polymerises, while below the critical concentration levels, a microtubule end depolymerises. Since microtubule plus end has a lower critical concentration of tubulin addition than the minus end, microtubules can undergo treadmilling in the minus to the plus-end direction (Waterman-Storer & Salmon, 1997). Treadmilling is possible when the free tubulin concentration is above the critical concentration for the microtubule plus end and below the critical concentration for the minus end. However, rate of treadmilling *in vivo* is significantly higher than *in vitro* (Waterman-Storer & Salmon, 1997). While treadmilling is an intrinsic microtubule property, its rate varies and depends not only on free tubulin concentration but also microtubule interactions with microtubule associated proteins (MAPs) regulating microtubule dynamics (Panda et al, 1999). Treadmilling could have a role in cell motility and trafficking.

Microtubules can also persist for a long time in a state when they neither grow nor shrink, so called “pause” state. This pause state must require stabilising agents but not much is known about microtubule caps, apart from a ring complex discussed later. Also, it is often unclear whether microtubules indeed suspend their activities at the plus ends when in pause state or if the subunit turnover is too subtle to be detected (Jiang & Akhmanova, 2011).

The term “dynamic instability” refers to the dynamic behaviour of a microtubule end where the polymer undergoes phases of growth and shrinkage. Dynamic instability happens at both ends of microtubules but it is more robust at the plus end (Panda et al, 1999). The growing microtubule can start rapidly depolymerising (catastrophe) followed by a return to the growing mode (rescue) (Figure 1.2.) (Gardner et al, 2013). Only the β-tubulin at the plus end with a molecule of GTP bound to its exchangeable site (E-site) can add another αβ-tubulin heterodimer, a process attributed to an irreversible GTP- to GDP hydrolysis (Desai & Mitchison, 1997; Heald & Nogales, 2002).

During GTP hydrolysis the energy is stored in the microtubule lattice as a mechanical strain (Desai & Mitchison, 1997). Loss of this GTP tubulin cap exposes the GDP tubulin and results in release of the strain which causes microtubule

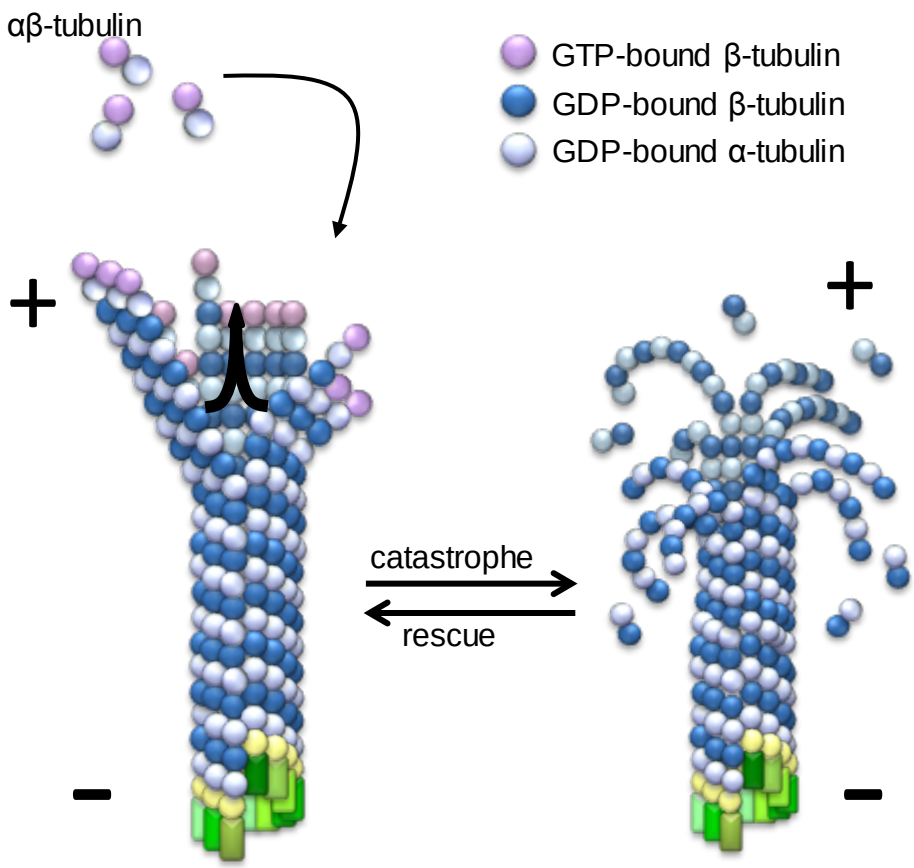

Figure 1.2 Dynamics of microtubule polymers
Microtubules polymerise by adding αβ-tubulin dimers to the plus ends. While both α and β-tubulin have bound GTP molecule only the β-tubulin can add another αβ-tubulin heterodimer to the plus end, a process attributed to an irreversible GTP- to GDP hydrolysis. Loss of GTP tubulin cap from the microtubule plus ends exposes the GDP tubulin and causes microtubule protofilaments to peel backwards from a microtubule filament causing its rapid depolymerisation, called catastrophe. Contrarily, microtubule rescue is the event when microtubules starts polymerising again, a process associated with gaining back the GTP cap by the microtubule.

protofilaments to peel backwards from a microtubule filament causing its depolymerisation (Figure 1.2) (Desai & Mitchison, 1997; Heald & Nogales, 2002). Faivre-Moskalenko et al. (2002) demonstrated that catastrophes are essential for positioning of microtubule organising centres (MTOCs) by investigating positioning of artificial MTOCs in microchambers containing already developed microtubule array. MTOCs started moving in the microchambers only after addition of a catastrophe promoting factor (Faivre-Moskalenko & Dogterom, 2002). Interestingly, microtubules undergo an aging process which is indicated by increased catastrophe rates in the long microtubules. Microtubules are required to accumulate several events before they undergo catastrophe (Gardner et al, 2013).

Microtubule rescue is the event when microtubule shortening ceases and the microtubule starts polymerising again, a process associated with gaining back the GTP cap by the microtubule (Figure 1.2) (Gardner et al, 2013). While it was shown that rescue events are not dependent on tubulin concentration, a study by Dimitrov et al. (2008) demonstrated that the rescue events may be attributed to features embedded in microtubule lattice (Gardner et al, 2013). Dimitrov et al. (2008) used a conformation-specific antibody, hMB11, recognising polymerised tubulin bound to a non-hydrolyzable analogue of GTP but not to a GTP-bound tubulin. The hMB11 antibody, in addition to microtubule end, decorated microtubules along their lattice giving a randomly distributed dot staining both *in vitro* and *in vivo*. These unhydrolysed GTP-tubulin islands become exposed upon microtubule depolymerisation and they can act as GTP cap and trigger microtubule rescue (Dimitrov et al, 2008). Interestingly, in neuronal cells hMB11 staining on microtubules is more abundant in axons than dendrites (Nakata et al, 2011). Therefore, the GTP tubulin incorporation into the microtubule lattice can be regulated and a cell-dependent event improving microtubule stability in cells such as neurons.

1.1.3. Nucleation of microtubules

Contrarily to the *in vitro* conditions, where microtubule nucleation can occur without aid of any nucleating factors, in *in vivo* conditions a nucleator is required (Teixido-Travesa et al, 2012). Microtubule nucleation and organisation is largely regulated by

MTOCs which are sites of proteins essential for performing these processes. The key player at the MTOCs is γ-tubulin which forms a platform for microtubule nucleation. 14 molecules of γ-tubulin assemble into a ~2.2 MDa ring structure (γ-TuRC) along with other proteins, γ-tubulin complex protein 2 (GCP2), GCP3, GCP4, GCP5 and GCP6 (Kollman et al, 2011). γ-tubulin small complexes (γ-TuSCs) are subunits of γ-TuRCs and they are composed of two γ-tubulin molecules associated with GCP2 and GCP3 (Kollman et al, 2011). Although a model is proposed where γ-TuRC serves as a template for microtubule nucleation, neither the exact structure of the ring nor the number of each of the subunits composing the complex are yet clear (Kollman et al, 2011).

While the presence of γ-tubulin in the centrosomal regions has a major role in microtubule nucleation, the γ-tubulin pool in the cytoplasm constitutes ~80% of the total, suggesting that it has a function at other sites (Moudjou et al, 1996). However, the nucleating activity of γ-TuRCs has been restricted to mitotic spindle, centrosome or spindle pole body (Choi et al, 2010; Kollman et al, 2011). γ-TuRCs, apart from their microtubule nucleating activity, have also been shown to stabilise microtubule minus ends by capping them (Anders & Sawin, 2011; Teixido-Travesa et al, 2012).

A conformational change of GCP3, induced by direct binding of attachment factor proteins anchoring γ-TuRCs to the MTOCs, was proposed to convert γ-TuRC to an active form and trigger microtubule nucleation (Kollman et al, 2010). Other mechanisms modulating γ-TuRC include its post-translational modifications, alternating γ-TuRC composition or regulation by targeting γ-TuRCs to specific cellular sites (Teixido-Travesa et al, 2012). However, the mechanisms which promote microtubule nucleation from γ-TuRCs still remain elusive.

1.2.The EB family of microtubule plus end-binding proteins

1.2.1. EB1 is an essential protein

End binding 1 (EB1) protein was found in a screen for interactors of Adenomatous polyposis coli (APC) which is a tumor suppressor. The name EB1 is attributed to the protein binding to the C-terminus of APC (Su et al, 1995). EB1 belongs to an

evolutionarily conserved group of EB proteins which track microtubule plus ends and regulate their dynamics (Su et al, 1995; Tirnauer & Bierer, 2000). EB proteins bind autonomously to the growing microtubules, exclusively to their plus ends (Bieling et al, 2008; Woods et al, 2013). Importantly, EB proteins are central to regulation of microtubule plus end dynamics by recruiting MAPs to the microtubule plus ends (Kumar & Wittmann, 2012; Woods et al, 2013). Being key players in regulation of microtubule dynamics, EB proteins have an essential role in processes such as establishment of cell polarity, spindle positioning and chromosome stability (Tirnauer & Bierer, 2000; Tirnauer et al, 2002).

Throughout the cell cycle, EB proteins associate preferentially with microtubule plus ends and centrosomes (Berrueta et al, 1998; Bu & Su, 2001; Mimori-Kiyosue et al, 2000). RNAi of *Drosophila melanogaster* EB1 (DmEB1) increases the number of nondynamic microtubules but it does not affect the overall microtubule organisation in interphase cells (Rogers, 2002). In mitosis, depletion of DmEB1 by RNAi affects spindle pole focusing, positioning and results in reduction in astral microtubules (Rogers, 2002). Defective spindle elongation and chromosome segregation was observed in Drosophila embryos injected with anti-EB1antibodies (Rogers, 2002). DmEB1 was shown to be essential for Drosophila development and viability. Neuromuscular defects and uncoordinated movement of hypomorphic *DmEB1* escaper mutants was observed (Elliott et al, 2005).

1.2.2. Conservation

While only one EB1 homologue is present in yeast, BIM1 in *Saccharomyces cerevisiae* (*S. cerevisiae*) and Mal3 in *Schizosaccharomyces pombe* (*S. pombe*), more than one EB protein has been identified in metazoa (Bu, 2003; Tirnauer & Bierer, 2000). Three genes have been identified in human, *EB1*, *RP1* and *EBF3*, encoding EB1 family proteins EB1, EB2 and EB3, respectively (Su & Qi, 2001). These proteins share amino acid identity of 57-66% and have a conserved domain structure (Schroder et al, 2011). Whereas there is only one EB1 protein expressed from the *EB1* gene, there are two EB2 proteins translated from different initiation codons from *RP1* and two EB3 proteins translated from differently spliced mRNA from *EBF3* (Su & Qi, 2001).

EB1 is expressed ubiquitously in different lines of human cultured cells. Also, DmEB1 is expressed ubiquitously in different tissues and at various developmental stages (Bu, 2003; Elliott et al, 2005). However, EB proteins have different expression patterns in some cell types. Straube et al. (2007) showed that EB3 level in undifferentiated cells is low and it significantly increases when cells start differentiating (Straube & Merdes, 2007). Contrarily, EB2 expression is switched off upon cell differentiation and EB1 level remained the same (Straube & Merdes, 2007). EB3 was also expressed preferentially in brain and it has an essential role, together with EB1, in maintaining the integrity of axonal initial segment (Leterrier et al, 2011; Nakagawa et al, 2000). EB proteins may have diverged in animals to regulate different aspects of microtubule dynamics in differentiated cells.

However, even though it has been 18 years since the discovery of the first members of this crucial protein family, many questions remain unanswered. Particularly interesting is the occurrence of the three EB homologues and different isoforms in mammals: are they functionally redundant or do they have distinct roles? While EB1 has been most extensively studied, not much attention has been given to EB2 and EB3. Also, studies of EBs particularly focused on dissecting the proteins at the cellular level, while the protein function in context of a whole organism has been neglected. The only study in higher organisms has been performed by Elliott et al. (2005) demonstrating that DmEB1 has an essential neuromuscular role in development of Drosophila. However, what is the protein's role in a developed organism? How is the protein function influenced, if at all, by the interaction with its numerous partners in a context of a multicellular organism? Finally, what are the sequence determinants which promote binding to EBs and do they differ between the family members? Answering these questions requires new tools which will allow targeting of specific interactions inside a developed organism.

1.2.3. Structure

EBs are small, globular proteins of ~30-kDa composed of two conserved domains, a ~130-residue N-terminal calponin homology (CH) domain and ~80-residue C-terminal dimerisation domain (Figure 1.3.). The CH and dimerisation domains are separated by an unstructured linker of ~70 residues (Askham et al, 2002; Bjelić et al,

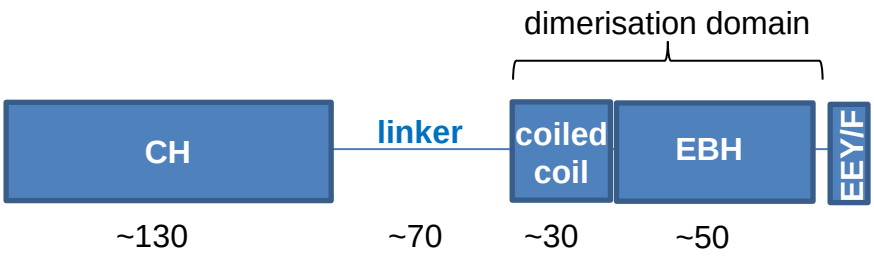

Figure 1.3 Schematic representation of EB1 domain organisation
EB1 proteins are small proteins of ~30kDa highly homologous accross the species. Three distinct domains make up EB1 proteins; calponin homology (CH) domain in the N-terminus followed by ~70 amino acid unstructured linker region and ~80 amino acid dimerisation domain. The dimerisation domain is composed of ~30 amino acid coiled coil and ~50 amino acid EB homology (EBH) domian. CH domain, present in many actin and tubulin-binding proteins, has microtubule-binding role in EB1 (Zimniak et al. 2009). Role of the unstructured linker region is unknown. The following coiled coil and EBH regions are both involved in formation of EB1 dimers. EBH domain recognizes SxIP motif carried by multiple microtubule plus end binding proteins. Conserved EEY/F motif at the very end of C-terminus which is specifically recognised by CAP-Gly domains of microtubule plus-end binding proteins.

2012; Slep & Vale, 2007). While the roles of the two conserved domains have been studied, the role of the linker is not known (Komarova et al, 2009).

1.2.3.1. The N-terminus of EB1 is a microtubule interaction region

The crystal structure of the N-terminal CH domain, responsible for interaction with microtubules, has been solved, showing a highly conserved fold (Hayashi, 2003; Komarova et al, 2009). The CH domains of human and budding yeast EB proteins are almost identical. They are formed by α-helices folded into a globule. The central hydrophobic helix, α3, is wrapped around by the remaining helices (Figure 1.4.) (Slep & Vale, 2007). The α6 helix contains many surface-exposed and highly conserved amino acid residues as well as conserved hydrophobic residues creating a groove (Figure 1.4). Hence, amino acids located in α6 helix may have an important role in protein-protein interactions. However, the microtubule plus end tracking activity of EB1 is attributed to residues located on one hemisphere of CH domain which is formed by α1 and a loop between α3 and α4 (Slep & Vale, 2007). De Groot et al. (2009) showed that mutation of Lys59 and Lys60 on CH domain completely abolished microtubule plus end tracking by EB1 (Figure 1.4).

The amino acid sequence of human EB2 in the CH domain, nearby a conserved region essential for microtubule binding, is different from the corresponding sequences on *EB1* and *EB3*. However, differences between *EB1* and *EB3* are less obvious (Komarova et al, 2009). The amino acid differences of CH domains between the three proteins can imply their different behaviour. In terms of microtubule plus end accumulation and catastrophe suppression both of EB1 and EB3 is more effective than EB2 (Komarova et al, 2009).

1.2.3.2. The C-terminus of EB1 is a partner-binding region

The C-terminal region of EB1 contains a coiled coil region, EB homology (EBH) domain and a disordered C-terminal tail (Bjelić et al, 2012).

The coiled coil region is a universal protein oligomerisation motif responsible for dimerisation of EB proteins (Akhmanova & Steinmetz, 2008; Honnappa et al, 2005). Although EB1 dimerisation is required for robust microtubule plus end tracking, an EB1 construct devoid of the dimerisation domain can still

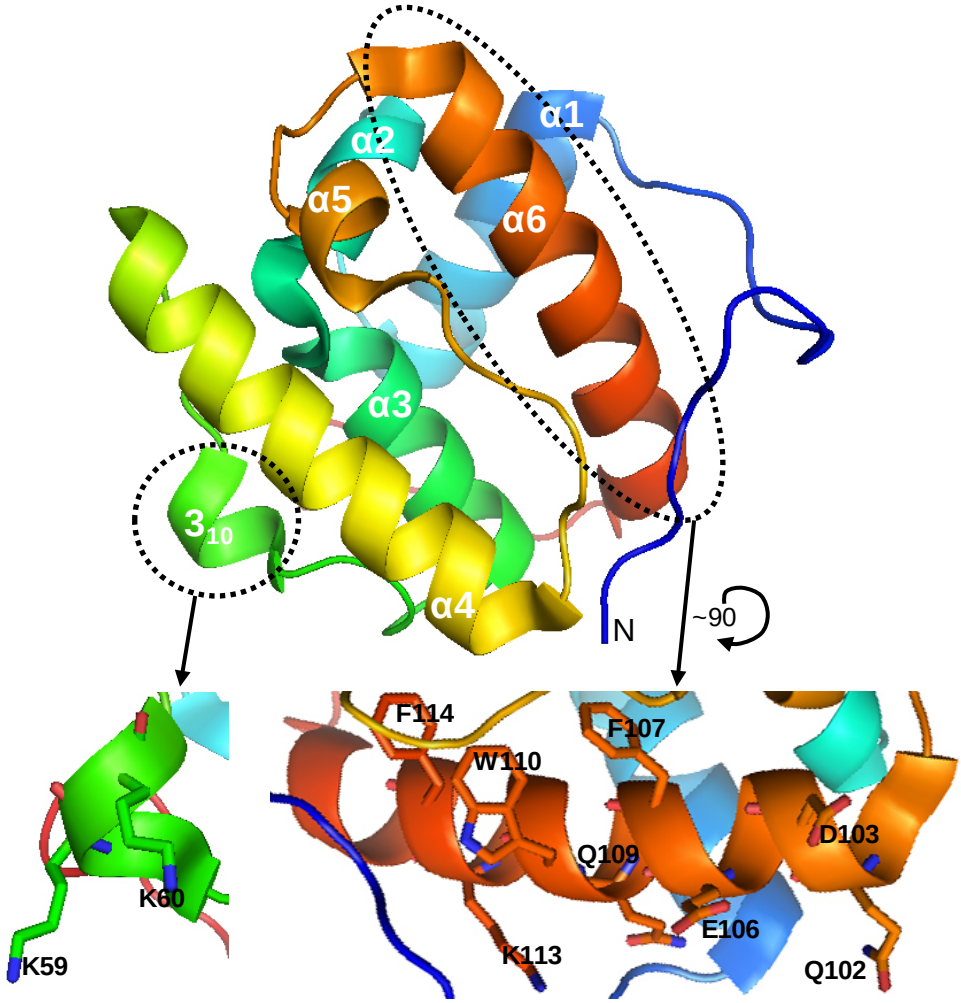

Figure 1.4 Structure of Calponin Homology domain of human EB1. The EB1 CH domain is formed by α helices that pack around hydrophobic α3 helix. The tubulin-binding site is located within loops α1 and α3- α4. The α3- α4 loop encompasses helix 3_{10} where are located lysines 59 and 60 which are essential for microtubule plus end tracking by CH of EB1. Highly conserved and surface exposed residues in loop α6 may have important role in protein-protein interactions. A conserved hydrophobic groove is created by F107, W110 and F114 and conserved electrostatic residues include Q102, D103, E106, Q109 and K113 (Slep et al. 2007). The protein model was generated in PyMOL.

weakly track growing microtubule plus ends *in vivo* (Skube et al, 2010). Homodimerisation was shown to be important for a partner binding by EB1 since residues from each of the EB1 molecules forming a homodimer contribute to contacts with microtubule-actin crosslinking factor (MACF) and abrogating EB1 homodimerisation compromised the partner binding (Slep, 2005). While all three, EB1, EB2 and EB3, form homodimers, only EB1 and EB3 can also form heterodimers (De Groot et al, 2009). Formation of heterodimers may be used to recognise diverse proteins for complex regulation of microtubules by EB proteins. Considering that the protein dimerisation is essential for its microtubule anti-catastrophe properties, regulation of EBs dimerisation is another interesting, yet unexplored, aspect of regulation of microtubule dynamics (De Groot et al, 2009; Komarova et al, 2009).

The EBH domain partially overlaps with the coiled coil region (Figure 1.3) (Akhmanova & Steinmetz, 2008). This ~50 amino acid domain is formed of an antiparallel four-helix bundle (Slep & Vale, 2007). A patch on the EBH domain surface is decorated by highly conserved residues forming a hydrophobic cavity. This hydrophobic cavity is a docking site used by a large group of SxIP (Ser-any amino acid-Ile-Pro) motif-containing proteins which regulate microtubule plus end dynamics (Akhmanova & Steinmetz, 2008; Slep & Vale, 2007).

The C-terminal tail of EBs contains EEY/F (Glu-Glu-Tyr/Phe) sequence motif which is also present at the C-terminus of CLIP-170 and α-tubulin (Mishima et al, 2007). EEY/F is a conserved recognition sequence for CAP-Gly (cytoskeleton-associated protein-glycine-rich) microtubule plus-end binding proteins (Honnappa et al, 2006). The acidic-aromatic tail of EB1 comprising the EEY/F sequence recognises GKNDG (Gly-Lys-Asn-Asp-Gly) motif located in the hydrophobic cavity of the globular CAP-Gly domain (Akhmanova & Steinmetz, 2008).

1.2.4. EB1 binds to microtubules and regulates their dynamics

1.2.4.1. EB1 associates with microtubule polymers

While EB1 and EB3 in CHO-K1 cultured cells display the same, comet-like localisation (~2 μm at the microtubule plus ends dispersing in the minus end

direction), the localisation pattern of EB2 is different. Immunostaining of EB2 shows subtle microtubule plus end association and even distribution along the microtubule lattice (Komarova et al, 2009). A study by Komarova et al. (2009) showed that binding and tracking of microtubule plus ends by EB1, EB2 or EB3 is independent of each other and that the proteins compete for microtubule plus end binding. Depletion of EB1 from CHO-K1 cultured cells redistributed EB2 to the plus ends, without affecting EB3 localisation. Similar redistribution of EB2 happened when both EB1 and EB3 were depleted. Depletion of either EB2 or EB3 had no effect on distribution of the remaining EBs (Komarova et al, 2009).

While EB1 binding to microtubule plus ends was demonstrated by several research groups, the binding mechanism has been tackled only recently and is not yet clear. The first question that was addressed was whether EB1 copolymerised with tubulin or whether it bound to the already polymerised tubulin at the microtubule plus ends. Bieling et al. (2007) showed that Mal3 does not bind to unpolymerised tubulin but it must recognise some features present on a microtubule polymer.

1.2.4.2. EB1 recognises different tubulin conformations

Different suggestions have been made as to what are the determinants on a growing microtubule recognised by EB1. One of the hypotheses was that EB1 recognised the GTP cap which was unlikely because the GTP-bound β-tubulin comprises a maximum of two heterodimers at the end of a protofilament while the EB1 binding region is much larger (Maurer et al, 2012). Also, if it was the nucleotide binding state of β-tubulin dictating EB1 affinity for a microtubule, one could observe a uniform EB1 binding along the microtubule lattice which is not the case. Instead, EB1 immunostaining appears comet-shaped at the microtubule plus ends where the signal is the strongest at the plus end and disperses in the minus-end direction. Kueh et al. (2009) reviewed increasing evidence that “structural plasticity”, defined as a change in structural state, of a microtubule drives the polymer dynamics rather than purely its chemical state. If EB1 is attracted to microtubules by particular tubulin conformations, this can explain why EB1 binding to the microtubule lattice is different from EB1 binding to the microtubule plus end region where tubulin is also GDP-bound.

A study by Maurer et al. (2011) further supports the idea that EB1 recognises different tubulin conformations. They demonstrated that Mal3 and EB1 have particularly strong affinity to the polymerised tubulin transitioning from GTP- to GDP-bound state, so in an intermediate conformation(s). Polymerising microtubules in presence of GTPγS, a slowly hydrolysable GTP homolog, resulted in robust Mal3 or EB1 accumulation along the microtubule lattice (Maurer et al, 2011). Hence, tubulin slowly changing its conformation during GTP hydrolysis may have a reflection in the comet-like immunostaining of EB1. The tubulin conformation favoured by EB1 remains at the microtubule plus end for ~8 seconds, a period of time when microtubule is decorated with Mal3 and EB1 (Bieling et al, 2007; Dixit et al, 2009). Also, it was shown that EB1 and Mal3 association with microtubules is very dynamic. Mal3 dwell time on a microtubule is ~0.28 second (or ~0.8 second for mammalian EB1) (Bieling et al, 2007; Dixit et al, 2009).

1.2.4.3. EB1 promotes conformational change of tubulin

However, does the tubulin conformation favoured by EB1 serve only as a platform for EB1 binding or does the EB1 binding to a microtubule affect tubulin conformation? Maurer et al. (2011) demonstrated that the lifetime of the conformational state at which Mal3 could bind to microtubule decreased along with an increase in Mal3 concentration. Hence, Mal3 can work as a catalyst of tubulin transition state (Maurer et al, 2011). Interestingly, addition of Mal3 *in vitro* increases catastrophe frequency and microtubule growth rate (Bieling et al, 2007; Komarova et al, 2009; Maurer et al, 2011; Vitre et al, 2008). It is possible that Mal3 dose-dependent conformational change on the microtubule reduces the Mal3 binding region hence increasing the risk of a catastrophe. Also the conformational change of tubulin facilitated by EB1 may accelerate closing of the microtubule tube and increase the polymerisation rate (Kumar & Wittmann, 2012). Indeed, addition of EB1 to microtubules polymerised in presence of DMSO and GMPCPP, known to induce unclosed microtubules, significantly increased the proportion of closed microtubules (Vitre et al, 2008). However, regulation of microtubule dynamics by EB1 in *in vivo* conditions is more complex and it may depend on EB1 interaction with the proteins recruited by EB1 to the microtubule plus ends.

1.2.4.4. The precise localisation of EB1 on microtubules is established

Maurer et al. (2012) showed that CH domains of EBs bind regularly between protofilaments (B-lattice) except for the seam of GTPγS-polymerised microtubules (A-lattice) (Maurer et al, 2012). Binding of a Mal3 CH domain fragment between the neighbouring protofilaments forming the B-lattice forms stabilising interprotofilament bridges. The Mal3 CH stabilisation effect on microtubule plus ends was predicted by the observation that Mal3 CH immunostaining started decaying from the microtubule plus ends several seconds prior to catastrophe (Maurer et al, 2012). Therefore, EB1 forms a protective structural cap at the microtubule plus ends.

Maurer et al. (2011) demonstrated that Mal3 CH domain was regularly distributed on a microtubule every 8 nm allowing prediction of 12 molecules of Mal3 CH domain for every 13 tubulin dimmers (Figure 1.5). This is in agreement with the measurements of Mal3-GFP fluorescence measured on microtubules at saturating concentrations and comparing fluorescence intensity to that of a GFP-labelled kinesin-1 which is known to bind one tubulin dimer (Maurer et al, 2011; Maurer et al, 2012). They also showed that the Mal3 CH domain binding occurs at the corner of four different αβ-tubulin heterodimers where two adjacent α-tubulins and two adjacent β-tubulins meet (Figure 1.5). This finding is consistent with EB1 not binding along the seam because such a tubulin arrangement does not exist at the seam (Maurer et al, 2012). Mal3 CH makes a contact with the β-tubulin helix whose structural rearrangement is triggered by GTP hydrolysis. Mutating a conserved amino acid residue, Q89, in Mal3 CH domain which contacts the β-tubulin helix affects microtubule binding behaviour (Iimori et al, 2012; Maurer et al, 2012). Hence, EB1 may sense β-tubulin conformation characteristic of a certain microtubule region.

1.2.5. EB1 functions in mitosis to regulate spindle dynamics

DmEB1 depletion by RNAi from Drosophila S2 cells resulted in aberrant chromosome segregation and a range of mutant spindle phenotypes, such as shorter and malformed spindles positioned away from the cell centre and defocused spindle

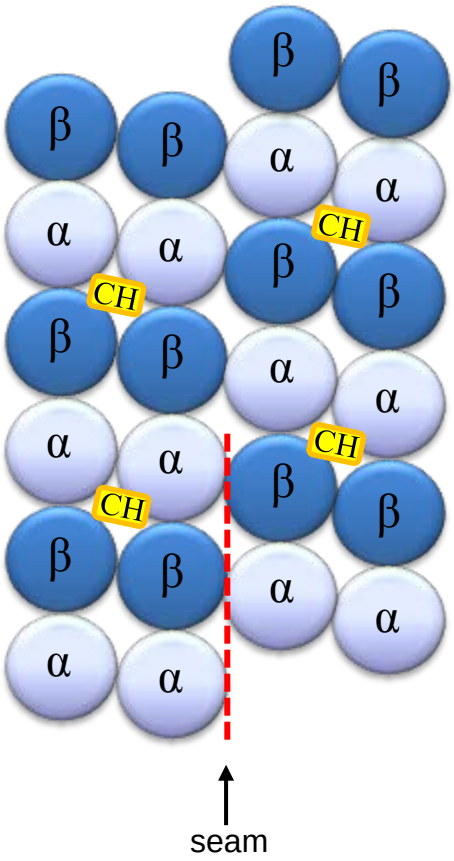

Figure 1.5 Model of EB1 binding site on a microtubule.
CH domain of EB1 binds between tubulin dimers of microtubule B-lattice; an arrangement where α tubulins of the neighbouring protofilaments lie next to each other. Such arrangement is not present at the seam (A-lattice). The binding occurs regularly at 8nm distance between α-tubulins towards the plus end and β-tubulins towards the minus end.

poles (Rogers, 2002). DmEB1 is required for microtubule plus end tracking by a minus end-directed motor protein Ncd, a product of *non-claret disjunctional*, which is a motor protein essential for spindle pole focusing (Goshima et al, 2005). Ncd cross-links the neighbouring kinetochore fibers (k-fibers) and helps in their focusing. Ncd was also shown to slide the neighbouring microtubules against each other (Oladipo et al, 2007). Such sliding along the spindle facilitates transport of microtubules, which do not originate from the centrosome, towards the centrosome. Although Ncd can transport microtubules towards the centrosomes, this is a dominant function of dynein, another minus end-directed motor protein, and Ncd's role is primarly in focusing k-fibers (Goshima et al, 2005). The DmEB1-dependent localisation of Ncd to the plus ends of nucleating centrosomal microtubules was proposed to have a role in spindle pole focusing as well as in capturing chromosomes by the centrosomal microtubules by Ncd which captures k-fibers and connects them to the spindle (Goshima et al, 2005).

EB1 is involved in modulating chromosomal attachments in mitosis. Mal3 deleted cells show mitotic delay where the time between initiation of SPB separation and anaphase onset significantly increases (Asakawa et al, 2005). Asakawa et al. (2005) demonstrated that in mitotic cells a spindle checkpoint protein, Bub1, which monitors bipolar chromosome attachment, in the absence of Mal3 protein localises to the kinetochores. Such Bub1 localisation is specific to incorrect chromosome attachment.

EB1 also participates in control of spindle length (Rogers, 2002; Zimniak et al, 2009). Zimniak et al. (2009) demonstrated that in *bim1* deletion mutants the elongation rate of mitotic spindle was reduced and the spindle was subsequently shorter. The spindle elongation and disassembly of spindle mid-zone is positively regulated by phosphorylation of Bim1 (Zimniak et al, 2009). In a Bim1 unphosphorylatable mutant long spindles were generated and spindle mid-zone disassembly was prevented. During spindle disassembly in the phosphorylation-deficient Bim1, a significant amount of Bim1 occupied the spindle mid-zone. Contrarily, in the wild-type cells the Bim1 zone in the mid-spindle gradually decreased and only small punctae of the protein were observed (Zimniak et al, 2009). EB1 depletion from Drosophila S2 or human HeLa cells results in astral

microtubules not being formed which may also contribute to the decrease of spindle length since the pulling forces exerted by cortical proteins on astral microtubules contribute to spindle elongation (Rogers, 2002).

Therefore, EB1 is involved in regulating various aspects of spindle organisation and dynamics.

1.2.6. EB1 is central to the microtubule plus end binding by MAPs

Although extensively studied, precise mechanisms of modulating microtubule dynamics by EB1 remain unclear. The effects that EB1 exerts on microtubules depend on EB1 interaction with other microtubule modulators. Although various microtubule plus end binding proteins can regulate microtubule dynamics, EB1 emerged as a central component of the plus end interaction network. EB1 can autonomously bind to the growing microtubules and recruit various proteins to the plus ends (Jiang et al, 2012). Contrarily, numerous plus end MAPs require EB1 to efficiently accumulate and track growing microtubule plus ends. The C-terminus of EB1 is involved in two distinct binding mechanisms required for EB1-mediated recruitment of MAPs to microtubules. The EB1 C-terminus is an interaction site for proteins containing Cap-Gly domain or/and SxIP motif (Honnappa et al, 2009).

1.2.6.1. EB1 interacts with CAP-Gly motif-containing proteins

Conserved from yeast to human, CAP-Gly is a protein domain rich in glycine and hydrophobic residues. The CAP-Gly domain was crystallised revealing a globular fold, composed of a short α-helix at the C-terminus, followed by three β-sheets formed by three, three and two antiparallel β-strands at the N-terminus (Li et al, 2002). An *in silico* search for similar structures showed that CAP-Gly domain architecture is unique (Li et al, 2002).

An amino acid segment GKNDG located in a hydrophobic cavity between β3 and β4 strand is the longest conserved motif in Cap-Gly and it is essential to target the acidic-aromatic tail of EB1 comprising the EEY/F sequence (Akhmanova & Steinmetz, 2008; Li et al, 2002; Weisbrich et al, 2007). Proteins containing CAP-Gly include MAPs such as cytoplasmic linker proteins (CLIPs) and the largest Dynactin subunit, $p150^{glued}$ (Schroer, 2004; Weisbrich et al, 2007). Although CAP-

Gly domains are generally known as tubulin-binding modules, these domains of CLIP-170, CLIP115 and p150^{glued} are also involved in interaction with EB1 (Ligon et al, 2003; Weisbrich et al, 2007). p150^{glued}, similarly to CLIP-170, uses CAP-Gly domain to localise to microtubule plus ends (Steinmetz & Akhmanova, 2008). The significance of CAP-Gly interaction with EEY/F is prominent since CLIP-170 tracking and binding specifically to the microtubule plus ends requires EB1 (Bieling et al, 2008; Dixit et al, 2009; Komarova et al, 2005).

1.2.6.2. EB1 interacts with SxIP motif-containing proteins

Proteins recruited by EB1 to the microtubule plus ends are structurally and functionally heterogeneous (Kumar & Wittmann, 2012). However, the majority of these MAPs are recruited to the microtubule plus ends using SxIP which interacts with EBH domain of EB1 (Figure 1.6) (Kumar et al, 2012). Interestingly, some of these proteins contain multiple SxIP motifs which act in concert to enhance microtubule plus end binding and tracking (Honnappa et al, 2009; Kumar & Wittmann, 2012). The most conserved amino acid residues of SxIP are isoleucine/leucine and proline which are involved in a hydrophobic interaction with EB1. Honnappa et al. (2009) investigated an interaction at atomic level between SxIP of MACF and C-terminus, amino acids 191-268, of EB1 (EB1c). Ser5477 of MACF SxIP forms a network of hydrogen bond interactions with conserved residues Arg222, Glu225, Gln229 and Tyr247 of EB1 (Figure 1.7) (Honnappa et al, 2009). The nonpolar Ile5479 and Pro5480 of MACF SxIP are deeply buried in the hydrophobic cavity on EB1c which is shaped by amino acid residues Phe216, Arg222, Glu225, Leu241 and Tyr247 located between two C-terminal helices in EB1 (Figure 1.7) (Honnappa et al, 2009; Kumar et al, 2012; Kumar & Wittmann, 2012). Since mutation of either isoleucine or proline of SxIP to polar amino acids abolished interaction with EB1 by all the SxIP proteins tested so far, these residues are essential for EB1 binding (Kumar et al, 2012; Kumar & Wittmann, 2012; van der Vaart et al, 2011).

Although essential, SxIP alone is not enough to mediate interaction with EB1. SxIP is located within a sequence region particularly rich in arginine and serine residues. The positive charge within the SxIP region provided by arginines and

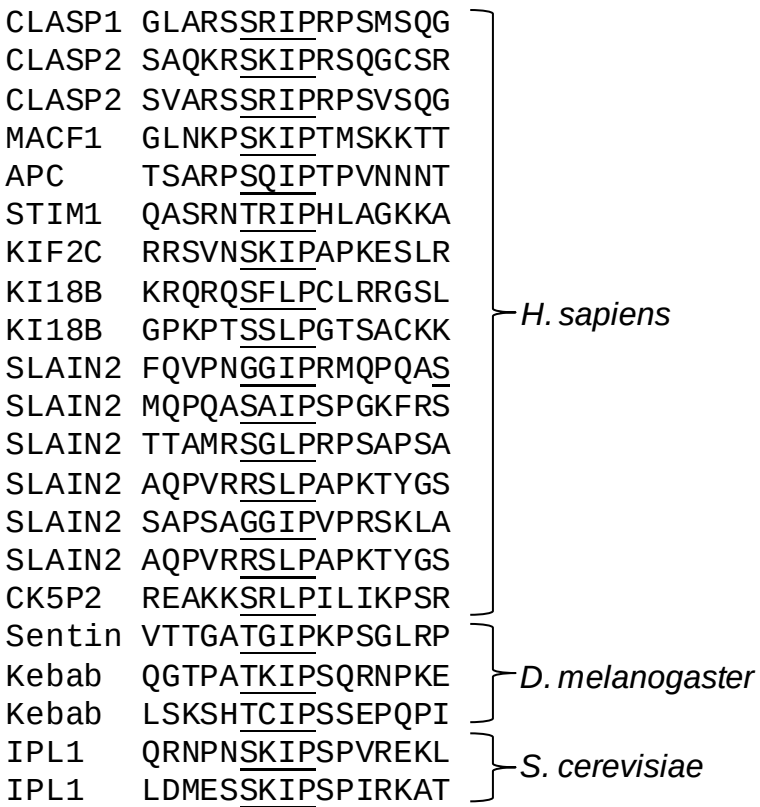

Figure 1.6 Fragments of proteins known to use SxIP motif for binding to EB1.

Alignment of 21 sequence fragments from 12 proteins whose interaction with EB1 was experimentally proven. Residues at positions corresponding to SxIP are underlined.

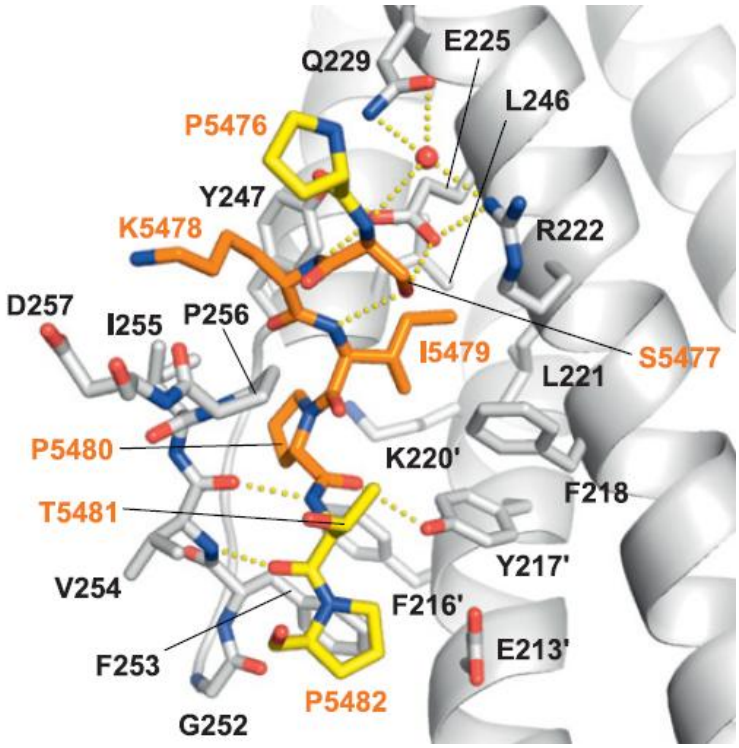

Figure 1.7 Atomic-level interaction network of MACF-EB1 complex. Nonpolar Ile5479 and Pro5480 of MACF SxIP are buried in hydrophobic cavity on EB1 and are essential for SxIP proteins' binding to EB1. The hydrophobic cavity on EB1 is formed by residues Phe216, Arg222, Glu225 and Tyr247 which are located between C-terminal helices of EB1. Conserved residues on EB1, Arg222, Glu225, Gln229 and Tyr247, form a network of hygrogen bond interactions with Ser5477 of MACF SxIP. The residues constituting SxIP motif in MACF are coloured in orange, the residues outside SxIP are in yellow and EB1 is coloured gray. Dashed yellow lines denote hydrogen bonds. The figure is adapted from Honnappa et al, 2009.

negative charge near the EB1 C-terminus are likely to contribute to the binding (Kumar et al, 2012). Additionally, EB1 interaction with SxIP proteins is negatively regulated by phosphorylation (Honnappa et al, 2009; Kumar et al, 2012).

Even though EB1 recruits many MAPs by SxIP, a novel Drosophila protein, Sentin, is a dominant partner of DmEB1 for promoting microtubule dynamics (Li et al, 2011). Sentin may be a functional homologue of mammalian SLAIN2 (Li et al, 2012a). Li et al. (2011) replaced the C-terminal fragment of DmEB1, which is responsible for binding to all of the known protein partners, with Sentin. They observed that the wild-type phenotype was restored after expression of the DmEB1-Sentin fusion in double RNAi DmEB1-Sentin cells. However, other MAPs interacting with EB1 may have more specific functions than Sentin, such as facilitating microtubule plus end association via EB1 with different organelles and structures inside the cells (Kumar & Wittmann, 2012). Also, different SxIP-containing proteins may be required to modulate specific processes inside the cells involving microtubule plus ends. An example is CLASP, whose microtubule plus end localisation is spatially regulated in fibroblasts (Lansbergen et al, 2006). CLASP also localises to the cell cortex, Golgi, kinetochores and spindle mid-zone (Lansbergen et al, 2006; Patel et al, 2012).

Therefore, the interaction of EB1 with MAPs containing SxIP is a very interesting mechanism required for regulation of microtubule dynamics, yet new and unexplored.

1.3. The Dis1/TOG family of proteins

The Dis1/TOG family of proteins has homologues across the species, from yeast to mammals. A Dis1/TOG family member, XMAP215 (*Xenopus* microtubule assembly protein), was first identified from egg extracts as a 215-kDa protein which promoted microtubule elongation ~10-fold (Brouhard et al, 2008; Gard & Kirschner, 1987). The Drosophila Mini spindles (Msps) protein of 227-kDa was identified as a factor responsible for keeping spindle integrity in cytological screen for mitotic mutants. A *msps* mutation results in formation of small additional spindles, defocused spindle poles and chromosome misalignment (Cullen et al, 1999). In meiotic spindles, Msps is responsible for maintaining bipolarity of acentrosomal spindles (Cullen & Ohkura,

2001). In interphase cells, Msps has an antipausing activity on microtubules (Brittle & Ohkura, 2005). Depletion of Msps from Drosophila S2 cells results in microtubules not extending towards the cell periphery and causes microtubule bundling (Brittle & Ohkura, 2005). Localisation of Msps is dynamic in dividing cells thus suggesting that Msps-microtubule association is cell cycle regulated. Msps localises to centrosomes in all mitotic stages, it spreads along the spindle in metaphase and anaphase and in telophase lower level of Msps immunostaining is observed at the spindle mid-body (Cullen et al, 1999). In interphase cells, Msps localises along the microtubules and Msps immunostaining is particularly strong at the microtubule plus ends (Brittle & Ohkura, 2005).

Interestingly, apart from being abundant in the dividing cells, Msps is highly expressed in brain, suggesting that the protein has also a role in nonproliferating cells (Charrasse et al, 1998; Cullen et al, 1999; Gard & Kirschner, 1987).

1.3.1. Structure

The characteristic feature of Msps and its homologues is the presence of multiple tumor overexpressed gene (TOG) domains at their N-termini (Figure 1.8 A) (Ayaz et al, 2012; Ohkura et al, 2001). Human ch-TOG, plant MOR1, XMAP215 and Msps have five TOG domains, Zyg-9 of nematode has three TOG domains and yeast Stu2, Alp14 and Dis1 have two TOG domains (Widlund et al, 2011). The higher eukaryote Msps homologues are likely to be monomeric while the yeast homologues form homodimers (Al-Bassam et al, 2007). Dimerisation of Stu2 is essential *in vivo* since the dimerisation mutants had growth defects. Also, the microtubule affinity of Stu2 is strongly reduced in the mutants lacking the dimerisation domain (Al-Bassam, 2006). The TOG domains are αβ-tubulin-binding modules (Ayaz et al, 2012). In higher eukaryotes and nematode, the TOG domains are followed by a variable region and a conserved C-terminal region (Al-Bassam et al, 2007). In yeast, TOG domains are followed by a basic linker and a coiled coil region which is used for the protein homodimerisation (Figure 1.8 A) (Al-Bassam, 2006).

The C-terminus of Msps is known to be an interaction region with D-TACC (Drosophila transforming acidic coiled-coil-containing) which is required for Msps localisation to spindle poles (Cullen & Ohkura, 2001; Lee et al, 2001). It was shown

(A)

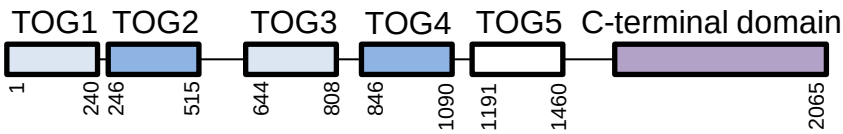

(B)

```
Msps TOG1   16 CVHKLWKARVDGYE 29
Msps TOG2  287 LEEKKWTLRKESLE 300
Msps TOG3  601 LVDSNWKNRLAAVE 614
Msps TOG4  869 MSDKDWKTRNEGLT 882
Msps TOG5 1199 MFHDDFRYHLKVIE 1212
Stu2 TOG1   18 LTYKLWKARLEAYK 31
Stu2 TOG2  336 ITSSKWKDRVEALE 349
```

Figure 1.8 Schematic representation of XMAP215 domain organisation and sequence conservation within TOG domains.
(A) Members of the higher order XMAP215 family are monomers. They contain five arrayed TOG domains in the N-terminal region and a conserved C-terminal region. TOG domains are classified into three groups based on sequence homology; TOG1 and TOG2 are group A, TOG2 and TOG4 are group B and TOG5 is group C. Each TOG domain is ~200 amino acids long and is composed of usually six HEAT repeats, which are involved in protein-protein interactions. (B) Sequence alignment of the first intra-HEAT loop fragments of different TOG domains from *D. melanogaster* (Msps) and *S. cerevisiae* (Stu2). The prominent position of surface-exposed tryptophan is crucial for microtubule binding (red box) and highly conserved accross the TOG domains and species, except for TOG5 (phenylalanine).

in a cell culture that a 502 amino acid long C-terminal fragment of XMAP215 localises strongly to centrosomes in mitosis and interphase (Popov et al, 2001). An N-terminal 1584 amino acid fragment of XMAP215 showed microtubule association which was further confirmed by another study, where the microtubule lattice binding domain was mapped to amino acids 1150 and 1325, a region between TOG4 and TOG5 (Widlund et al, 2011). In Stu2, the microtubule lattice binding region is localised after the TOG repeats, in the ~100 amino acid long linker (Wang & Huffaker, 1997).

TOG domains consist of ~200 amino acids and each of the domains is composed of, usually six, HEAT repeats (Figure 1.9 A) (Al-Bassam et al, 2007). HEAT repeats, present in a variety of proteins, are ~40 amino acid residues long and occur in block of 3 to 22 tandem repeats (Groves et al, 1999; Kobe et al, 1999). Considering the functional diversity of proteins containing HEAT repeats it was proposed that HEATs are involved in protein-protein interactions (Kobe et al, 1999; Ohkura et al, 2001). Although the sequence similarity between individual HEAT motifs is low, the motifs have a common architecture forming α-helical antiparallel structures that stack side by side and form elongated domains (Figure 1.9 A) (Kobe et al, 1999). The highest degree of conservation between HEAT repeats of a TOG domain was mapped to amino acid residues in intra-HEAT loops (Figure 1.8 B) (Al-Bassam et al, 2007; Slep, 2009). Apart from being conserved between the TOG domains of the same protein, these residues are also conserved across the Dis1/TOG family (Al-Bassam et al, 2007). A tryptophan residue present on a loop of the first HEAT repeat of TOGs, except TOG5 (phenylalanine), is a prime determinant of TOG domain interaction with tubulin (Slep, 2009). A highly conserved salt bridge, which is located directly below Trp292, forces this tryptophan residue to be exposed at the protein surface (Figure 1.9 B) (Slep & Vale, 2007). Single mutation of either Trp21 on TOG1 or Trp292 on TOG2 of Msps to glutamic acid reduced binding to αβ-tubulin and the double mutation inhibited the binding (Slep & Vale, 2007). Therefore the tryptophan on TOGs is critical for αβ-tubulin-binding. Similarly, mutating conserved Lys151 in first TOG domain (TOG1) of Stu2 in a loop of fourth HEAT repeat inhibited tubulin binding (Al-Bassam et al, 2007). Hence the conserved residues in intra-HEAT loops appear to mediate TOG-tubulin binding. The crystal

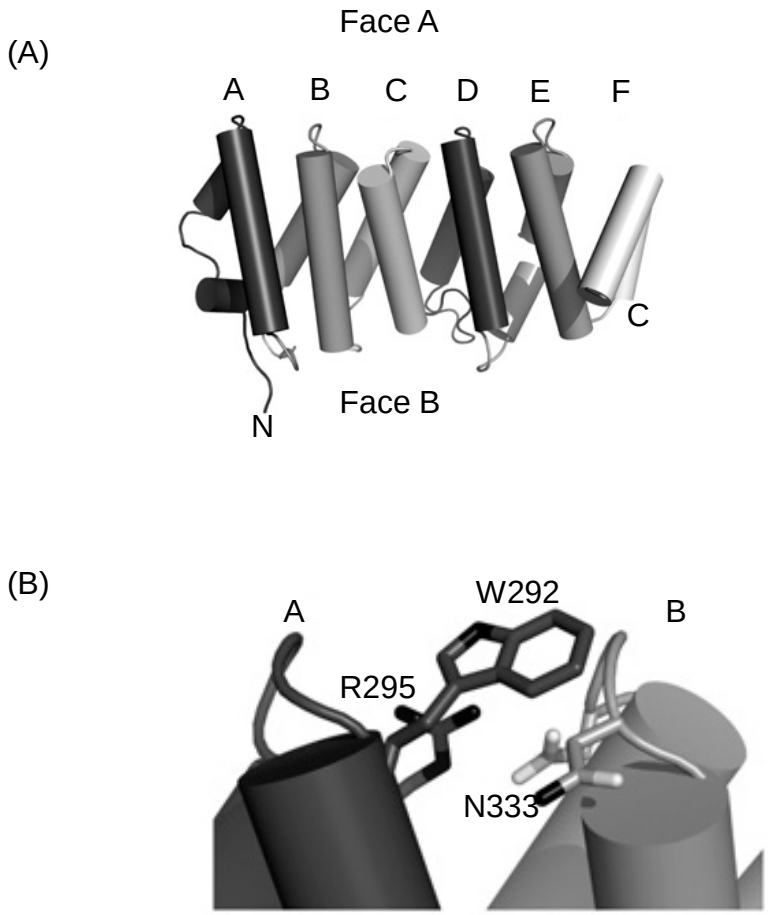

Figure 1.9 TOG2 domain structure of Drosophila Msps.
(A) TOG domains are structures made of usually six HEAT repeats stack side by side and form elongated domains. Each HEAT repeat is formed of two helices connected by intra-HEAT loops (on face A) which contain highly conserved and surface exposed residues. Contrarily, inter-HEAT loops connecting individual HEAT repeats (on face B) do not have a high degree of conservation. (B) Trp292 in intra-HEAT loop of face A is highly conserved between TOG domains and is a major determinant of a TOG domain interaction with tubulin. Trp292 is forced to the surface by the salt bridge between Asp331 and Arg295 located directly below it. The figure is adapted from Slep (2009).

structure of Stu2 TOG1 in complex with αβ-tubulin confirms that the intra-HEAT loops are major determinants in αβ-tubulin binding by Stu2 (Ayaz et al, 2012).

1.3.2. Microtubule Binding

Dis1/TOG family proteins contain a variable number of TOG domains, yeasts have two TOGs, nematode three and higher eukaryotes have five TOGs. Based on sequence similarity, TOG domains of Dis1/TOG family can be classified into three groups. TOG1 and TOG3 are group A, TOG2 and TOG4 are group B and TOG5 is group C (Figure 1.8 A) (Currie et al, 2011; Slep, 2009). Thus, it is possible that the higher eukaryote Dis1/TOG family members evolved by duplicating TOG domains to efficiently polymerise tubulin.

Dis1/TOG proteins bind free tubulin dimers. While it was shown that XMAP215 and Msps bind αβ-tubulin with 1:1 stoichiometry, two molecules of the yeast homologue, Stu2, are required to bind an αβ-tubulin dimer. Stu2 homodimerises via the C-terminal coiled coil regions to efficiently bind tubulin (Al-Bassam & Chang, 2011). Although the role of the fifth TOG domain of eukaryote Dis1/TOG proteins, TOG5, remains unclear, there is an indication that it may be enhancing binding of the Dis1/TOG proteins to tubulin (Al-Bassam & Chang, 2011; Widlund et al, 2011).

Slep et al. (2007) showed that Stu2 domains, TOG1 or TOG2 as well as TOG1 and TOG2 added *in trans*, can bind tubulin dimers. However, TOG1 interaction with tubulin heterodimer is much stronger than interaction of TOG2 with tubulin heterodimer (Al-Bassam, 2006). Neither of Msps fragments, TOG1 or TOG2 nor TOG1 and TOG2 acting *in trans*, bind tubulin. However, Msps fragment containing TOG1 and TOG2 in tandem binds tubulin dimer indicating that the region that links TOG1 with TOG2 has, possibly a structural, role in tubulin binding.

1.3.3. Regulation of Microtubule Dynamics

XMAP215 stays bound to a growing microtubule during multiple rounds of tubulin addition, which is different from EB1, a protein discussed earlier that also tracks growing microtubule plus ends autonomously but associates with microtubules dynamically. Also differently to EB1, XMAP215 tracks not only growing but also

the depolymerising microtubule ends. XMAP215 acts as an antipausing factor of microtubule dynamics. It catalyses microtubule growth at physiological tubulin concentrations by adding up to 25 tubulin dimers into each 13 protofilaments and it depolymerises microtubules at low tubulin concentrations. XMAP215 and Stu2 are elongated, rod-shaped proteins with multiple flexible joints, presumably the inter-TOG regions, when they are not in a complex (Brouhard et al, 2008; Cassimeris et al, 2001). However, XMAP215 becomes well ordered when in complex with tubulin; XMAP215 wraps around a tubulin dimer adopting a globular conformation. The architecture of XMAP215 bound to tubulin is similar to that of the Stu2 homodimer in complex with tubulin. The Stu2 homodimer also forms a compact complex with tubulin. Together with a quick dissociation of the Stu2 homodimer-αβ-tubulin complex, a model was proposed where Stu2 homodimer captures αβ-tubulin, positions it at the growing end of a microtubule and dissociates from the assembled αβ-tubulin (Al-Bassam, 2006).

More recently a structural study involving crystallisation of Stu2 TOG1 with αβ-tubulin shed more light on Stu2-mediated microtubule polymerisation mechanism. It is apparent from the crystal structure that the curvature of the tubulin heterodimer facilitates TOG1 binding. Although TOG1 can still bind to straight αβ-tubulin, the binding is less tight (Ayaz et al, 2012). TOG1 and TOG2 binding to tubulin discriminates between curved and straight tubulin heterodimer conformations. Tubulin adopts straight conformation when in microtubule body and curved when free or at the very ends of a microtubule. Both TOG1 and TOG2 preferentially bind curved αβ-tubulin which does not exist in the microtubule body (Ayaz et al, 2012). Stu2 homodimer might associate to microtubule plus ends through TOG2 domains, which preferentially recognise conformation of αβ-tubulin at the microtubule plus ends, and incorporate tubulin heterodimer using TOG1 (Ayaz et al, 2012). Deletion of both TOG1 and TOG2 domains results in Stu2 associating with the microtubule body and abolishes plus end binding (Al-Bassam, 2006). The ability of Stu2 to recognise different tubulin conformations is consistent with Stu2 being a microtubule polymerisation catalyst.

XMAP215 targets both microtubule body and plus ends. XMAP215 bound to microtubule body diffuses along the microtubules towards the plus end where it

accumulates and persists for several rounds of tubulin addition and accelerates tubulin addition (Brouhard et al, 2008). However, XMAP215 accelerates microtubule depolymerisation in absence of tubulin.

1.3.4. Regulation of Mitotic Spindle Architecture

Since Msps depleted cells exhibit a number of spindle defects, Msps has an essential role in maintaining correct spindle architecture in the dividing cells.

Msps interaction with D-TACC was demonstrated to have a key role in stabilisation of microtubules within the spindle of Drosophila embryos. A pool of D-TACC-Msps complexes at the centrosomes can be phosphorylated by Aurora A to bind and stabilise microtubule minus ends (Barros, 2005). The minus end stabilisation by D-TACC-Msps complex is exclusive to the centrosomes. A phosphorylation site on TACC3, a *Xenopus* homologue of D-TACC, targeted by Aurora A is conserved amongst species (Kinoshita et al, 2005). Microtubule stabilisation by TACC3-XMAP215 complex was proposed to protect spindle microtubules from microtubule depolymerising protein, MCAK. In the presence of TACC3, XMAP215 counteracts MCAK depolymerising activity which allowed for the microtubule nucleation from centrosomes. Thus TACC3 presumably enhances XMAP215 activity at the centrosomes (Kinoshita et al, 2005). The protection of microtubules at the centrosomes from depolymerising activity of MCAK is crucial to prevent formation of multipolar spindles (Holmfeldt et al, 2004).

1.3.5. Interplay with EB1

Msps and EB1 are both key players in regulation of microtubule dynamics. Although EB1 alone has mild effects on acceleration of microtubule growth rate *in vitro*, it is essential to maintain microtubule dynamics *in vivo* and in cell extracts (Niethammer et al, 2007; Vitre et al, 2008). Msps significantly increases microtubule polymerisation rate but the *in vitro* reconstitution assays proved that alone it is not sufficient to fully restore microtubule growth rates seen in cells. EB1-Msps interplay was investigated in context of regulation of microtubule polymerisation rate. Although microtubule growth is not dependent on direct EB1-Msps interaction, both of the proteins are essential and sufficient to restore robust microtubule growth *in*

vitro (Zanic et al, 2013). It was shown *in vitro* that EB1 and Msps increased microtubule polymerisation by up to 20 μm min^{-1}, the levels seen *in vivo*. Since fast polymerisation activity of Msps relies on its TOG domains which release a tubulin dimer once straightened upon incorporation into a microtubule, it was suggested that EB1 speeds up Msps polymerisation activity because it accelerates protofilament straightening through enhancement of lateral interactions between tubulin dimers (Ayaz et al, 2012; Vitre et al, 2008; Zanic et al, 2013). Van der Vaart et al (2009) showed that SLAIN2 (a human homologue of Sentin), a MAP which interacts with EB1 using the SxIP, interacts also with ch-TOG. Inhibition of ch-TOG interaction with SLAIN2 results in microtubule growth defects and disruption of microtubule array in interphase (van der Vaart et al, 2011). The microtubule plus end localisation of Sentin or SLAIN2 depends on interaction with EB1 (Li et al, 2011; van der Vaart et al, 2011). Therefore, this indirect EB1-Msps interaction, via a MAP, gives a new insight to the regulation of microtubule plus end dynamics.

1.4. Peptide aptamers

1.4.1. Peptide aptamers as a powerful tool in genetic studies

A multitude of cellular processes are regulated by protein interaction networks. Two types of genetic approaches, forward and reverse genetics, are used to elucidate protein functions within a network. The forward genetics relies on generation of random genetic mutants and selecting those which display a desired phenotype. Identifying the genes responsible for the phenotype, along with biochemical data on their interaction partners, gives the researcher an idea about the roles these genes play and their positions within a network. In reverse genetic analysis, an approach which is opposite to the forward genetics, individual genes are manipulated and the phenotype is observed to address the question of what is the possible role of the gene.

However, there are limitations with regards to studying a protein function when mutating it at a DNA level. Knocking out a gene essential for cell proliferation makes it difficult to study the gene function in a developed organism unless conditional mutants, such as temperature sensitive mutants, are available. Also, even

though RNAi can be used to deplete the messenger RNA and thus inhibit protein expression, the pool of the protein which had already been produced remains intact. Thus RNAi is not sufficient if it targets transcription of a stable protein whose half-life is long because the original protein pool would likely sustain its functions inside the cell. However, the protein levels would be reduced if the cell undergoes a sufficient number of divisions which is not the case in the differentiated cells.

An alternative approach is the use of peptide aptamers. The name “peptide aptamer”, coming from a combination of Latin word “aptus” which means “fitting” and Greek “meros” meaning “part”, resulted from similarity of these molecules to the nucleic acid aptamers which are nucleic acid fragments binding to various molecular targets (Seigneuric et al, 2011). Peptide aptamers were originally described as double constrained peptides displayed in the active site of thioredoxin (TrxA) that were designed to function inside a cell and bind to their protein targets (Colas et al, 1996). They usually contain a 10-20 amino acid peptide fragment, so-called “variable region”, which can be either constrained from both sides by the protein sequence from which it is displayed or, less often, the variable region can be singly constrained by fusing it to one of the protein termini. These small, novel molecules advanced protein-protein interaction research and drug target discovery as well as understanding of protein interaction domains. What distinguishes peptide aptamers from unconstrained peptides or antibodies is their small size, stability and solubility, which relies on their fusion to a “scaffold” protein from which they are displayed as well as specificity to a certain region on a target protein resulting in disruption of particular protein-protein interactions (Crawford et al, 2003; Hoppe-Seyler et al, 2001; Wickramasinghe et al, 2010). Also, as peptide aptamers are expressed inside the cells, they do not pose delivery problems.

1.4.2. Design of peptide aptamers

1.4.2.1. Selection

Peptide aptamers can be applied in both forward and reverse genetic studies. In forward genetics a peptide library is screened for production of a desired cellular phenotype and such peptide aptamers and their target proteins can be selected for

further studies (Crawford et al, 2003). In the reverse genetics, a researcher finds peptide aptamers binding to a protein of interest and selects them for subsequent *in vivo* studies (Crawford et al, 2003; Geyer, 2001). Both, *in vitro* and *in vivo* selection methods have been reported. Various display platforms have been used for the *in vitro* selection of peptide aptamers, ranging from the display on surfaces such as phage, yeast, flagella of *Escherichia coli* as well as ribosomes (Geyer & Brent, 2000; Li et al, 2012b; Yeh et al, 2013). The *in vivo* selection of peptide aptamers is very common and probably more suited than an *in vitro* selection if one wants to perform further studies involving expressing these peptide aptamers in an organism. The first reported yeast two-hybrid (Y2H) screen for peptide aptamers was performed to find interactors of human cyclin dependent kinase 2 (Cdk2) (Colas et al, 1996). The tested interactors inhibited Cdk2 activity and bound to it with a dissociation constant in a nanomolar range (Colas et al, 1996). Y2H takes an advantage of transcription factor being split into two parts, a transcription activation domain (AD) and a DNA-binding domain (BD), which fused to proteins interacting with each other bring the AD and the BD in a close proximity (Figure 1.10). Three common features of Y2H screens for peptide aptamers binding to a protein of interest are:

- A vector which carries DNA fragments from a library encoding different peptide aptamers fused to an AD of a transcription factor, the so-called "prey". The most commonly used transcription factor is GAL4.
- A vector which carries DNA encoding the protein of interest fused to a DNA-BD of the transcription factor, the so-called "bait".
- Reporter genes downstream of the activating sequence. Interaction of the bait- and prey-fused proteins is detected due to BD and AD being brought together. The proximity of the two domains results in the activation of a downstream reporter gene (Figure 1.10). The common choice of the reporter genes are auxotrophic markers such as *ADE2*, *HIS3*, *LYS2*, *LEU2* or *URA3* (Hoppe-Seyler et al, 2004). Thus, the selection of yeast carrying the interacting peptide aptamers is possible by plating them on media deficient in an appropriate nutrient. Often a second reporter gene is introduced, such as *lacZ*, which has an enzymatic activity which can be quantified thus giving an information about bait-prey interaction strength (Hoppe-Seyler et al, 2004).

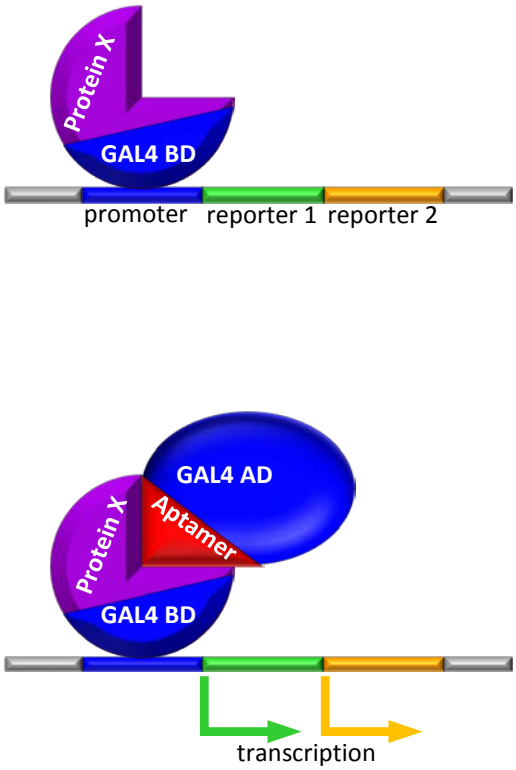

Figure 1.10 Strategy for detecting peptide aptamers interacting with a protein of interest by yeast two-hybrid
Plasmid encoding a protein of interest fused with DNA binding domain (BD) of Gal4 is introduced into yeast which has the reporter genes *lacZ* and *HIS3* under the control of the *GAL1* promoter. Yeast are cotransformed with a plasmid expressing a library of peptide aptamers fused with activation domain (AD) of Gal4. Tranformants containing peptides interacting with the protein fused with BD of Gal4 reconstitute GAL4 activity causing expression from reporter genes.

1.4.2.2. Scaffolds for peptide aptamer display

The most common protein used as a scaffold for peptide aptamer display is TrxA of *E. coli*. It is a protein of 12 kDa found in many eukaryotic and prokaryotic species (Holmgren, 1989). TrxA is a cytoplasmic protein which can be expressed inside the cells at high levels without toxic effects (Colas et al, 1996; LaVallie et al, 1993). Importantly for its use as a peptide aptamer scaffold, TrxA is stable and soluble thus often it is fused to other proteins to improve their solubility (Geyer, 2001; LaVallie et al, 1993). To display a peptide aptamer from TrxA, a random sequence fragment from a library is inserted into a biologically active site of TrxA abolishing its enzymatic activity (Klevenz et al, 2002). Importantly, a peptide insertion into this site does not affect the protein which retains its native folding (LaVallie et al, 1993; Lu et al, 1995). The active site sequence of TrxA is a good spot for presenting the peptides because it forms a loop on the protein surface and makes the peptides accessible (Lu et al, 1995). While being most commonly used, TrxA-based peptide aptamers were reported not to express stably in human cultured cells (Woodman et al, 2005). Also, peptide aptamers double constrained within the loop on TrxA are enclosed by cysteine residues which can cause disulfide bond formation when in an oxidative environment. Thus, it has to be taken into consideration that a peptide displayed on TrxA may adopt a different conformation and become inactive when shifting between oxidative and reducting environments. However, alternative scaffolds have been proposed which can be applied accordingly to a need. An example of another scaffold for display of double constrained peptides is stefin A triple mutant (STM). STM was designed by Woodman et al (2005) and shown to confer stability in systems such as bacteria, mammals and yeast. STM is based on human stefin A, a small protein whose folding is independent of disulfide bonds, thus it can be applied in intra- and extracellular systems (Davis et al, 2009; Woodman et al, 2005). Examples of other protein scaffolds used for a double constrained display of peptides include green fluorescent protein (GFP) or a derivative of staphylcoccal nuclease (SNase).

While the double constraint of peptides can be advantageous because of their usually higher proteolytic stability, the conformations that can be adopted by

these double constrained peptides are highly limited (Colas et al, 1996; Geyer & Brent, 2000). Therefore, single constrained peptides were displayed as a direct fusion to the C-terminus of GAL4-AD by Yang et al. (1995) for selection in Y2H. They found several peptide interactors binding to the retinoblastoma (Rb) protein, one of which bound with ~10 μM affinity. Also, singly constrained peptides displayed on a phage as a fusion to the N-terminus of pIII, a phage coat protein, in search for concanavalin A interactors showed mid-micromolar range of binding (Oldenburg et al, 1992). However, the peptide aptamers with double constrained peptide fragments very often showed target binding affinity in nanomolar range (Colas et al, 1996; Fabbrizio, 1999). Thus, even though single constrained peptide interactors can be selected more easily from a library because of the higher conformational variability, their binding affinity to a target protein may not be as high as the binding of peptides whose folding is double constrained.

Klevenz et al. (2002) addressed the question of whether exchange of a peptide aptamer scaffold to a different scaffold, from which a peptide was not originally displayed, would affect the peptide aptamer affinity to its target. This study is important because, if a scaffold exchange did not affect a peptide-protein interaction, one could screen a library of single constrained peptide interactors and then double constrain the interacting peptides within a different scaffold to improve their affinity to a target protein. Variable peptide regions of three TrxA-based peptide aptamers were shifted to alternative scaffolds, doubly-constraining catalytically inactive derivative of SNase or GFP, as well as to singly-constraining GAL4-AD, rendering the peptides partially flexible (Klevenz et al, 2002). Only one of the peptides continued binding to its target protein when displayed from SNase, GFP or GAL4-AD, the other two lost a detectable binding activity (Klevenz et al, 2002). The authors explained the loss of binding with peptides adopting different folding in different scaffolds while the one which retained the binding, in both doubly-constrained and singly-constrained form, adopted a strong intrinsic stability, thus not requiring a support from a scaffold constraining it from both sides (Klevenz et al, 2002). While it is not known whether the affinity of that peptide for its target improved when the scaffold was changed in the research described by Klevenz at al. (2002), Cohen et al. (1998) reported improving a peptide-protein binding affinity

1000-fold by displaying an originally single constrained peptide from the double-constraining TrxA scaffold.

Therefore, peptides whose folding relies on a double-constraint from a scaffold may not show a target-binding activity when screened in a context of another scaffold. Thus it is necessary to rethink the experimental design for peptide aptamer screening because changing the scaffold may not be an option for some peptides.

1.4.3. Applications

1.4.3.1. Biomedical research - identification of drug targets

Perturbing a target proteins' function is a general approach to validate a drug target and it is often done by methods which reduce the proteins' expression levels or abolish its expression (Baines & Colas, 2006). However, inadequate validation of a drug target is a significant problem in drug discovery (Colas, 2008). Peptide aptamers are a very powerful alternative for target validation in the drug discovery process because, similarly to therapeutic ligands, they bind to a specific site on a protein thus disturbing a particular interaction rather than all the interactions in which a protein is involved (Baines & Colas, 2006). Therefore, peptide aptamers enable one to verify, at a cellular or an animal model level, whether a therapeutic ligand would revert a pathological phenotype associated with a disease. A selected peptide aptamer which produces a desired therapeutic effect can be potentially used as a therapeutic itself or the crystal structure information, coming from co-crystallising a peptide aptamer with its target, can be used for screening potential small molecule inhibitors *in silico* or their rational synthesis (Crawford et al, 2003). Alternatively, a peptide aptamer can be applied in a competitive displacement assay where a pool of small molecule ligands are selected based on their ability to displace the peptide aptamer (Dibenedetto et al, 2013). Such selected interactors can become precursors for therapeutic drugs.

The druggable sites on a protein can be mapped using peptide aptamers if the target protein structure is known or if it can be modelled by homology (Pamonsinlapatham et al, 2008). In AptaPrint technology a target protein structure is

visually investigated for presence of structural features, such as putative binding pockets or protein-protein interaction sites, and amino acid mutations are introduced into such molecular surfaces (Baines & Colas, 2006). Next a pool of peptide aptamers previously selected for binding to the wild-type version of the mutated protein are screened to examine whether they retain binding ability to each of the protein mutants. The peptide aptamers which no longer bind to a mutant version of the target are likely to bind to the mutated site (Baines & Colas, 2006). The pitfalls of AptaPrint include limitations of the software used to build a homology model of a protein which was not crystallised and structural modifications which may arise when mutating the protein target (Baines & Colas, 2006; Hoppe-Seyler & Butz, 2000).

1.4.3.2. Biomedical research - biosensing in diagnostics

Another potential implementation peptide aptamers have is in disease diagnostics where they can be used on various protein detection platforms. Since peptide aptamers are highly selective towards their targets, they can be applied to detect a mutant form of a protein causing a disease as well as distinguish between different protein isoforms (Davis et al, 2009). Thibaut at al. (2012) reported a novel peptide aptamer-based enzyme-linked immunosorbent assay (ELISA) used for detection of antibodies against anti-human platelet antigen antibodies (HPA-1a). In neonatal alloimmune thrombocytopenia (NAIT), a pregnant woman generates HPA-1a antibodies against the foetus which may destroy foetal platelets (Thibaut et al, 2011). Therefore, early detection of HPA-1a in maternal blood is essential. The advance of this method comes from abandoning human platelets, used in current NAIT diagnostics to detect HPA-1a antibody, which pose storage problems and can differ between the batches coming from different donors (Thibaut et al, 2011). In their assay, Thibaut et al. (2011) used TrxA-displayed peptide aptamer, specifically binding to HPA-1a antibody, coated onto a microtitration plate, followed by sequential incubations with human serum and Fc fragment-specific antibody conjugated to HRP. Addition of an HRP substrate allows for detection of a reaction product by optical density.

Another successful biomedical application of peptide aptamers was reported by Murray et al. (2007) who obtained peptide aptamers with high specificity to anterior gradient-2 (AG-2). AG-2 is the most abundant, upregulated protein in Barrett's epithelium, a proliferative condition causing abnormal change in cells of oesophagus (Murray et al, 2007). Since Barrett's epithelium is strongly associated with esophageal adenocarcinoma, development of a biomarker assay for detection of AG-2 in a patient's biopsy serum could help to target the disease early (Murray et al, 2007). They identified two peptide aptamers binding with high specificity to AG-2 which were used to affinity-purify AG-2 from a crude clinical biopsy lysate to near homogeneity. Interestingly, three attempts to obtain monoclonal antibodies specific to AG-2 did not yield antibodies effective enough in similar purification or diagnostic experiments (Murray et al, 2007).

Park et al. (2011) developed a peptide aptamer biosensor for detection of hepatotoxicity marker, alanine aminotransferase (ALT) enzyme, a biomarker of liver damage. The advance of their biosensor over the those currently in use is that the peptide aptamer-based biosensor detects ALT itself rather than its enzymatic activity (Wu et al, 2011). Thus, they provided an alternative for development of biosensors to detect almost any protein target regardless of its physico-chemical activities. The biosensor platform described by Park et al. (2011) and other peptide aptamer-based platforms which couple peptide aptamer-target protein binding to the electrochemical detection methods offer a powerful, label-free technique which could find a clinical application.

1.4.3.3. Basic Research - identifying pathway components and binding motifs

Peptide aptamers can be widely applied in identifying components of biological pathways and learning the binding motifs. The origin of the peptide aptamer work is attributed to Colas et al. (1996) who found fourteen TrxA-based peptide aptamers which could bind human Cdk2 *in vitro* (Hoppe-Seyler et al, 2004). While neither of them interacted with two unrelated control proteins, some of the peptide aptamers interacted with other Cdks. This was explained by these peptide aptamers binding to different regions on Cdk2, some of which can be conserved within the Cdk protein family (Colas et al, 1996). This pioneering work was followed by many researchers

investigating biological pathway components also using peptide aptamers to target different protein sites.

Similarly to Colas et al. (1996), Butz et al. (2000) in their search of peptide aptamers binding to human papillomavirus (HPV) E6 also found peptide aptamers which could bind to E6 proteins of other HPV types indicating a structural homology between the proteins. Moreover, several of the identified peptide aptamers contained motifs similar to those found in natural binding partners of E6 and proposed to be E6 protein binding motifs (Butz et al, 2000). Some of these peptide aptamers induced apoptosis of HPV-positive cancer cells by targeting the E6 protein which has an antiapoptotic potential (Butz et al, 2000). Also a screen where peptide aptamers were selected to outcompete DP for E2F binding isolated a peptide aptamer with a four amino acid motif which is present on DP and is conserved across the species (Fabbrizio, 1999). They showed that the motif on DP is essential for the progression through the cell cycle because it allows for DP/E2F heterodimerisation. Therefore, peptide aptamers could help to identify new protein interactors by giving an idea of the functional motifs used for interaction with the target protein and thus ease finding drug targets.

Another example of successful peptide aptamer application to dissect a biological pathway and narrow down an interaction to a motif level was presented by Wickramasinghe et al. (2010) who isolated a peptide aptamer named “swiggle”. Swiggle interacts specifically with the LLY motif of Membrane-Type 1 Matrix Metalloproteinase (MT1-MMP) intracellular domain (ICD). Expression of MT1-MMP, a major player implicated in extracellular matrix remodelling, is associated with processes promoting tumour progression such as tumour cell invasion and metastasis (Uekita et al, 2001). However, the only information on MT1-MMP interaction involving its ICD comes from the studies in which the domain was either partially or completely deleted (Wickramasinghe et al, 2010). Wickramasinghe et al. (2010) applied swiggle in their research and showed that it outcompetes a protein interactor required for MT1-MMP internalisation, and that the LLY motif of ICD is essential for the interaction between MT1-MMP and its internalisation partner (Wickramasinghe et al, 2010). They also showed that peptide aptamers can be found to interact with domains as small as 21 amino acids of MT1-MMP ICD.

Even though not yet extensively explored, peptide aptamers were used in living organisms. Kolonin et al. (1998) expressed two peptide aptamers against Cdk proteins in Drosophila, each resulting in rough eyes associated with cell division defects. They showed by overexpressing Cdks, in peptide aptamer-expressing Drosophila, that the effect of these peptide aptamers on cell cycle progression is dosage-dependent (Kolonin & Finley, 1998). Moreover, the peptide aptamers were selected in Y2H for binding to Cdk1 or Cdk2 and this specificity was demonstrated in *in vitro* assay and was preserved upon expression in Drosophila. By expressing in Drosophila, peptide aptamers were applied to target Wnt signalling pathway which is an essential and highly conserved pathway for an animal development (Yeh et al, 2013). Expressing a peptide aptamer in Drosophila wing targeting β-catenin (β-cat), one of the Wnt pathway effector proteins, resulted in bubbles and blisters on the wing and growth defects. Yeh et al. (2013) further explored a crosstalk between the Wnt and Notch pathways showing that Ankyrin (ANK) repeats motif on Notch1 is a regulatory region for the Wnt pathway. Therefore, peptide aptamers can be expressed in living organisms as they retain their target binding and successfully applied to dissect interactions within a network.

1.4.3.4. Basic Research - peptide aptamer biotechnology

Peptide aptamers can be applied to assess peptide motif specificity required for a target protein binding. Dibenedetto et al. (2013), having found a peptide aptamer binding to two unrelated human proteins, wanted to dissect its target specificity. They randomly mutagenised the peptide aptamer to generate a library comprising of 1200 variants and a subset of the variants was picked by chance and examined for binding to either one or other protein target. They observed that substitution of an amino acid at a particular position to isoleucine conferred the peptide aptamer specificity to one of the proteins, while tyrosine at that position resulted in binding the other protein target (Dibenedetto et al, 2013). Such peptide aptamer evolution approach can improve its specificity to a target thus having a potential application in obtaining peptide aptamers specific to a target protein and discriminating between related proteins.

It has been shown that peptide aptamers selected from a peptide library of random sequences often bind to a site on a protein target which is physiologically significant (Warbrick, 2006). An example is a screen for peptide aptamers binding to proliferating cell nuclear antigen (PCNA) which yielded peptide aptamers binding to a site used for PCNA binding by its known partner p21. Thus, peptide aptamers can guide a researcher to a protein domain which is significant for biological interactions and even narrow down the search to the protein site level.

Peptide aptamers can be potentially used to map an interaction site used by a protein to bind its partner. Warbrick et al. (1995) to map the minimum PCNA binding site on $p21^{WAF1}$ first, using Y2H, established the regions on each of the two proteins involved in their interaction. To narrow down the interaction region on $p21^{WAF1}$ to the residues critical for the binding, they generated overlapping peptide fragments of the $p21^{WAF1}$ region and binding efficiency of each $p21^{WAF1}$-derived peptide to PCNA was detected by ELISA (Warbrick et al, 1995).

Also Hall et al. (2011) used a whole protein fragment as a peptide aptamer. To kill *Trypanosoma brucei,* the binding of tbBRCA2 and RAD51, which is essential to mediate recombination repair, was perturbed. Induction of peptide aptamer encompassing the BRC motif of tbBRCA2 (which is essential for RAD51 binding) significantly slowed down growth of *T. brucei* (Hall et al, 2011). Thus, it was shown that a protein motif-derived peptide aptamer can have an inhibitory effect on this protein function.

Peptide aptamers atop of their basic function which is binding to the target proteins can be engineered to have additional functions. Hence, peptide aptamer harbouring a nuclear localisation signal (NLS) was used to direct its protein target from cell cytoplasm to the nucleus (Colas et al, 2000). Such protein depletion from a compartment where it plays a biological function by redirecting it to a compartment where it has no activity results in its functional knockout. Also Colas et al. (2000) demonstrated that a target protein can be modified using peptide aptamers. By fusing a peptide aptamer to a ubiquitin ligase, one can target the protein interactor of such peptide aptamer to induce its ubiquitination (Colas et al, 2000; Crawford et al, 2003). Therefore peptide aptamers can be further modified to act as a shuttle for enzymes to modify proteins of interest.

1.5. Project aims

There are limitations to study post-mitotic roles of Msps and DmEB1, particularly in a developing organism, as these proteins are essential for cell division. To overcome these limitations, new tools are required. I aimed to develop new tools which would allow inactivating the proteins at specific time and space at a whole organism level. More specifically, I aimed to

1) generate a *msps* temperature-sensitive Drosophila to inactivate Msps

2) select peptide aptamers interfering with Msps and DmEB1 functions. This also reveals what residues promote binding to Msps and DmEB1.

CHAPTER 2

Materials and methods

2.1. Standard materials

2.1.1. Buffers

Buffers were prepared as in Sambrook et al., 1989 (Sambrook et al, 1989; Sambrook & Russell, 2001). Most of the non-temperature-sensitive solutions were sterilised by autoclaving, the temperature-sensitive solutions were filtered using 0.2 µm Millex syringe filters (Millipore) or bottle top filters (TPP).

2.1.2. Enzymes and chemicals

Chemicals used in this study were supplied by Sigma, Invitrogen, Fisher Scientific and BDH and were of analytical grade. Restriction enzymes were provided by New England BioLabs (NEB) and Promega. Taq DNA polymerase (Roche) and primeSTAR HS DNA polymerase (TaKaRa) were used throughout.

2.1.3. Antibodies

Antibodies used for Drosophila S2 cell immunostaining were as follows

	antibody	**dilution used**	**make**
primary	Mouse anti-tubulin (dm1A)	(1:250)	Sigma
	Mouse anti-GFP	(1:500)	Molecular Probes
	Rabbit anti-GFP	(1:500)	Molecular Probes
	Rabbit anti-EB1	(1:200)	(Elliott et al, 2005)
	Rat anti-Sentin	(1:50)	by the Ohkura lab (unpublished)
	Sheep anti-CLIP-190	(1:500)	(Dzhindzhev, 2005)
secondary	Anti-mouse Cy3	(1:500)	Jackson Labs
	Anti-mouse Alexa Fluor 488	(1:1000)	Molecular Probes
	Anto-rabbit Cy3	(1:2000)	Jackson Labs
	Anti-rabbit Cy5	(1:2000)	Molecular Probes
	Anti-rabbit Alexa Fluor 488	(1:200)	Molecular Probes
	Anti-rat Cy3	(1:500)	Jackson Labs
	Anti-sheep Cy3	(1:1000)	Jackson Labs

2.2. DNA techniques

Standard DNA techniques were used throughout (Sambrook et al, 1989). Kits were used according to the manufacturer's instructions: QIAquick PCR Purification Kit

(Qiagen) to purify PCR products, HiSpeed Plasmid Midi Kit (Qiagen) for large scale purification of DNA from bacteria and Wizard Plus SV Minipreps DNA Purification System (Promega) for small scale purification of DNA from bacteria.

2.2.1. DNA Sanger sequencing

DNA sequencing reaction [25 x (96°C x 30 sec + 50°C x 15 sec + 60°C x 4 min) + 4°C hold] was performed in thermocycler using BigDye polymerase (Life Technologies) and 0.8 pmol/µl sequencing primer and analysed by Sanger sequencing services at Genepool (Edinburgh).

2.2.2. Gateway cloning for generation of peptide aptamer constructs

To allow for efficient gene transfer between cloning vectors while maintaining the reading frame, genes encoding peptide aptamers were cloned into pDONR221 donor vector as follows. The genes were flanked by attB1 and attB2 sites, for recombination with pDONR221, using polymerase chain reaction (PCR) by including these sites in primers (oKMT43: GGGGACCACTTTGTACAAGAAAGCTGGGTCCACGATGCACAGTTGAAGT GAA and oKMT44: GGGGACAAGTTTGTACAAAAAAGCAGGCTCCAAAATCTGTATGGCTTAC CCATACG). These PCR products were run on an agarose gel to confirm their sizes. The PCR products were cloned into pDONR221 donor vector using Gateway BP Clonase II enzyme mix (Invitrogen) following the manufacturer's instructions. The destination vectors pAGW or pARW were used for the expression of an aptamer fused to a GFP or mRFP under the *actin5C* promoter in S2 cells, and pPGW was used for expression of an aptamers fused to GFP under the *UASp* promoter in Drosophila. To introduce a gene of interest to a destination vector, Gateway LR Clonase II enzyme mix (Invitrogen) was used and the reaction was performed according to the manufacturer's instructions. *Escherichia coli* (*E. coli*) One Shot TOP10 (Invitrogen) cells, [F- *mcrA* Δ(*mrr-hsd*RMS-*mcr*BC) Φ80*lac*ZΔM15 Δ *lac*X74 *rec*A1 *ara*D139 Δ(*araleu*)7697*gal*U *gal*K *rps*L (StrR) *end*A1 *nup*G], were used throughout and bacterial transformations were carried following the manufacturer's instructions.

2.3. Yeast techniques

2.3.1. Construction of bait plasmids

Vector pGBT9 was used to construct all bait plasmids. Msps, DmEB1, HsEB1 or HsEB3 coding sequences were flanked, using PCR, by ~50 nucleotide fragments complementary to pGBT9 upstream and downstream of the EcoRI site on pGBT9 by inclusion of these fragments in primers. The PCR products were run on agarose gel to confirm their sizes and purified using PCR purification kit (QIAGEN). A gene was inserted by gap repair into pGBT9 vector linearised by digestion with EcoRI in Y190 *S. cerevisiae* strain. To confirm insertion of a gene into the vector, PCR was performed from a yeast colony (as in 2.3.4) using primers to amplify the plasmid region including the putative insertion site and sequenced.

2.3.2. Construction of prey plasmids

pACT2 was used throughout as a prey vector. Prey plasmids containing D-TACC or α-tubulin coding sequence were constructed in the same manner as bait plasmids, except using the prey vector (pACT2). To express double constrained peptide aptamers, pACT2 plasmid was used with TrxA coding sequence cloned into it (gift from Emma Warbrick, Dundee).

2.3.3. Making libraries for expression from prey plasmid

Deoxyoligonucleotides were synthesised commercially (Eurofins), encoding 16 random amino acids (for NNK library) or 13 random with fixed Ser-x-Ile-Pro (for SxIP library) followed by stop codon and flanked by 48 bp at 5’ and 21 bp at 3’complementary to the sequence upstream and downstream of the EcoRI restriction site in pACT2. The complementary strands to the deoxyoligonucleotides were polymerised by a single polymerisation (98°C x 10 sec + 50°C x 10 sec + 72°C x 10 min + 4°C hold) using PrimeSTAR HS DNA polymerase (TaKaRa). The primer contained the further 29 bp fragment of pACT2 adding it to the 3’ end of the deoxyoligonucleotide fragments.

Deoxyoligonucleotide was synthesised commercially (Eurofins), encoding 13 random amino acids with fixed Ser-x-Ile-Pro, flanked by 48 bp at 5' and 24 bp at 3'complementary to the sequence upstream and downstream RsrII restriction site in TrxA sequence. A further 24 bp complementary fragment was added to the 3' end by inclusion in a primer by a single polymerisation reaction as previously.

2.3.4. Amplification of a gene from a yeast colony

To prepare template for PCR from yeast genomic DNA, a yeast colony was picked into an Eppendorf tube with 10 µl of 0.02M NaOH freshly made from 10M NaOH. The tube was vortexed briefly and incubated for 5 min at 100°C. Immediately after the incubation, the tube was put on ice and, once cold, condensation was spun down in a table top centrifuge. The cells were suspended and used as a template in a PCR reaction [94°C x 2 min + (94°C x 30 sec + 55°C x 30 sec + 68°C x 1min/kb) x30 + 68°C x 10min + 4°C hold] using Taq polymerase.

2.3.5. Yeast two-hybrid methods

2.3.5.1. Screening for peptide aptamers

Growth, maintenance and transformation of *S. cerevisiae* were carried out according to (Guthrie & Fink, 2004). Y190 *S. cerevisiae* strain (*MATa leu2-3 112 ura3-52 trp1-901 his3-D200 ade2-101 gal4D gal80 D cyhR URA3::GAL1-lacZ, LYS2::GAL1-HIS3*) was used for all Y2H analyses. Yeast carrying a bait plasmid were cotransformed with linearised prey vector and a library of the variable DNA fragments for insertion into the prey plasmid. In order to test for expression from *HIS3*, transformants were plated on yeast minimum media, YMM (6.7g Difco Yeast Nitrogen base without amino acids, 20g Glucose, 1L distilled water) supplemented with 20 mM 3-Amino-1,2,4-triazole (3-AT) and essential amino acids (adenine), incubated for 1 week and plates were examined for formation of colonies. Where growth occurred, a colony was picked and patched on YMM plate with 10 mM 3-AT and adenine and incubated for 3 days. Where growth occurred, a colony was patched on a YMM agar plate without 3-AT and allowed to grow for one day. A plate was replicated to two copies and positive and negative control yeast for expression from

lacZ were patched on one of the replicas. Yeast were allowed to grow for one day and β-galactosidase activity was assayed on plate by overlay with 0.72% X-Gal (Guthrie & Fink, 2004). Yeast from one of the replica plates, corresponding to yeast patches which produced β-galactosidase on the other replica, were used to isolate single colonies by streaking the yeast on YMM plate with 10 mM 3-AT and then YMM without 3-AT. Single colonies were, as previously, patched on YMM, allowed to grow, plates were replicated and and β-galactosidase activity was assayed on plate by X-Gal overlay. PCRs were performed from yeast colonies (as in 2.3.4) which produced β-galactosidase to amplify from prey plasmid a library insert sequence and the flanking region, 127 bp of the 5' and 138 bp of the 3'. To exclude that activation of *lacZ* reporter gene was caused by random mutation in yeast or a plasmid, the DNA was used together with linearised prey vector to cotransform yeast carrying a bait plasmid. The DNA was also sequenced. Transformants were assayed on plates for β-galactosidase activity as previously and these true positives which produced blue colouration were stocked in glycerol.

2.3.5.2. Selecting strongest Y2H interactors

Y2H was performed and transformants were assayed on plates for β-galactosidase activity, as previously. Transformants which expressed β-galactosidase were assayed in liquid as in Miller et al. (1972) with the following modifications (Miller, 1972). 1 ml of yeast cultured overnight in liquid at 30°C with constant shaking were diluted 3 ml media. After 3 hours A_{600} was measured. If A_{600} was 0.5-1.0, the incubation was stopped. 1 ml of yeast cell culture was centrifuged for 1 min in a table top centrifuge at 14000 rpm. Supernatant was discarded, not disturbing the pellet, followed by adding 400 µl Z buffer (60 mM Na_2HPO_4, 40 mM NaH_2PO_4, 10 mM KCl, 1 mM Mg_2SO_4, 1 mM dithioerythritol, 0.2% (v/v) sarcosyl, pH7) and 100 µl of 4 mg/ml ortho-Nitrophenyl-β-galactoside. Cells were resuspended by pipetting and incubated in a water bath at room temperature for 15 min and then at 30°C until the colour developed. 500 µl of 1 M Na_2CO_3 was added and the solution was spun down for 10 min in a table top centrifuge at 14000 rpm. The A_{420} of the supernatant was measured. The β-galactosidase activity was calculated as A_{420}/A_{600} ratio. The assay

as performed in replicas (usually three) and average of A_{420}/A_{600} was calculated for corresponding yeast clones.

2.4. Techniques of Drosophila cell culture

2.4.1. Culturing and transfecting Drosophila S2 cells

Drosophila S2 cells were cultured in tissue culture flasks at 27°C in Schneider's Drosophila medium (Gibco by Life Technologies) supplemented with 10% Foetal Bovine Serum (FBS) heat inactivated (Gibco by Life Technologies). The cells were split twice a week to 6 x 10^6 cells/ml in 5 ml culture. Cells were transfected with a recombinant expression vector for transient expression studies using Effectene Transfection Reagent kit (Qiagen) and following the manufacturer's instructions.

2.4.2. Coating coverslips with Concanavalin A (ConA)

Glass coverslips (1 mm thick, VWR international) or 35 mm glass bottom Petri dishes (MatTek Corporation) were washed in distilled water, 3 x 5 min, then submerged for 30 min in 0.5M HCl and, next washed with distilled water, 3 x 5 min and then with 100% ethanol for 30 min. The coverslips were allowed to air-dry before dipping them individually in 0.5 mg/ml ConA (Calbiochem) and they were air-dried again. The coverslips were stored at 4°C.

2.4.3. Fixing Drosophila S2 cells

Cells were first adhered to ConA coverslips by incubating a coverslip submerged in 1 ml of 6 x10^5 cells/ml culture at 27°C for 2 hours. After removing the media, and cold methanol fix (90% methanol, 3% formaldehyde, 5mM Na_2CO_3 at pH 9) was applied after chilling it on dry ice. The coverslips were incubated for 15 min at -80°C and 15 min at room temperature. The coverslips were rinsed and stored in washing buffer, PBS-T (0.1% Triton X-100 in PBS: 137mM NaCl, 2.7mM KCl, 10mM Na2HPO4.2H2O, 2mM KH2PO4, pH7.4).

2.4.4. Immunostaining of Drosophila S2 cells

Cells fixed on coverslips coated with ConA were incubated at room temperature for 1 hour in blocking buffer (10% FBS in washing buffer from 2.4.3), followed by

incubation for 1 hour with the primary antibodies in blocking buffer. The coverslips were rinsed and washed 3 x 5 min with PBS-T, followed by 1 hour incubation with secondary antibody solution in blocking buffer. Following rinsing and 3 x 5 min washing with PBS-T, coverlips were incubated for 10 min with 0.4 µg/µl DAPI diluted in PBS-T. The coverslips were then washed twice in PBS-T and once with PBS and mounted on glass slides using mounting medium (2.5% propyl gallate, 85% glycerol).

2.4.5. Adhering Drosophila S2 cells for live imaging

ConA coverslips were submerged in 1 ml of 0.5 x 10^5 cells/ml culture at 25°C and incubated for 2 hours.

2.5. Microscopy techniques

2.5.1. Analysis of fixed Drosophila S2 cells

Following cell fixation and staining, as described, images were taken with an Axioplan 2 microscope (Zeiss) attached to a CCD camera (Hamamatsu) controlled by OpenLab 2.2.1 software (Improvision). To measure Sentin or CLIP-190 signal at the microtubule plus ends, the method was used as described by Dzhindzhev et al. (2005), with the following modifications. The plus end signal was calculated using the formula S–B, where S is the total pixel intensity for a particular plus end signal and B is the total pixel intensity of the local background. The local background signal intensity was measured, of the same size as plus end signal area, at one side of a plus end signal area. Three plus end signals were measured in at least ten separate interphase cells. Measurements were made using OpenLab 2.2.1 (Improvision).

2.5.2. Analysis of live Drosophila S2 cells

Cells were first adhered to Petri dishes (MatTek Corporation) coated with ConA by incubating the dish with 1 ml of 0.5 x 10^6 cells/ml culture at 27°C for 2 hours. Cells were imaged using an Axiovert (Zeiss) spinning disc microscope.

2.6. Protein techniques

2.6.1. Expression of MBP and MBP-DmEB1 recombinant proteins

E. coli bacterial culture (F–, *omp*T, *hsd*S_B (r_B–, m_B–), *dcm*, *gal*, λ(DE3), pLysS, Cm^r**)** carrying pSC23 or pSC22 plasmids (provided by Sara Clohisey) for expression of MBP or MBP-DmEB1 respectively were grown overnight at 37°C in LB medium with 50 µg/ml ampicillin with constant shaking. Following 1:100 dilution, a bacterial culture was grown until OD_{600} was 0.4 – 0.6. To induce protein expression, isopropyl β-D-1-thiogalactopyranoside (IPTG) was added to a final concentration of 1 mM and the culture was grown for additional 4 hours. Bacterial culture was next spun down at 4000 rpm for 10 min and pellets were either processed immediately or stored at -20°C.

2.6.2. Purification of MBP and MBP-DmEB1 recombinant proteins

To lyse the bacteria, a pellet was suspended in 1/10 of the original culture volume in ice cold PBS buffer supplemented with Complete EDTA-free protease inhibitors, 1 mM phenylmethylsulfonyl fluoride, a pinch (picked with the wider end of a 200 µl pipette tip) of lysozyme, 3mM dithiothreitol and 0.5 M EDTA, and mixed well and left on ice for 30 min. The suspension was sonicated in short bursts (5 sec ON, 10 sec OFF) for a total ON-time of 2 min. The lysate was centrifuged at 4°C and 14000rpm in a JA-25.50 rotor of Beckman Avanti-25 centrifuge for 30 min and the supernatant was passed through a 0.2 µm syringe filter. The proteins were affinity purified using 1 ml MBPTrap HP column (GE Healthcare) on ÄKTA system (GE Healthcare) at the flow rate 1 ml/min. The column was equilibrated with five column volumes of the wash buffer (1mM EDTA, 1mM DTT in PBS). One-step elution was applied by injection of ten column volumes of 100% elution buffer (1mM DTT, 10mM maltose in PBS). The elute was collected in 0.5 ml fractions. The proteins were further purified by size exclusion chromatography using 24 ml Superdex 200 10/300 GL column (GE Healthcare) on ÄKTA system (GE Healthcare) at the flow rate 0.5 ml/min. The column was equilibrated with 1.5 column volumes of the buffer (1mM DTT in PBS). One 0.5 ml fraction from the affinity purification containing the protein was injected. 1.5 column volume of 0.5 ml fractions were collected, the

protein peak eluted at 11 ml. Protein purity was assessed by SDS-PAGE using standard methods (Sambrook et al, 1989).

2.7. Affinity measurements by isothermal titration calorimetry (ITC)

ITC experiments were conducted using MicroCal Auto-iTC$_{200}$ (GE Healthcare). All peptides used were commercially synthesised (Eurogentec). They were weighed out as solids and dissolved in 100% DMSO. 1 μM MBP or MBP-DmEB1 was loaded into the cell with 20 μM peptide in the titrating syringe. MBP, MBP-DmEB1 and peptide were analysed in the same buffers (120 mM NaCl, 2.7 mM KCl, 30 mM NaH_2PO_4, 1 nM DTT, 2% DMSO, pH 7.4). The titration experiments were performed at 25°C. MBP or MBP-DmEB1 was titrated with increasing concentrations of a peptide. The resulting heats were integrated using Origin (OriginLab) software by fitting to a single-site binding model provided by the software package. Experiments were done in at least three replicas.

2.8. Drosophila techniques

Standard Drosophila handling techniques were used (Ashburner et al, 2005). Drosophila were grown on standard yeast agar medium (107g agar, 442 brewers yeast, 786g glucose, 714g maize, 57g yeast, 32g nipagin, 32ml propionic acid, 200ml ethanol) at 25°C or 18°C. Drosophila lines used in this work were as follows:

genotype	**source**
w[1118]	Bloomington Stock Centre
y w; Act5C-GAL4/TM6B	Lab stock
w; msps^{A}/TM6C	By A. Brittle and H. Ohkura, unpublished
y w; msps^{P}/TM6C	(Cullen et al, 1999)
w; pKMT138 P[w^{+m}, UAS-GFP-aptamer 37]/TM6C	This work
w; pKMT224 P[w^{+m}, UAS-GFP-aptamer 37dimer]/TM6C	This work
w; pKMT139 P[w^{+m}, UAS-GFP-aptamer Perfect]/TM6C	This work
w; pKMT210 P[w^{+m}, UAS-GFP-aptamer Perfect dimer]/TM6C	This work
w; pKMT217 P[w^{+m}, UAS-GFP-aptamer T14]/TM6C	This work
w; pKMT98 P[w^{+m}, UAS-GFP-aptamer C2]/TM6C	This work

w; pKMT99 P[w^{+m}, UAS-GFP-aptamer C28]/TM6C	This work
w; pKMT23(pAB106) P[w^{+m}, $msps^{E190K}$]/TM6C	This work
w; pKMT23(pAB106) P[w^{+m}, $msps^{E190K}$] $msps^{A}$/TM6C	This work

2.8.1. Generating genetic recombinants

To obtain Drosophila mutants carrying both transgenic *msps[E190K]* and *msps* null mutation at the same third chromosome Drosophila were crossed as depicted on a crossing scheme in Figure 2.1.

2.8.2. Expressing peptide aptamers

Peptide aptamers were expressed in Drosophila by crossing them as described in chapter 4 and 5.

2.8.3. Drosophila temperature shifts

Temperature shift experiments of Drosophila pupae or Drosophila which emerged out of pupae case were performed as described in chapter 5. Young adult Drosophila, after shifting them to restrictive temperature, were monitored daily and their abilities to climb up a vial wall were assessed by tapping vials of mutant and control Drosophila side by side and then allowing the Drosophila to climb up. Drosophila coming from temperature shifts of pupae were dissected out of pupae case, if they had not not emerged themselves, and analysed under the microscope. Drosophila which emerged out of pupae case and could walk were knocked upside-down and their recovery was compared to the control Drosophila.

2.9. Statistics

Statistical analyses were performed as described in chapters 3 and 4 using following websites http://in-silico.net/tools/statistics and http://www.fon.hum.uva.nl/Service/CGI-Inline/HTML/Statistics.html

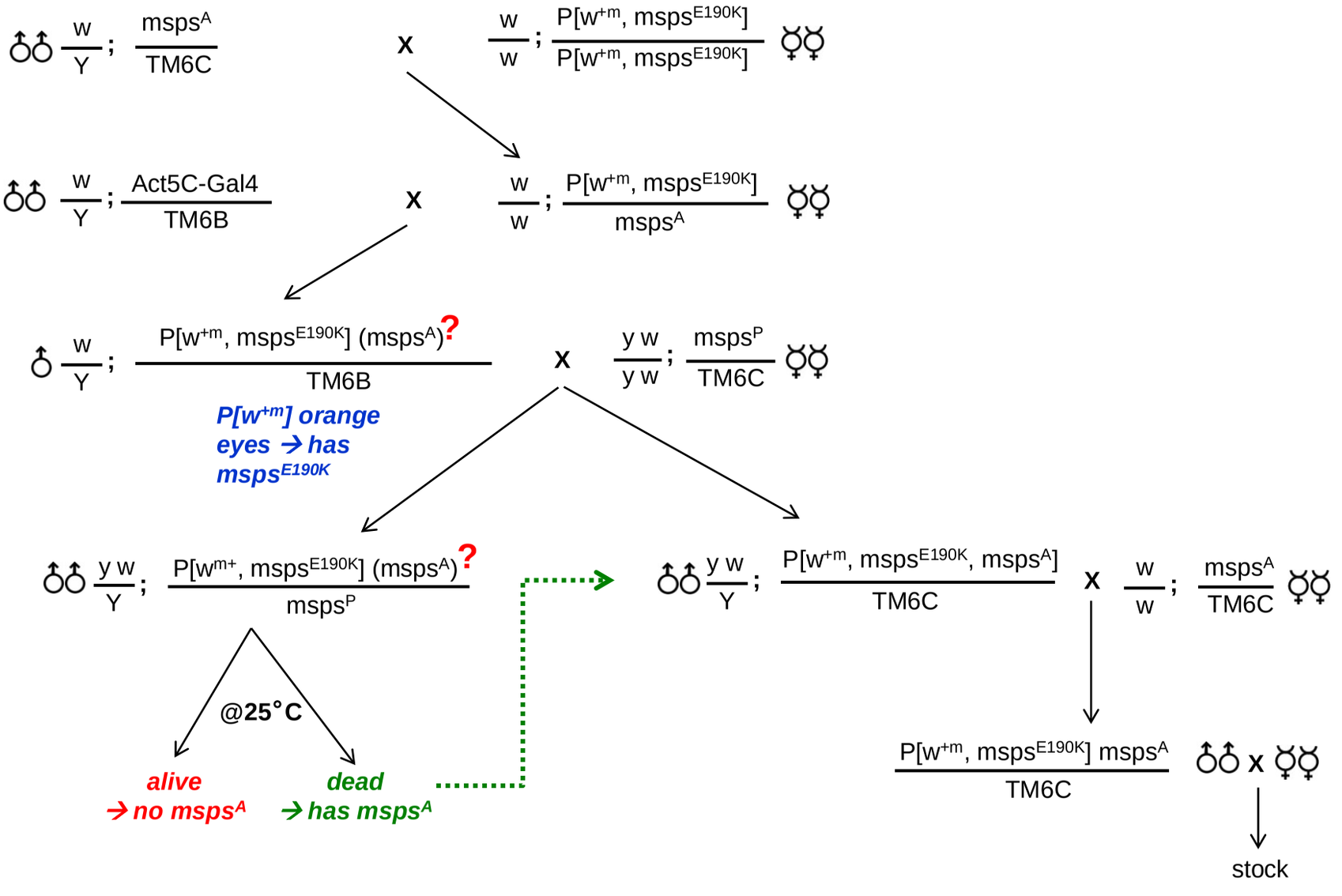

Figure 2.1 Generating genetic recombinants

To obtain Drosophila mutants carrying both transgenic *msps[E190K]* and *msps* null mutation at the same third chromosome, *P[w+m, mspsE190K]* homozygous flies were crossed with *mspsA/TM6C*. Individual male Drosophila with orange eyes resulting from this cross, were crossed with *msps* null mutant Drosophila, *mspsP/TM6C*, and the progeny was tested for viability at 25°C. Drosophila which carried two *msps* null alleels (*mspsA* and *mspsP*), but not the wild-type *msps*, were dead. Siblings of these double mutants were stocked.

CHAPTER 3

Identification of peptide aptamers to EB proteins

3.1. Single constrained peptide aptamers to DmEB1

3.1.1. Making bait plasmid

EB proteins recruit many MAPs to the microtubule plus ends by a consensus Ser-x-Ile-Pro sequence on these MAPs. Since many proteins have SxIP but do not bind to EB1, amino acids in the region surrounding SxIP are likely also involved in the binding. In other words SxIP is required but not sufficient for the binding. I aimed to establish the amino acid determinants in the region flanking SxIP which promote strong binding to DmEB1, by large scale screening for peptide aptamers. I screened a library encoding single constrained peptides, displayed from the C-terminus of GAL4-AD. The single constraint promotes higher conformational variability of peptides making it easier to select singly constrained peptides than the double constrained peptides. The N- and C-terminus of a double constrained peptide is fused to a protein from which it is displayed making this peptide less flexible.

I constructed a bait plasmid containing the DNA encoding full length DmEB1 by inserting the DNA into EcoRI site of Y2H bait vector (pGBT9) by gap repair in yeast on transformation (Figure 3.1). Gap repair relies on homologous recombination between the same sequences on two different DNA fragments. Therefore, to allow insertion into the bait vector by gap repair, sequences of 50 bases upstream and 50 bases downstream of the EcoRI site of the bait vector were added to either end of the DmEB1-coding sequence by PCR through inclusion of the sequences in the primers. A Y2H strain of yeast was transformed with a mixture of the bait vector linearised by EcoRI and the PCR product, and plated on selective media for the bait plasmid.

Next, to confirm that the bait plasmid had a correct insert, yeast transformants were tested by amplifying the insert by PCR. After confirming the correct insert size (~1 kb) on agarose gel, I sequenced this PCR product and confirmed that no mutation was introduced during construction. This transformant was stored in glycerol for future experiments.

3.1.2. Making prey plasmid library

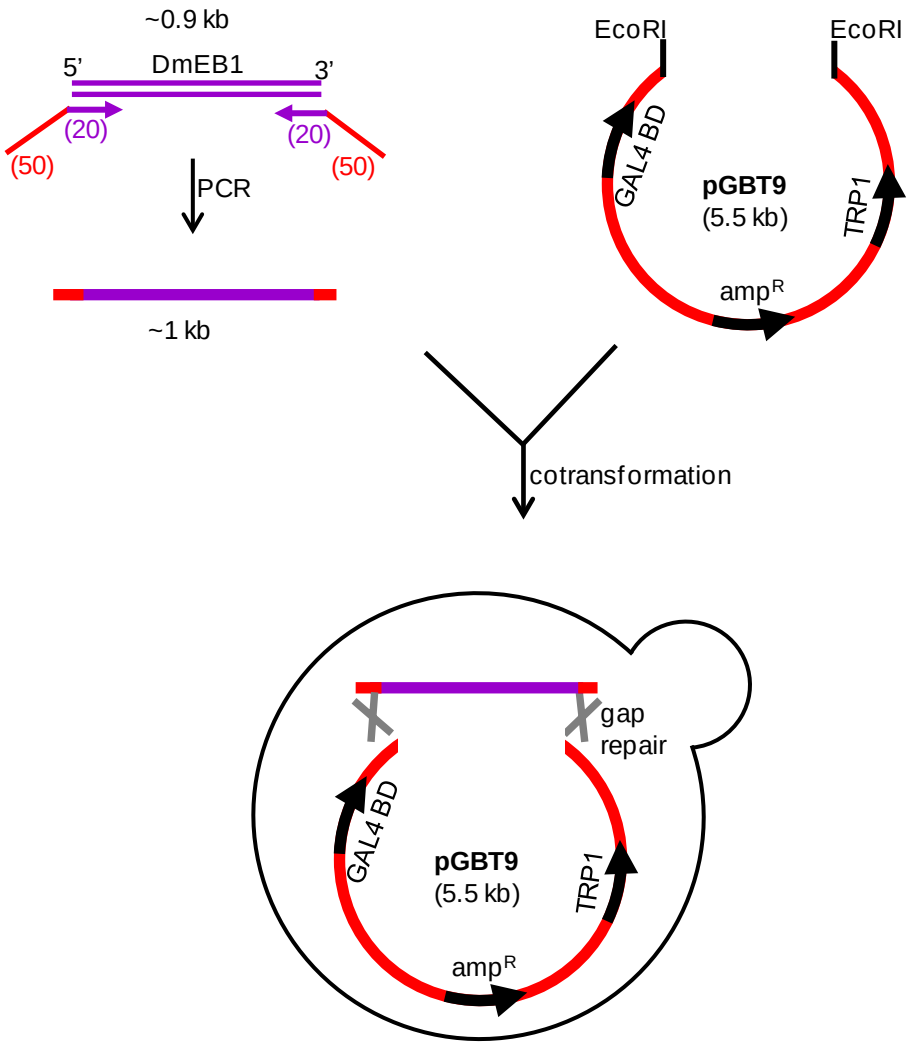

Figure 3.1 Making bait plasmid
To make bait plasmids, ~50 nucleotide fragments complementary to pGBT9 bait vector (red) upstream and downstream of the EcoRI site on pGBT9 were added to DmEB1 (purple) using PCR, by inclusion of these sequences in primers. Yeast (Y190) were cotransformed with the PCR product and pGBT9 vector linearised with EcoRI for inducing the gap repair.

I aimed to find peptide aptamers which bind tightly to the C-terminal EBH domain. To identify these peptide aptamers, after constructing bait plasmid, I next constructed Y2H prey plasmid library. Instead of a library encoding completely random peptides, I fixed codons for SxIP which were preceded by 5 and followed by 7 random amino acids and a stop codon (Figure 3.2). Random amino acids were encoded by NNK codons, where N represents any of the four bases and K represents guanine or thymine. Using NNK reduced bias among the amino acids (for example frequency of codons for arginines was reduced from six to thee) and included a complete set of standard amino acids (Mena & Daugherty, 2005). NNK also allowed to avoid UAA and UGA stop codons. To allow the insertion into a prey vector (pACT2) by gap repair in yeast on transformation, a pool of single-stranded (ss) DNAs was first commercially synthesised. These DNAs contained sequences encoding 16 amino acids and the stop codon flanked by sequence corresponding to the prey vector sequences upstream (48 nucleotides) and downstream (21 nucleotides) of the EcoRI site on the vector. Next, I synthesised complementary strands to the ssDNAs by using a primer partially complementary to 3' end of the ssDNAs and adding further 29 nucleotides complementary to the prey vector sequence by inclusion of the sequence in the primer (Figure 3.2). By performing a single polymerase reaction instead of a PCR, I added the complementary strand. This minimised the likelihood of screening the same sequences multiple times.

To verify the quality of the Y2H prey plasmid library, yeast were cotransformed with the prey vector linearised at EcoRI site and the above DNA encoding the random peptides with fixed SxIP, and plated on media selective for the prey plasmid but not activation of reporters. To test the DNA fragments were inserted into Y2H prey vector by gap repair, the region embracing the insert site on the prey plasmid was amplified by PCR from 11 yeast transformants and sequenced. Six of the 11 prey plasmid library fragments encoded 13 random amino acids and the fixed SxIP motif followed by the stop codon as originally designed (Figure 3.3). Premature stop codons were present in 4 other DNA fragments, but they were located after the codons for SxIP (Figure 3.3). Only 1 out of the 11 DNA fragments did not have an insert (not shown).

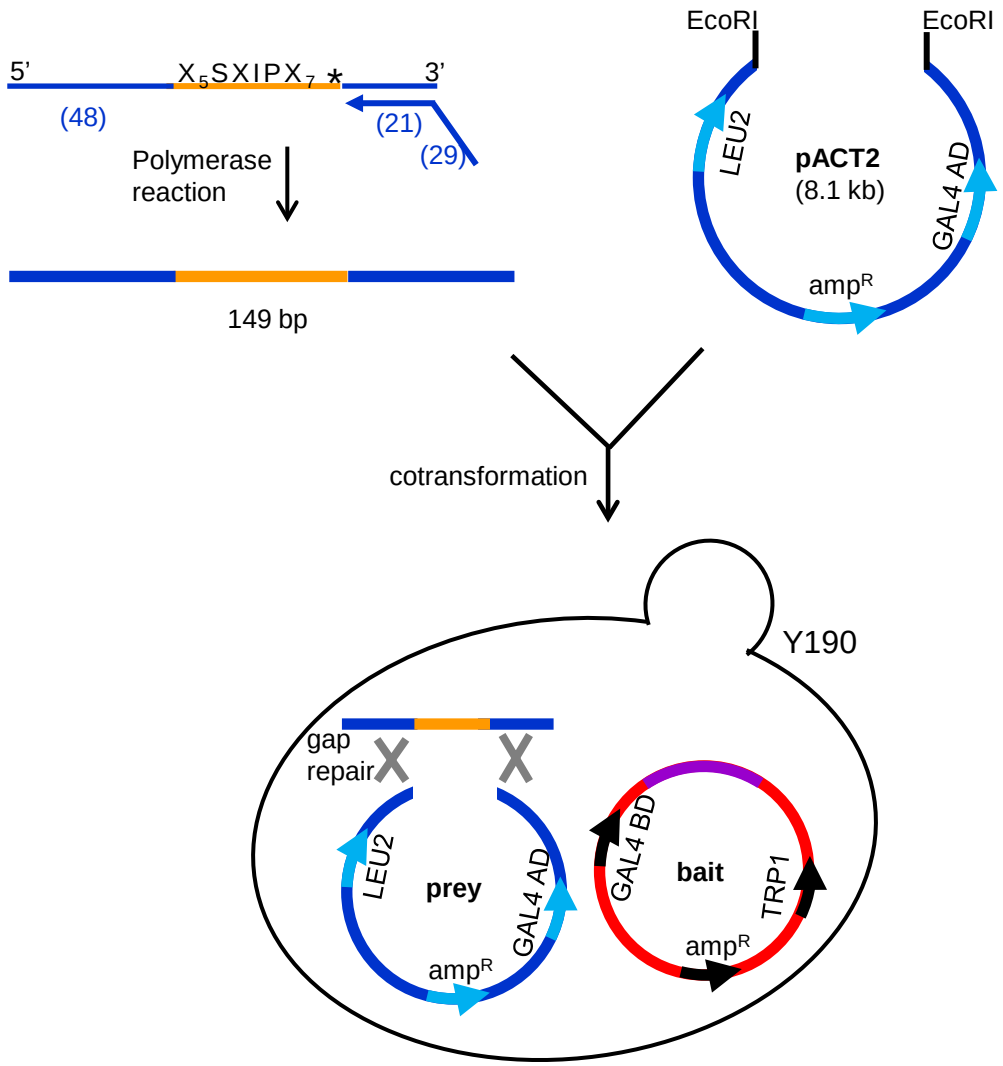

Figure 3.2 Generating prey plasmid library by gap repair.
To make prey plasmid library, oligonucleotide was synthesised whose core region encodes Ser-x-Ile-Pro preceded by 5 and followed by 7 random residues (xxxxxSxIPxxxxxxx), followed by a stop codon (TGA) and flanked by 48 nt at the 5' end and 21 nt at the 3' end, each of which corresponds to the sequence upstream and downstream of the EcoRI restriction site on the prey vector pACT2. A further 29 nt were added to the 3' end through inclusion in a primer during synthesis of the complementary strand. Y190 carrying a bait plasmid was cotransformed with a DNA fragment as above and a prey vector linearised by EcoRI.

```
1  WQYLQSVILGVKI-ASC
2  TRLSFSTIPGHAKPIV-
3  GLLTSSAIPFAGELAQ-
4  PPCIYSNIPDVYG-LR-
5  RRGFLSGIP-LRQGAG-
6  PTRWKSLIPVWWGHIL-
7  LAAGESAIPPTWMQPF-
8  VLCCGSGIPL-RWPLL-
9  SEGE-SGIPLGGVGFE-
10 ERGRVSSIPCHRFLRG-
```
(* * *)

Figure 3.3 The amino acid sequences encoded by unselected clones from the prey SxIP library

Yeast were cotransformed with linearised prey vector and DNA encoding random peptides with fixed SxIP flanked by sequences corresponding to fragments of 5' and 3' on linearised prey vector for gap repair. Transformants were plated on media selective for the prey plasmid but not activation of reporters. The region embracing the insert site on the prey plasmid was amplified by PCR from 10 clones picked at random and sequenced. Fixed SxIP motif is denoted with asterisks, bold indicates translated sequence.

To determine whether amino acids encoded in the SxIP prey plasmid library occurred at random at each position a further 39 transformants were sequenced. The sequences were a heterogeneous mixture of nucleotides (Figure 3.4). The encoded peptides appeared to be composed of amino acid mixture without any amino acids dominating and each of the peptides was unique (Figure 3.5). To verify whether the occurrence of amino acids at subsequent positions encoded in the SxIP library was random, a chi-squared test was performed. The amino acid occurrence at each position was scored for ~40 peptides and compared to the expected number of each amino acid, which was calculated taking into account the number of codons by which each of the amino acids can be encoded using NNK. The amino acids occurrence at all 13 positions was random ($p > 0.01$) (Figure 3.6).

Since 91% of the peptide fragments contained SxIP and amino acids were encoded at random at the subsequent positions within the SxIP library, I concluded that the library was of a good quality.

3.1.3. Optimizing screening conditions and screening the prey plasmid library

Before performing Y2H screen on a large scale, I optimised the conditions of yeast transformation with the SxIP library. A number of small scale yeast transformations were performed altering the amounts of the linearised prey vector and the SxIP library fragments. The optimal amounts of the linearised vector and the fragments to transform 5 ml of 1-2 x 10^7 cells/ml yeast were 0.5 µg of each.

Then, I optimised the concentration of 3-AT, an inhibitor of histidine biosynthesis, for selection of interactors. Increased level of a reporter expression, *HIS3*, required for yeast to survive on 3-AT reduced the background growth allowing to select bait-prey plasmid interactors. I cotransformed yeast carrying DmEB1 bait plasmid with linearised prey vector and the SxIP library and plated on media containing 10, 20, 25, 30, 35, 40 and 50 mM 3-AT. Growth of these transformed yeast was severely inhibited when plated on media containing ≥20 mM 3-AT. I concluded that 3-AT concentration as low as 20 mM was enough to suppress growth of yeast expressing background levels of *HIS3*.

To perform the large scale Y2H screen, 50 µg of each the linearised prey vector and the SxIP library fragments were used to transform 500 ml of 1-2 x 10^7

Figure 3.4 The composition of the unselected SxIP prey plasmid library
The DNA sequences of random unselected clones from SxIP prey plasmid library were obtained by sequencing. The sequences were a heterogeneous mixture of nucleotides. K = G/T, n = A/T/C/G

```
          * **
1   ELYTWSWIPSDVCGVA-
2   FMQSRSGIPEMVRGLG-
3   GSWCGSIIPMVRLAQG-
4   AGRIGSTIPRQLHVDH-
5   TETQNSSIPALWRWLS-
6   QLALVSAIPSVSLYKL-
7   VVRAVSVIPLWGQGGG-
8   RRMHPSSIPQRVDWAR-
9   S-SLLSRIP-MPERGC-
10  GLHVFSKIPLHVMTRV-
11  LKASLSNIPRLRVQTR-
12  RFLSQSNIPMLSLSCI-
13  GLGLGSAIPLVDRDGA-
14  IGRTSSGIPPCPYRSG-
15  RVSIGSMITNCFTSHD-
16  WELLGSSIPWYPFTYR-
17  SPSGRSRIPGADMGRF-
18  GRPGASAIPCRYRRE--
19  LCCSLSWIP-FGEVYQ-
20  GWLR-SSIPQLGGNCS-
21  GMCWLSGIPVGLGGLK-
22  SRLCASLIPDL-EMRS-
23  PR-RTSCIPTACLERY-
24  CGAGYS-IPSRSG-FQ-
25  GVLVVSDIPRVTPHQG-
26  QYGSISWIPMRGGYDC-
27  GVLNPSCIPGRSVGSA-
28  QEVDGSGIPTAAHWVI-
29  IRWTSSIIPAVRLIKL-
30  PRSAVSEIPSTCWAI--
31  RPCRWSGTP--SVNAQ-
32  R-SYQSIIPE--RWRS-
33  LRYSWSGIPWVRGLLE-
34  SLAWRSRIPKGRSIPVG
35  YSGE-S-IPLKLVCTIV
36  WDAMGSSIPWR-HAAF-
37  QCWCYSWIPGVVRGPTC
38  RLLRGSHIP-KWCGTV-
39  PCV-GSRIPHSRVDSR-
```

Figure 3.5 Amino acid sequences of peptides encoded in SxIP prey plasmid library
Yeast were cotransformed with linearised prey vector and DNA encoding random peptides with fixed SxIP flanked by sequences corresponding to fragments of 5' and 3' on linearised prey vector for gap repair. Transformants were plated on media selective for the prey plasmid but not activation of reporters. The region embracing the insert site on the prey plasmid was amplified by PCR from clones picked at random and sequenced. Fixed SxIP motif is denoted with asterisks, bold indicates translated sequence.

	position																	Average amino acid occurrence	
	-5	-4	-3	-2	-1	S	x	I	P	+1	+2	+3	+4	+5	+6	+7	+8	observed	expected
Ala	1	0	5	2	2	0	3	0	0	2	3	1	0	3	3	3	0	2.15	2.44
Arg	6	7	3	4	3	0	4	0	0	3	6	6	6	3	5	4	0	4.62	3.66
Asn	0	0	0	1	1	0	2	0	0	1	0	0	0	2	0	0	0	0.54	1.22
Asp	0	1	0	1	0	0	1	0	0	1	1	2	1	2	2	1	0	1.00	1.22
Cys	1	3	3	3	0	0	2	0	0	1	2	2	2	1	2	2	1	1.92	1.22
Glu	1	3	0	1	0	0	1	0	0	2	0	0	3	1	1	1	0	1.08	1.22
Gln	4	0	1	1	2	0	0	0	0	2	1	0	1	1	2	3	0	1.38	1.22
Gly	8	3	3	3	9	0	6	0	0	3	2	4	5	8	3	5	1	4.85	2.44
His	0	0	1	1	0	0	1	0	0	1	1	0	3	1	1	1	0	0.85	1.22
Ile	2	0	0	2	1	0	3	38	0	0	0	0	0	2	1	3	0	1.08	1.22
Leu	3	6	7	4	4	0	1	0	0	4	5	3	5	1	4	2	0	3.77	3.66
Lys	0	1	0	0	0	0	1	0	0	1	2	0	0	0	2	1	0	0.62	1.22
Met	0	2	1	1	0	0	1	0	0	3	2	0	2	1	0	0	0	1.00	1.22
Phe	1	1	0	0	1	0	0	0	0	0	1	1	1	0	1	2	0	0.69	1.22
Pro	3	2	1	0	2	0	0	0	38	1	0	3	1	0	2	0	0	1.15	2.44
Ser	4	2	5	6	2	39	5	0	0	4	1	5	1	2	3	4	0	3.38	3.66
Thr	1	0	1	3	1	0	1	1	1	2	1	1	1	2	3	1	0	1.54	2.44
Trp	2	1	3	2	3	0	4	0	0	3	1	2	1	4	0	0	0	2.00	1.22
Val	1	4	2	2	4	0	1	0	0	1	7	5	5	2	2	3	1	3.08	2.44
Tyr	1	1	2	1	2	0	0	0	0	0	1	1	1	2	2	1	0	1.15	1.22
*	0	2	1	1	2	0	2	0	0	4	2	3	0	1	0	1	36	1.46	1.22
Different from expected	±	-	-	-	±	n/a	-	n/a	n/a	-	-	-	-	-	-	±	n/a		

Figure 3.6 The frequencies of amino acids at each position encoded by unselected prey plasmid clones from SxIP library.
Yeast carrying DmEB1 bait were cotransformed with SxIP prey plasmid library and plated on non-selective media. Prey plasmid inserts of randomly picked clones were sequenced and occurrence of amino acids at subsequent positions in these sequences was scored. The observed amino acid occurrence excludes the fixed amino acids (shadowed). Each position was tested using chi-squared test for statistical differences from the frequency expected from random DNA sequences. No significant differences were observed. "–", $p \geq 0.05$. "±", $0.01 \leq p < 0.05$.

cells/ml yeast. The transformants were plated on media with 20 mM 3-AT and clones which grew on the media were further patched on the minimal media and overlaid with X-galactose to test expression from the second reporter gene, *lacZ*. Blue colouration indicated expression from the *lacZ* reporter gene.

To estimate how many peptides I screened during one round of the large scale transformation, I plated onto histidine containing media an aliquot of yeast transformed with linearised prey vector and the SxIP library, and an aliquot of yeast transformed with the linearised prey vector only. I estimated that I screened between 0.5 and 1 million peptides encoded on the SxIP prey plasmid library in each transformation.

In total I screened ~5 million peptides and I found ~500 transformants which grew on 3-AT media and turned blue when overlaid with X-galactose indicating both reporter genes were activated.

3.1.4. Certain amino acid residues flanking SxIP promote peptide binding to DmEB1

I aimed to find amino acids in region flanking SxIP which promote binding to DmEB1. DNA encoding the SxIP-containing peptides was amplified and sequenced from 45 yeast transformants found in Y2H screen which activated both reporters. It appeared that the encoded peptides were rich in arginine and the occurrence of some of the amino acids was not random at certain positions (Figure 3.7 and 3.8).

To test whether the occurrence of particular amino acids at certain positions in the vicinity to SxIP was significantly different in selected peptides than unselected peptides, chi-squared test was performed. I scored an amino acid occurrence at each position encoded by the 45 sequenced DNA fragments and compared them with the amino acids scored for the 39 peptides from the unselected SxIP library (unselected peptides) (Figure 3.8). Since occurrence of amino acids Lys and Arg at -5, Thr at -4, Arg and Phe at -2, Arg and Val at -1, Arg and Lys at x, Arg and Val at +1, Trp at +2, Val at +3, Gly at +4, Arg at +5 and Gly at +7 was significantly different in selected than unselected peptides ($p < 0.01$), I concluded that these amino acids promote binding of the SxIP-containing peptides to DmEB1 (Figure 3.9).

	position																	Average amino acid occurrence	
	-5	-4	-3	-2	-1	S	x	I	P	+1	+2	+3	+4	+5	+6	+7	+8	observed	expected
Ala	4	6	1	4	1	0	0	0	1	0	0	1	3	5	0	0	0	2.00	2.81
Arg	14	5	10	8	17	0	29	0	0	26	6	12	6	13	10	5	0	12.38	4.22
Asn	1	3	2	0	1	0	0	0	0	0	0	0	2	2	3	0	0	1.08	1.41
Asp	0	0	0	0	0	0	0	0	0	0	1	0	0	1	0	1	0	0.23	1.41
Cys	0	1	5	0	0	0	0	0	0	0	0	3	0	1	2	0	1	1.00	1.41
Glu	1	2	0	0	0	0	0	0	0	0	0	0	1	1	3	0	0	0.62	1.41
Gln	2	1	0	2	2	0	0	0	1	0	0	2	1	0	1	1	0	1.00	1.41
Gly	3	6	5	8	2	0	1	0	0	0	1	3	24	4	6	14	1	6.00	2.81
His	1	0	0	2	0	0	0	0	0	0	0	0	0	1	1	0	0	0.38	1.41
Ile	1	2	0	0	0	0	0	44	0	2	0	2	0	0	0	0	0	0.54	1.41
Leu	3	0	1	1	1	0	7	0	0	0	4	4	2	1	2	3	3	2.46	4.22
Lys	6	1	3	2	5	0	7	0	0	2	0	3	1	0	2	2	0	2.62	1.41
Met	0	1	2	1	0	0	0	0	0	0	2	0	0	1	1	1	0	0.69	1.41
Phe	1	1	2	4	0	0	0	1	0	0	1	1	0	0	0	1	0	0.92	1.41
Pro	1	4	2	0	3	0	0	0	43	1	1	0	0	1	2	2	0	1.31	2.81
Ser	4	0	4	4	1	45	1	0	0	2	0	0	2	3	4	8	0	2.54	4.22
Thr	0	6	1	0	2	0	0	0	0	0	0	3	1	0	1	2	0	1.23	2.81
Trp	0	4	0	4	0	0	0	0	0	0	26	0	0	6	1	2	0	3.31	1.41
Val	3	1	7	3	9	0	0	0	0	12	0	11	2	3	4	2	2	4.54	2.81
Tyr	0	1	0	2	0	0	0	0	0	0	3	0	0	0	0	1	0	0.54	1.41
*	0	0	0	0	1	0	0	0	0	0	0	0	0	2	2	0	38	0.38	1.41
Different from expected	+	±	+	+	+	n/a	+	n/a	n/a	+	+	+	+	+	-	+	n/a		

Figure 3.7 The frequency of amino acids at each position encoded by prey plasmid clones selected from SxIP library interacting with DmEB1 bait.

Yeast carrying DmEB1 bait were cotransformed with SxIP prey plasmid library and selected for bait-prey interaction. Prey plasmid inserts were sequenced and occurrence of amino acids at subsequent positions in these sequences was scored. The observed amino acid occurrence excludes the fixed amino acids (shadowed). Each position was tested using chi-squared test for statistical differences from the frequency expected from random DNA sequences. Occurrence of amino acids at most positions (except +7) was not random. "+", $p \leq 0.01$, "±"; $0.01 < p < 0.05$, "-"; $p \geq 0.05$.

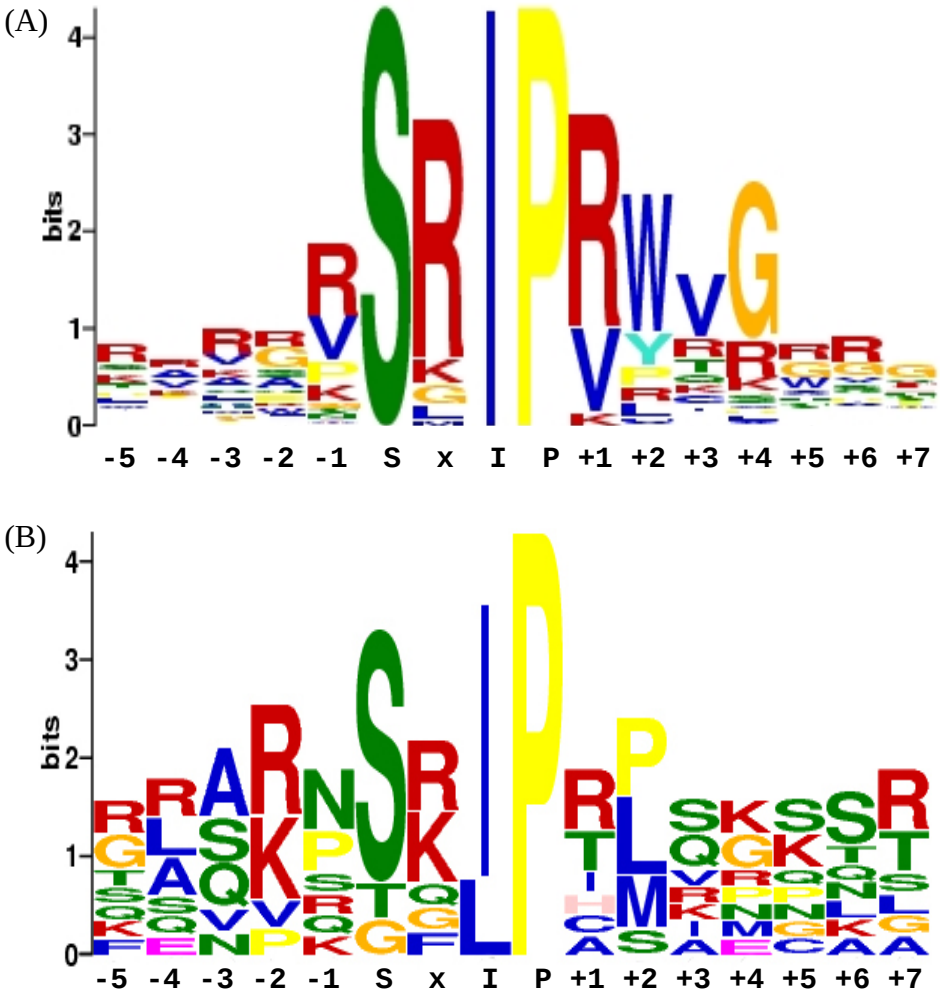

Figure 3.8 Sequence bias within SxIP motif and flanking region promoting binding to EB1

(A) Amino acids of peptide aptamers selected from SxIP library for interaction with DmEB1. Peptide aptamers selected from SxIP library revealed that some amino acids flanking SxIP are overrepresented and promote interaction with DmEB1. (B) EB1-recruited +TIPs that contain confirmed SxIP motifs. SxIP sequence logo was derived from an alignment of SxIP motifs of known SxIP proteins (accession numbers: Q7Z460, O75122, Q9UPN3-2, P25054, Q13586, Q99661, Q86Y91, Q9P270, Q9VUA5, Q96SN8, Q9VQ69, P38991) from *D. melanogaster*, *S. cerevisiae* and *H. sapiens*.

The total height of each stack indicates the "information content" at that position (measured in bits). The height of symbols within the stack reflects the relative frequency of the corresponding amino acid at that position. The subsequent positions within the sequences are labeled -5 to +7. The figures were generated using www.meme.nbcr.net server by submitting 16 amino acid long sequences in fasta format.

Position	-5	-4	-3	-2	-1	S	x	I	P	+1	+2	+3	+4	+5	+6	+7
amino acid letter code	R K	T A G R	R V	F A R G W S	R V		R K L			R V	W R	V R	G R	R W	R G	G S

Figure 3.9 Amino acids promoting binding of peptide aptamers to DmEB1
Peptides interacting with DmEB1 were selected from SxIP prey plasmid library in Y2H. Occurrence of amino acids at subsequent positions (-5 to +7) in these peptide aptamers was scored. The frequencies of amino acids at each position were compared between these peptide aptamers and peptides from SxIP prey plasmid library not selected for DmEB1 binding. Some amino acids occurred more frequently in peptide aptamers than in unselected peptides ($p < 0.01$) and are marked with yellow background. Amino acids occurring most frequently in peptide aptamers to DmEB1 are presented.

3.1.5. Designing an artificial peptide aptamer to DmEB1

By large scale screening of peptides for binding to DmEB1 combined with statistical analysis of occurrence of each of the amino acids at subsequent positions, I revealed that some of the amino acid residues promote binding to DmEB1. I aimed to find out whether a peptide made by combining these amino acids which promote binding to DmEB1 into one sequence of, what I called, an "aptamer Perfect" would bind to DmEB1 (Figure 3.9).

I tested DmEB1 interaction with aptamer Perfect by Y2H. DNA encoding aptamer Perfect, flanked by sequence allowing for gap repair with prey vector, was commercially synthesised. I cotransformed yeast containing DmEB1 bait plasmid with linearised prey vector and DNA encoding the aptamer Perfect and plated on selective media. Overlay of the transformants with X-galactose turned them blue, indicating that the clones activated expression from the *lacZ* reporter gene. Correct DNA construct and sequence encoding the aptamer Perfect was confirmed by PCR and sequencing.

To exclude the possibility that a spontaneous mutation in the prey plasmid or yeast caused reporter gene activation, I amplified the DNA encoding aptamer Perfect and the flanking sequences from a transformant. Yeast with DmEB1 bait plasmid were cotransformed with the amplified DNA and linearised prey vector and overlaid with X-galactose. Blue colouration was observed, so I concluded that presence of DNA encoding the aptamer Perfect, not a spontaneous mutation in plasmid or yeast, caused expression from the *lacZ*.

3.1.6. Identifying strongest single constrained peptide aptamers to DmEB1

In Y2H assay, the strength of protein interaction correlates with reporter gene expression levels. I aimed to categorise the strength of interaction by assessing expression levels from the *lacZ* on plate. As a positive control of strong bait-prey plasmid interaction, I used yeast transformed with bait and prey plasmid carrying *S. cerevisiae SPO13* and *S. pombe plo1+* genes which are known to have high affinity for each other (personal communication, Hiro Ohkura). This yeast patch gave a very dark blue colouration when overlaid with X-galactose. For negative control, I transformed yeast with a bait plasmid and an empty prey vector. Since the prey

plasmid had no insert, I expected no specific expression from the reporter gene. Indeed, yeast overlaid with X-galactose remained white.

I aimed to roughly categorise the yeast clones into three groups producing light, medium or dark blue colouration. The clones selected in Y2H screen were patched along with the negative and the positive controls on the same plate. Yeast were allowed to grow and were next overlaid with X-galactose. Examining all the yeast patches simultaneously allowed for more accurate comparison of the colour intensity between the patches allowing for the clone categorisation. However, this classification was based on visual examination rather than quantification. A yeast patch could have given a darker colouration if it was represented by a bigger number of yeast in a patch. Also, I was not able to discriminate between many of the clones within each of the three groups. I concluded that this method was good enough to get a general idea of how strongly each of the clones interacted with DmEB1 but it was not good enough to get a better insight and that a quantitative method was required.

A more quantitative assay has been developed to measure expression from the *lacZ* reporter gene. In this assay β-galactosidase cleaved o-nitrophenyl-β-D-galactoside (ONPG) to yield galactose and o-nitrophenol (ONP). When ONPG is in excess over the enzyme in a reaction, the production of ONP per unit time is proportional to the concentration of β-galactosidase (Estojak et al, 1995). To quantitatively assay β-galactosidase activity, yeast found in Y2H screen were first cultured in liquid media. Absorbance of each of the yeast cultures at 600 nm (A_{600}) was measured to determine yeast cell density. Then yeast cells were permeabilised to release the β-galactosidase and incubated with ONPG. The A_{420} was measured after the cell debris were removed. The ratio of A_{420}, which is proportional to concentration of ONP, and A_{600}, which reflects the yeast cell density used in the assay, gives an indication of the amount of the β-galactosidase per cell.

The assay was performed for 281 out of 472 the yeast clones found in Y2H screen as well as the yeast transformant for the aptamer Perfect in batches of up to 50 clones and in three independent replicas. For the negative control, yeast transformant containing DmEB1 bait plasmid and the empty prey vector was used. To compare between the batches, I included three aptamers, 155, 172 and 188, to all assays. These three clones were chosen because they appeared in the first experiment and

they were all giving similar absorbance readings. Average of the A_{420}/A_{600} from three experiments for each yeast clone was calculated. Between 5 and 10 clones from each batch which gave the highest A_{420}/A_{600} (a total of 51 clones) were further assessed together (Figure 3.10). The transformant expressing aptamer Perfect gave one of the highest A_{420}/A_{600} (Figure 3.10). Thus the amino acids at subsequent positions which were each shown to promote binding to DmEB1, also promote strong binding when they act in concert. Twelve transformants with the highest A_{420}/A_{600} were further analysed.

3.1.7. Confirming interaction with DmEB1

I aimed to exclude a possibility that expression from the *lacZ* reporter gene in the transformants found in the Y2H was caused by a spontaneous mutation in plasmid or yeast. Twelve clones were analysed which showed highest β-galactosidase expression in liquid assay (Figure 3.10).

Inserts encoding the variable peptide region of prey plasmids were amplified from yeast transformants. Yeast containing the DmEB1 bait plasmid were cotransformed with these amplified DNAs and linearised prey vector DNA. Yeast from all the transformations expressed from the *lacZ* reporter gene as confirmed quantitatively in liquid assay for β-galactosidase activity. Therefore, a possibility that a spontaneous mutation in yeast or plasmid caused expression from the reporter gene was excluded.

To exclude the possibility of mutations introduced into the DNA inserts during their amplification in PCR, I sequenced them and compared with the sequence of the original plasmid. The corresponding DNA sequences were identical. To rule out the possibility that these peptides encoded on prey plasmids activate expression from the *lacZ* reporter gene by binding to the GAL4 binding domain, rather than binding to DmEB1 fused with the GAL4 binding domain, transformations were performed where yeast carrying empty bait vector were cotransformed with the linearised prey vector DNA and the DNA encoding each of the peptides and plated on selective media. All the transformants overlaid with X-galactose remained white indicating that there was no expression from the reporter gene. I concluded that these

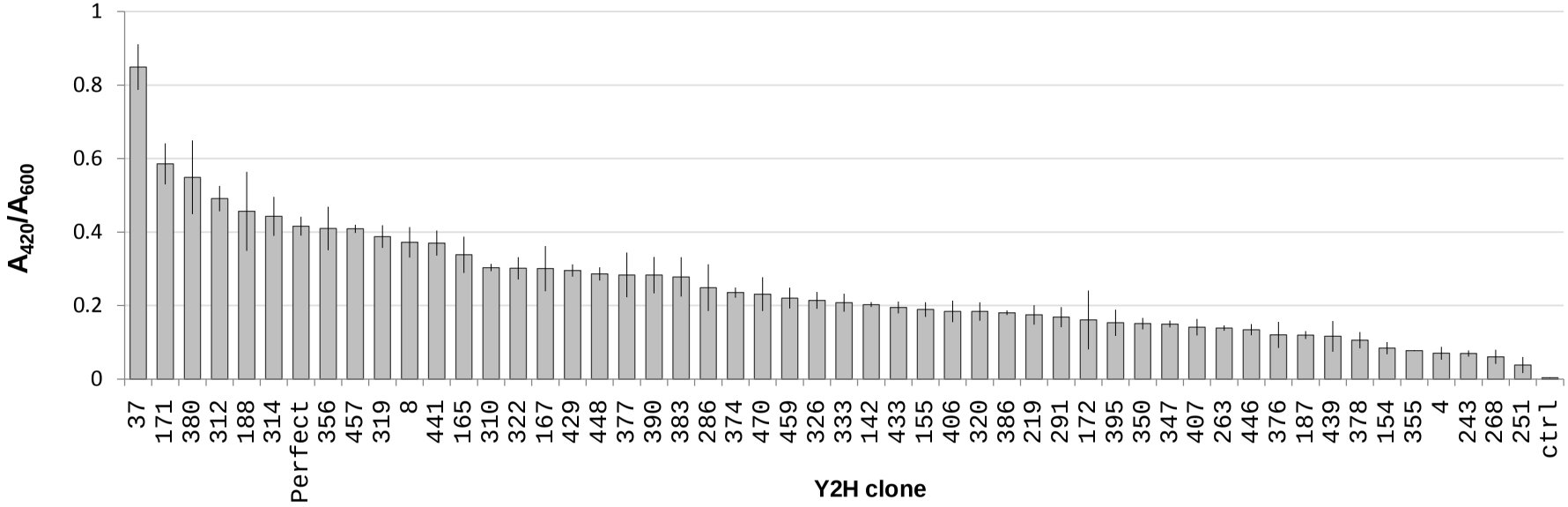

Figure 3.10 Strength of two-hybrid interactions of the strongest aptamers and aptamer Perfect with DmEB1.
The expression of the reporter gene *LacZ* was measured by a quantitative assay for β-galactosidase activity and normalised for the cell density (A_{420}/A_{600}). The empty bait plasmid was used as a control (ctrl). The bars represent standard error of the mean (SEM; n=3), numbers correspond to an SxIP clone.

peptides, hereafter named peptide aptamers, interact with DmEB1 at Y2H level (Figure 3.11).

3.1.8. Aptamer Perfect binds to DmEB1 within nM range

To determine affinity of aptamer 37 or Perfect to DmEB1, I performed ITC experiment. ITC measures heat absorbed or generated when molecules interact to calculate binding constant (K_d) (Turnbull & Daranas, 2003).

Maltose binding protein (MBP) or MBP-DmEB1 were produced in bacteria and purified by affinity chromatography followed by size-exclusion chromatography. Protein purity was assessed by running protein samples on SDS-PAGE (Figure 3.12 A, B). The only protein bands on the gel corresponded to the masses of MBP-EB1 and MBP in the corresponding lanes. Peptides corresponding to aptamer Perfect or a shorter version of aptamer 37 (RCVSRSKIPKLCLSWYLIR) missing seven C-terminal amino acids, were commercially synthesised. The shorter version of aptamer 37 was used because the deleted fragment is unlikely to contribute to interaction with DmEB1 (Buey et al, 2012). A study of an interaction between EB1 and a peptide derived from a MAP and containing SxIP showed that seven amino acids following SxIP are the most critical for the peptide-EB1 binding (Buey et al, 2012). Additionally, deleting a fragment of aptamer 37 which included hydrophobic amino acids may improve the solubility of the peptide improved.

Each of the peptide aptamers dissolved in 100% DMSO was next diluted to obtain the same buffer conditions as those of MBP and MBP-DmEB1 (120 mM NaCl, 2.7 mM KCl, 30 mM NaH_2PO_4, 1 nM DTT, 2% DMSO, pH 7.4) and titrated into solutions of MBP-DmEB1 or MBP for control. Heat changes resulting from the binding reactions were recorded. Also, the buffer alone was titrated into the MBP-DmEB1 or MBP solutions to later subtract the background heat changes generated by titration of the buffer from the heat changes generated by titrating the peptide aptamers in this buffer (Figure 3.13).

As no significant heat change was recorded when titrating aptamer Perfect to MBP solution, I concluded that the peptide aptamer did not interact with MBP (Figure 3.13). However, titrating aptamer Perfect into MBP-DmEB1 caused

Aptamer	Variable region
37	RCVSR*SK*I*PKLCLSWYLIRAREIYES-
171	LQSRRSRIPRWVGCRQ-
380	RSRTRSRIPRWVGFVQ-
312	RRAGKSRIPVAVRQSSCFELERSMNRRY-
188	RWVGVSRIPRWVGWES-
314	GRCRVSRIPRWVGGIK-
Perfect	RTRGRSRIPRWVGRRG-
356	RKRAPSRIPVLKRWPA-
457	PGKYVSKIPVWRGGRM-
319	LKLKRSRIPVPTKVRGDSSSRDL-
8	IKRGRSKIPRWIGDQH-
439	EYRGVSRIPVWKGRGT-
165	ITTRPSLIPRWVGRGG-

Figure 3.11 Strongest single constrained peptide aptamers to DmEB1
Interaction strength of peptide aptamers to DmEB1 was assessed by quantitative assay measuring expression of the reporter gene *LacZ.* Twelve peptide aptamers that proved strongest interaction in Y2H assay were sequenced. Asterisks denote codons for the fixed SxIP motif.

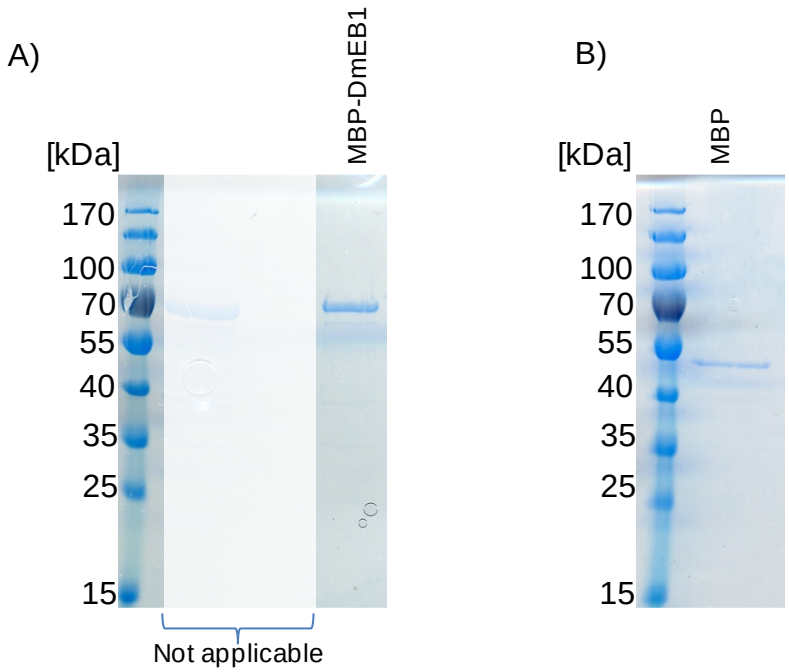

Figure 3.12. SDS-PAGE analysis of MBP-DmEB1 and MBP purification

Cleared bacterial lysate from E. coli containing MBP or MBP-DmEB1 protein was loaded on a MBPTrap HP column (1 ml) for affinity purification and the protein were eluted with 10mM maltose and collected in 0.5 ml fractions. A fraction from the affinity purification containing MBP or MBP-DmEB1 were loaded onto 24 ml Superdex 200 10/300 GL columns for purification by size exclusion chromatography and 1.5 column volume of 0.5 ml fractions were collected. Protein purity was assessed by SDS-PAGE using standard methods. The elution fractions containing the protein peak for (A) MBP-DmEB1 and (B) MBP were visualised on 12% SDS-PAGE gels.

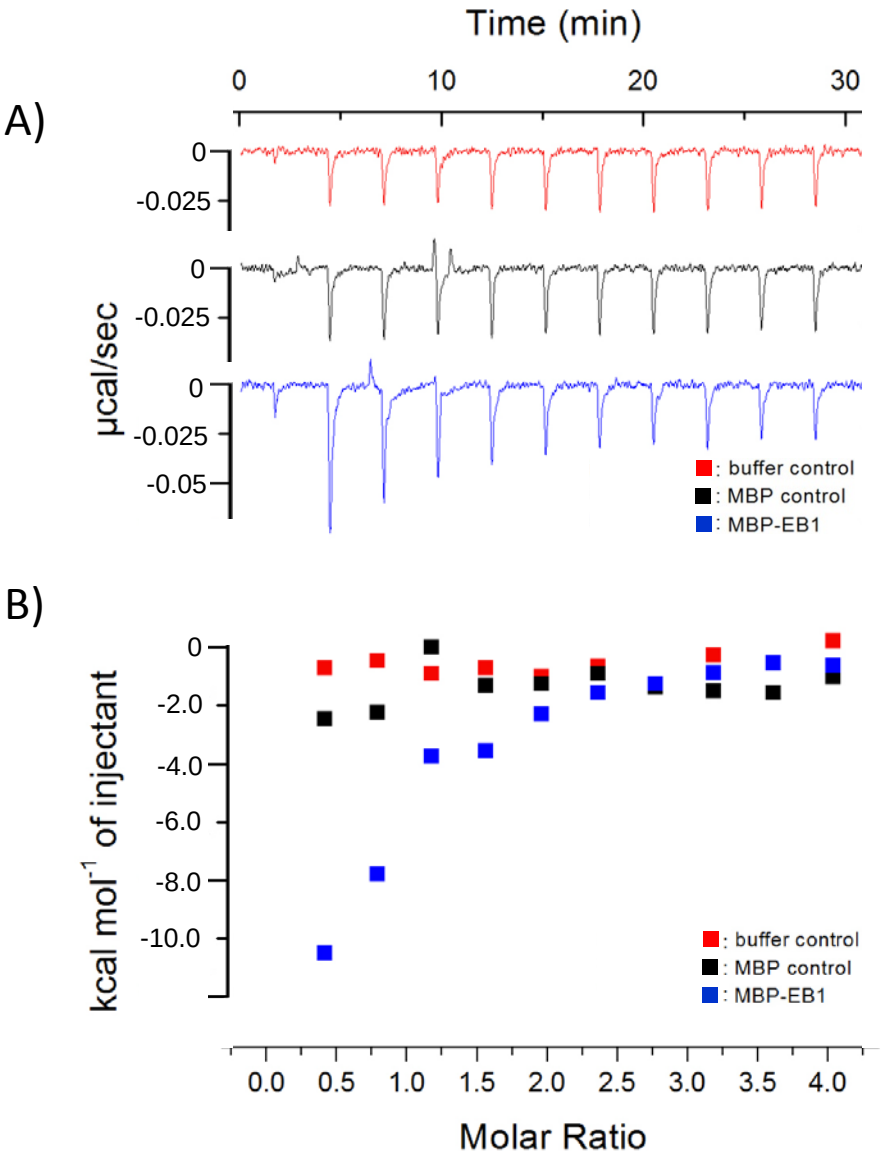

Figure 3.13 Binding of aptamer Perfect to MBP-DmEB1 or MBP
Isothermal titration calorimetry (ITC) shows a high affinity of aptamer Perfect to DmEB1. (A) Raw ITC data showing that aptamer Perfect interacts with MBP-fused DmEB1, but not MBP *in vitro*. Heat released by titrations of 20 µM aptamer Perfect into 1 µM solution of MBP-DmEB1 (blue), MBP (black) and buffer alone (red). Each peak corresponds to one injection. An initial smaller injection was followed by ten injections. For MBP-DmEB1, the heat became smaller for each injection, as the binding site became saturated. For buffer and MBP, it stayed constant, as heat was released only from dilution of the peptide without specific binding. (B) Integrated heat peaks were plotted against the molar ratio of the peptide to MBP-DmEB1.

significant heat changes (Figure 3.14). From these data, K_d of ~300 ± 80 nM was calculated.

Titrating aptamer 37 into MBP-DmEB1 solution resulted in exothermic followed by endothermic spikes indicating that aptamer 37 solubilises only upon injecting it into the solution. To overcome the solubility problem, I reversed the experimental design by injecting concentrated MBP-DmEB1 into a diluted solution of aptamer 37. However, because I did not have enough concentrated MBP-DmEB1 the experiment was not completed.

The C-terminal fragment of human EB1 was shown to bind an APC-derived C-terminal peptide, containing SxIP, with 5 μM affinity (Honnappa et al, 2005). I concluded that affinity of aptamer Perfect to DmEB1 is significantly higher than that of APC to EB1.

3.2. Peptide aptamers to reveal variability within SxIP motif for DmEB1 binding

3.2.1. Some amino acid variations in SxIP are tolerable for DmEB1 binding

Sequence variants of the consensus SxIP have been shown to exist amongst EB1 interactors using this motif for binding to EB1. While proline in the SxIP looks to be invariant, serine is often replaced by threonine and isoleucine by leucine. Lysine and arginine often occupy the "x" position. I aimed to determine what amino acids within the motif promote binding to DmEB1 and whether other variants than Ser/Thr-x-Ile/Leu-Pro are also possible. I performed Y2H as previously described using the prey plasmid library ("XXXX library") encoding the aptamer Perfect where SRIP was substituted by NNK codons for random amino acids (Figure 3.15).

The peptides encoded in the prey plasmid library appeared to have a mixture of amino acids at the four positions encoded by NNK without any of the amino acids dominating (Figure 3.16). All the prey plasmid library fragments encoded the aptamer Perfect where SRIP was substituted with random amino acids at positions X1, X2 and X3, as verified by the statistical analysis (Figure 3.17). P-value for position X4 was < 0.01 indicating that amino acids at X4 in the library were not random, Phe and Leu appeared much more frequently than expected (Figure 3.17).

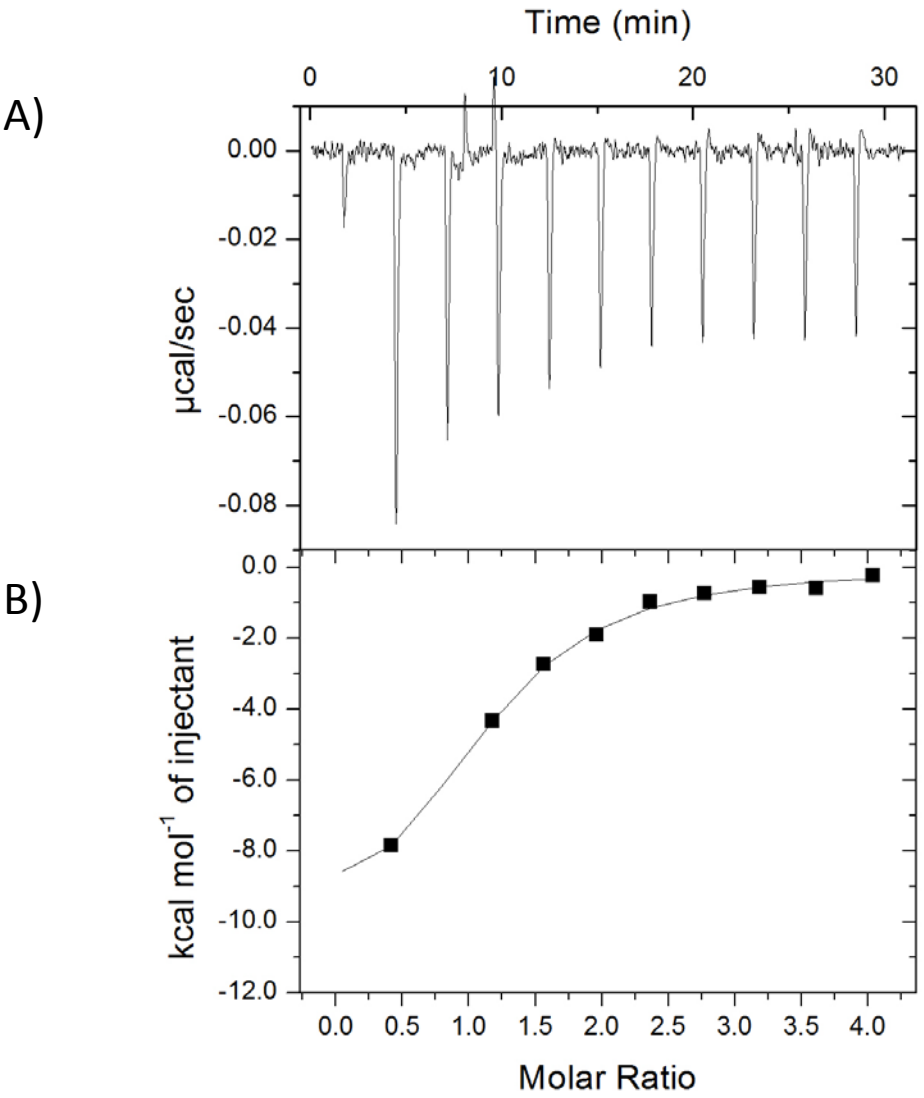

Figure 3.14 Binding of aptamer Perfect to MBP-DmEB1
A) Raw data for titrations of 20 µM aptamer Perfect into 1 µM solution of MBP-DmEB1. Each peak corresponds to one injection. An initial smaller injection was followed by ten injections. Heat released by titrations of 20 µM aptamer Perfect into 1 µM solution of MBP-EB1. Each peak corresponds to one injection. An initial smaller injection was followed by ten injections. The heat became smaller for each injection, as the binding site became saturated. (B) Integration of the data, corrected for the heat of dilution, and plotted against the molar ratio of the peptide to MBP-EB1. The line represents the fit to the single-site binding model generated by the ORIGIN program.

Figure 3.15 Construction of XXXX prey plasmid library

DNA sequence encoding the Perfect peptide (CGAACCCGAGGCCGATCCCGAATTCCACGATGGGTGGGCCGACGAGGCTGA) was used, where the DNA fragment encoding SRIP (TCCCGAATTCCA) was replaced with a fragment encoding four random amino acids (NNKNNKNNKNNK). N = A/T/C/G, K = G/T.

```
    *****     ********
1   RTRGRRWRFRWVGRRG-
2   RTRGRLFCSRWVGRRG-
3   RTRGRSGNFRWVGRRG-
4   RTRGRDLVFRWVGRRG-
5   RTRGR-HAARWVGRRG-
6   RTRGRRGRARWVGRRG-
7   RTRGRLRGCRWVGRRG-
8   RTRGRWPFLRWVGRRG-
9   RTRGRLELPRWVGRRG-
10  RTRGRVEYLRWVGRRG-
11  RTRGRL-LRRWVGRRG-
12  RTRGRR-YFRWVGRRG-
13  RTRGRL-LRRWVGRRG-
14  RTRGRMGRWRWVGRRG-
15  RTRGRLILFRWVGRRG-
16  RTRGR-KMLRWVGRRG-
17  RTRGREWSLRWVGRRG-
```

Figure 3.16 Amino acid sequences of peptides encoded in XXXX prey plasmid library

Yeast were cotransformed with linearised prey vector and DNA encoding XXXX prey plasmid library flanked by sequences corresponding to fragments of 5' and 3' on linearised prey vector for gap repair. Transformants were plated on media selective for the prey plasmid but not activation of reporters. The region embracing the insert site on the prey plasmid was amplified by PCR from clones picked at random and sequenced. Fixed sequence is denoted with asterisks, bold indicates variable sequence.

	Position				Average amino acid occurrence	
	X1	X2	X3	X4	observed	expected
Ala	0	0	1	2	0.75	1.13
Arg	3	1	3	2	2.25	1.69
Asn	0	0	1	0	0.25	0.56
Asp	1	0	1	0	0.25	0.56
Cys	0	0	1	1	0.50	0.56
Glu	1	2	0	0	0.75	0.56
Gln	0	0	0	0	0.00	0.56
Gly	0	3	1	0	1.00	1.13
His	0	1	0	0	0.25	0.56
Ile	0	1	0	0	0.25	0.56
Leu	6	1	4	4	3.75	1.69
Lys	0	1	0	0	0.25	0.56
Met	1	0	1	0	0.50	0.56
Phe	0	1	1	6	2.00	0.56
Pro	1	1	0	1	0.75	1.13
Ser	1	0	1	1	0.75	1.69
Thr	0	1	0	0	0.25	1.13
Trp	1	2	0	1	1.00	0.56
Val	1	0	1	0	0.50	1.13
Tyr	0	0	2	0	0.50	0.56
*	2	3	0	0	1.25	0.56
Different from expected	-	-	-	+		

Figure 3.17 The frequencies of amino acids for each position encoded by unselected prey clones from XXXX library.
Yeast carrying DmEB1 bait were cotransformed with XXXX prey plasmid library and plated on non-selective media. Prey plasmid inserts of randomly picked clones were sequenced and occurrence of amino acids at subsequent positions in these sequences was scored. Each position was tested using chi-squared test for statistical differences from the frequency expected from random DNA sequences. No significant differences were observed for position X1, X2 and X3. Amino acid occurrence on position X4 was not random. "+", $p \leq 0.01$, "-"; $p \geq 0.05$.

Although some amino acid bias can be observed in the library, which could have been caused by some synthesis issues, all the amino acids are represented even though some are rare. A stop codon followed the all the 18 amino acid sequences as designed.

The XXXX library was screened as previously described. I screened ~1 million peptides and found 57 transformants which activated both reporter genes. To analyse the amino acid composition within the fragment encoded by the NNK codons, I sequenced the region including the insertion site on prey plasmids in these 57 transformants. The encoded peptides had the same amino acid sequence apart from the positions encoded by NNK codons, as designed. Amino acids at positions X1, X2, X3 and X4 occurred not at random, as verified by statistical analysis (Figure 3.18).

Notably, Ser/Thr-x-Ile/Leu-Pro are also common amino acids in SxIP of natural DmEB1 interactors. These amino acids were amongst the most frequently occurring at the corresponding positions of DmEB1 interactors selected from the XXXX library. Chi-squared test was performed to analyse whether the occurrence of most frequent amino acids at each of the four positions was significantly different in these peptides selected for DmEB1 binding than in the random peptides encoded in the XXXX library. Since occurrence of amino acids S and T at position X1, Arg and Leu at X2, Ile and Leu at X3 and Pro at X4 was significantly different in selected than unselected peptides ($p < 0.01$), I concluded that these amino acids promote binding of the SxIP proteins to DmEB1 (Figure 3.19). Finding these amino acids, Ser/Thr-x-Ile/Leu-Pro, promoting binding to DmEB1 is consistent with finding these amino acids within SxIP of natural DmEB1 interactors. Interestingly, I additionally found that the most conserved positions X1, X3 and X4 allowed for amino acid variants other than the so far observed Ser/Thr-x-Ile/Leu-Pro in natural protein interactors of EB1. Additionally to the known amino acid variants, Cys and Gly were observed at X1, Arg, Met, Phe, Val at X3 and Ala and Leu at X4 (Figure 3.20 A). Almost all amino acids were found at X2 (Figure 3.20 A).

3.2.2. S-x-I/L-P in SxIP motif promote strong binding to DmEB1

	Position				Average amino acid occurrence	
	X1	X2	X3	X4	observed	expected
Ala	0	1	0	5	1.50	3.56
Arg	0	13	1	0	3.50	5.34
Asn	0	2	0	0	0.50	1.78
Asp	0	2	0	0	0.50	1.78
Cys	4	1	0	0	1.25	1.78
Glu	0	0	0	0	0.00	1.78
Gln	0	0	0	0	0.00	1.78
Gly	3	5	0	0	2.00	3.56
His	0	4	0	0	1.00	1.78
Ile	0	0	32	0	8.00	1.78
Leu	0	10	17	1	7.00	5.34
Lys	0	3	0	0	0.75	1.78
Met	0	4	1	0	1.25	1.78
Phe	0	0	1	0	0.25	1.78
Pro	0	0	0	51	12.75	3.56
Ser	41	2	0	0	10.75	5.34
Thr	9	0	0	0	2.25	3.56
Trp	0	4	0	0	1.00	1.78
Val	0	2	5	0	1.75	3.56
Tyr	0	4	0	0	1.00	1.78
*	0	0	0	0	0.00	1.78
Different from expected	+	+	+	+		

Figure 3.18 The frequency of amino acids at each position encoded by prey plasmid clones selected from XXXX library interacting with DmEB1 bait. Yeast carrying DmEB1 bait were cotransformed with XXXX prey plasmid library and selected for bait-prey interaction. Prey plasmid inserts were sequenced and occurrence of amino acids at subsequent positions in these sequences was scored. Each position was tested using chi-squared test for statistical differences from the frequency expected from random DNA sequences. Occurrence of amino acids at positions X1-X4 was significantly different from expected ($p \leq 0.01$). "+", $p \leq 0.01$, "±"; $0.01 < p < 0.05$, "-"; $p \geq 0.05$.

Position	X1	X2	X3	X4
amino acid letter code	S T	R L S	I L V	P A

Figure 3.19 Amino acids in XXXX region promoting binding of peptide aptamers to DmEB1
Peptides interacting with DmEB1 were selected from XXXX prey plasmid library in Y2H. Occurrence of amino acids at subsequent positions (X1-X4) in these peptide aptamers was scored. The frequencies of amino acids at each position were compared between these peptide aptamers and peptides from XXXX prey plasmid library not selected for DmEB1 binding. Some amino acids occurred more frequently in peptide aptamers than in unselected peptides ($p < 0.01$) and are marked with yellow background. Amino acids occurring most frequently in peptide aptamers to DmEB1 are presented.

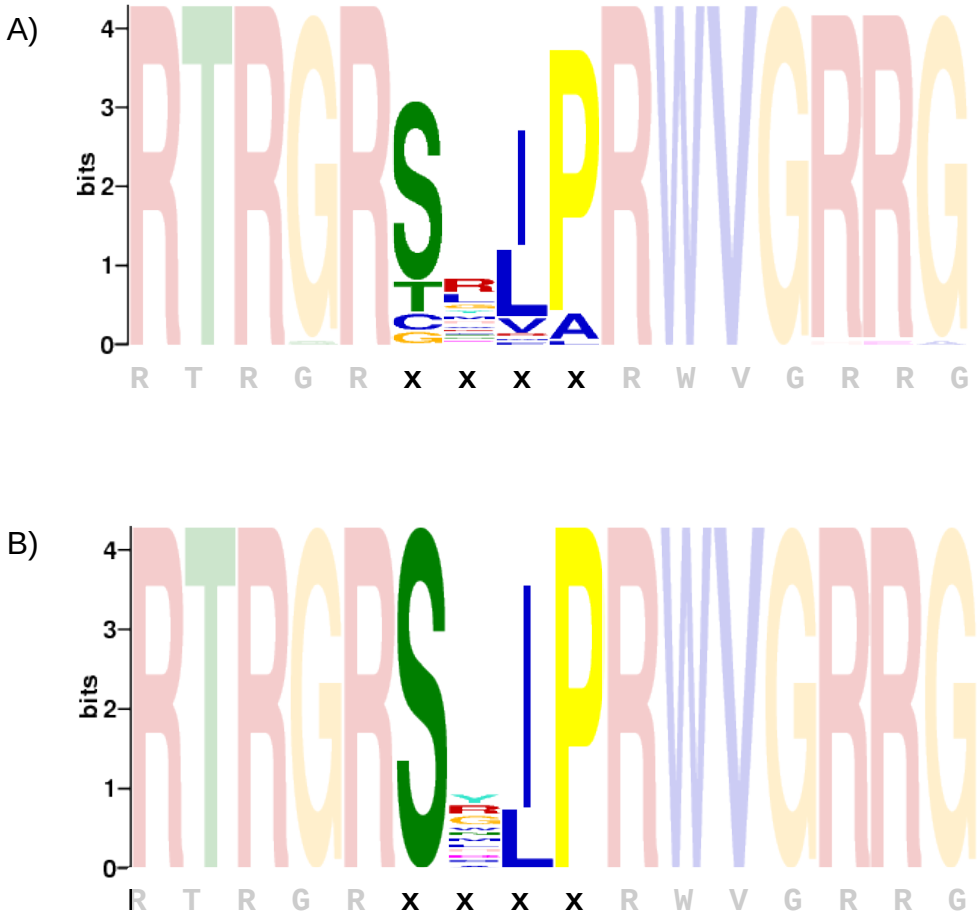

Figure 3.20 Sequence bias within SxIP motif promoting binding to DmEB1

Residues within the SxIP motif overrepresented among interactors showing any interaction with DmEB1 (A) and among the 15 strongest DmEB1 interactors (B) selected from a library based on the aptamer Perfect sequence in which SRIP was replaced with 4 random residues (XXXX library). The total height of each stack indicates the "information content" at that position (measured in bits). The height of symbols within the stack reflects the relative frequency of the corresponding amino acid at that position. The subsequent positions within the sequences are labeled -5 to +7. The figures were generated using www.meme.nbcr.net server by submitting 16 amino acid long sequences in fasta format.

Although some amino acid variation within SxIP is allowed for peptide binding to DmEB1, I investigated which amino acid variants in SxIP promote strong binding by measuring expression from the *lacZ* reporter gene as previously.

The quantitative liquid assay was performed for all 57 the yeast clones found in Y2H screen in three independent replicas. For the negative control, yeast transformant containing DmEB1 bait plasmid and the empty prey vector was used. To compare between the batches, I included aptamer 37 to all assays (Figure 3.21). All of the 15 strongest peptide aptamers invariably have Ser and Pro at positions X1 and X4 respectively and either Ile or Leu at position X3 (Figure 3.20 B). I concluded that these amino acids promote strong binding to DmEB1.

3.3. Improving binding of peptide aptamers to DmEB1

3.3.1. Oligomerising peptide aptamers

Proteins recruited to microtubule plus ends by EB1 often have more than one SxIP motifs. Also, it was shown that a dimerised SxIP motif enhanced MACF, one of EB1 interactors, accumulation at polymerising microtubule plus ends in human cultured cells (Honnappa et al, 2009). Thus, I aimed to design oligomerised aptamer 37 and Perfect.

Since the genes encoding for these oligomers need to express efficiently in both yeast and Drosophila cells, codon usage in these organisms was taken into account when designing genes for the peptide oligomers. Codons which constituted less than 10% of the total codon usage for a particular amino acid in the organisms were not used. To minimise recombination between DNA encoding for each peptide repeat within the genes encoding the oligomers, a combination of various codons was used to encode the same amino acid sequences (Figure 3.22). The gene for the aptamer Perfect oligomer encoded 7 aptamers Perfect separated by Ser-Gly-Ser-Gly (SGSG) linkers (Figure 3.22). Aptamer 37 oligomer was encoded by a gene for 4 aptamers 37 separated by SGSG linkers (Figure 3.22). To allow gap repair, the sequences were further flanked by DNA complementary to the prey vector fragments upstream (115 nucleotides) and downstream (101 nucleotides) of the EcoRI site on

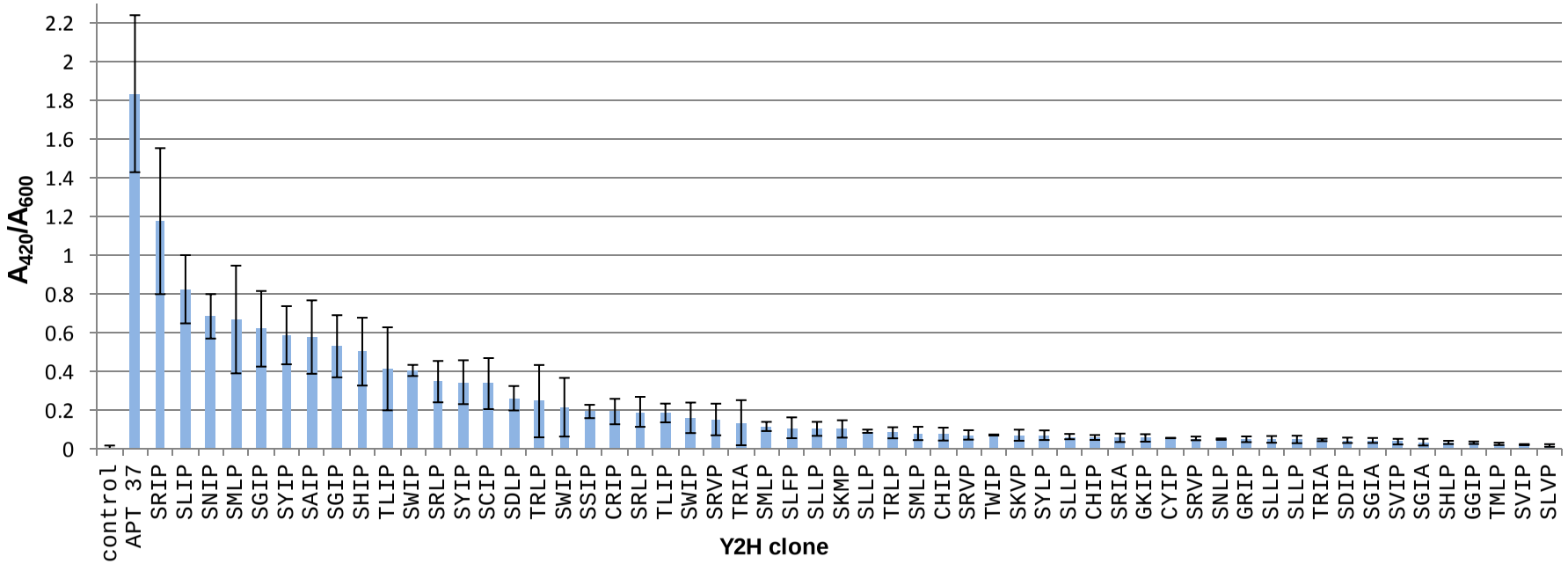

Figure 3.21 Strength of two-hybrid interactions between DmEB1 and aptamers from XXXX library

Y2H interactions between DmEB1 and aptamers from a screen of peptide sequences in which SRIP of aptamer Perfect was replaced with 4 random residues. Strength of Y2H interactions was measured by a quantitative assay for β-galactosidase activity and normalised for the cell density (A_{420}/A_{600}). The assay was performed using three independent cultures. The labels on X axis represent amino acid sequence of the region corresponding to SxIP, error bars are SEM.

A) Tetramer aptamer 37

```
R   C   V   S   R   S   K   I   P   K   L   C   L   S   W   Y   L   I   R   A   R   E   I   Y   E   S   S   G   S   G
cgt tgt gtt tcc cgt tcc aaa att cca aaa ttg tgt ttg tcc tgg tat ttg att cgt gct cgt gaa att tat gaa tcc tcc ggt tcc ggt
agg tgt gtg tcg agg tcg aaa ata cct aaa ctt tgt ctt tcg tgg tat ctt ata agg gca agg gaa ata tat gaa tcg tcg ggc agt ggc
aga tgc gtc agt aga agt aag atc ccc aag ctg tgc ctg agt tgg tac ctg atc aga gcc aga gag atc tac gag agt agt gga tcg gga
cgt tgc gta agc aga agc aag ata ccg aaa ttg tgc ttg agc tgg tac ctt att agg gcg aga gaa att tac gaa agc
```

B) Septamer aptamer Perfect

```
R   T   R   G   R   S   R   I   P   R   W   V   G   R   R   G   S   G   S   G
cgt acg cgt ggt cgt agc cgt att ccg cgt tgg gtg ggt cgt cgt ggt tcc ggt agt ggt
cgt acc aga ggt cgt tcc cgt ata cca cgt tgg gta ggt aga agg ggt agc ggc tcc ggc
aga act aga ggc aga tcg aga atc ccc agg tgg gtc ggc cgt aga ggc agt gga agc gga
aga acg aga ggt aga agc aga atc ccg aga tgg gtg ggc aga aga ggc tcg ggc agc ggt
agg aca agg gga agg agt agg ata cct cgt tgg gtc ggt agg agg gga tcc gga tcg ggc
agg acg cgt ggt agg agc agg att ccg agg tgg gtg gga cgt cgt gga agt ggt tcc gga
cgt act agg ggt aga tcg cgt atc cct aga tgg gta gga aga cgt ggc
```

Figure 3.22 Tetramerised aptamer 37 and septamerised aptamer Perfect

DNA sequences encoding (A) aptamer 37 tetramer and (B) aptamer Perfect septamer. In both cases aptamer repeats were separated by SGSG linkers. To minimise risk of recombination between DNA encoding for each peptide repeat within the genes encoding the oligomers, combination of various codons was used to encode the same amino acid sequences.

the vector. Genes were commercially synthesised and introduced onto ampicillin resistant cloning vectors.

3.3.2. Effect of peptide aptamer oligomerisation on binding to DmEB1

To establish whether the oligomerised aptamers, 37 and Perfect, bind DmEB1 stronger than the monomers, I measured the strength of interaction by Y2H.

The genes encoding the oligomerised peptides along with the flanking sequences upstream and downstream of the EcoRI site on the vector allowing for gap-repair were amplified from the commercially synthesised plasmids. Transformations were performed where yeast carrying DmEB1 bait plasmid were cotransformed with prey vector linearised at EcoRI site and either the amplified 37 tetramer or Perfect septamer DNA, and plated onto selective media for yeast carrying bait and prey plasmids. Sequencing showed that tested transformants with DNA encoding 37 tetramer carried plasmid with the correct sequence, as designed. Although some of the transformants with DNA encoding Perfect septamer carried the correct plasmid, there were also transformants which carried a gene encoding two repeats of aptamer Perfect or a gene encoding four repeats. Thus, the prey plasmid inserts underwent recombination in some of the transformants in yeast. Having these additional oligomers of aptamer Perfect, Perfect dimer and Perfect tetramer, I decided to dimerise peptide 37, too. DNA for 37 dimer was obtained by amplifying a fragment of a gene encoding 37 tetramer and, to allow gap repair, the gene for 37 dimer was flanked by DNA complementary to fragments of prey vector, as previously.

To measure the expression from *lacZ* reporter gene in five transformants carrying prey plasmids with DNA for 37 dimer, 37 tetramer, Perfect dimer, Perfect tetramer and Perfect septamer, activity of β-galactosidase was assessed in liquid as previously described. Transformants carrying the genes encoding aptamer 37, Perfect and empty prey vector were included in the assay for better comparison and control.

A_{420}/A_{600} for Perfect dimer was almost three times higher than that for aptamer Perfect (Figure 3.23). 37 dimer peptide showed almost half A_{420}/A_{600} value compared to aptamer 37 (Figure 3.23). However, Perfect tetramer, Perfect septamer or 37 tetramer only very weakly activated the reporter expression (Figure 3.23).

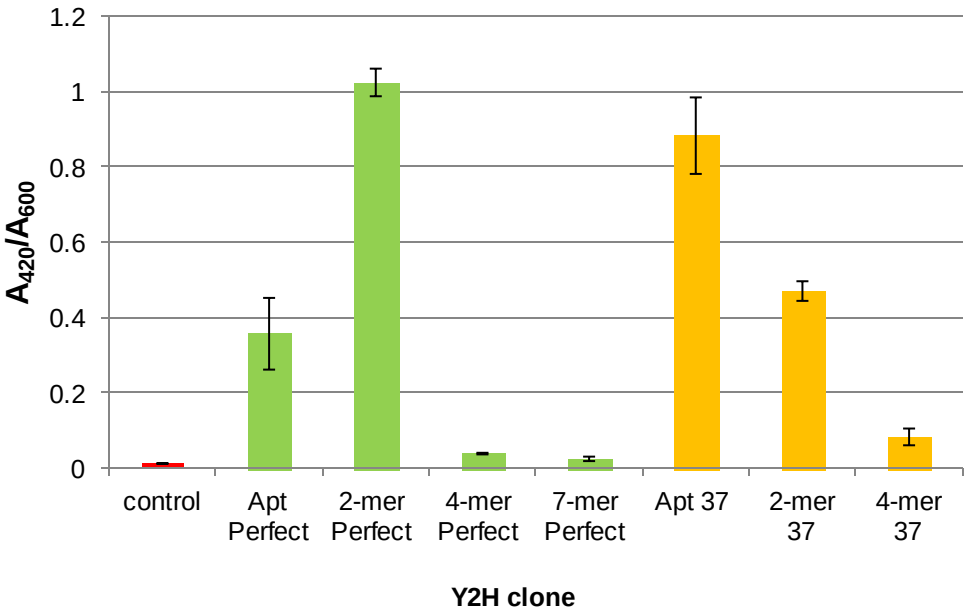

Figure 3.23 Strength of two-hybrid interactions between DmEB1 and aptamers from XXXX library

Y2H interactions between DmEB1 and multimerised aptamers 37 and Perfect. Strength of Y2H interactions was measured by a quantitative assay for β-galactosidase activity and normalised for the cell density (A_{420}/A_{600}). The assay was performed using three independent cultures, error bars are SEM.

Thus, the oligomerised aptamers 37 and Perfect interacted strongly with DmEB1 only as the dimers. Dimerised peptide Perfect interacted stronger with DmEB1 comparing to the monomer, while the dimerised peptide 37 interacted with DmEB1 weaker than the monomer.

3.4. Double constrained peptide aptamers to DmEB1

3.4.1. Screening the prey plasmid library

Although single constrained peptide aptamers displayed from a scaffold protein as its terminal fusion are conformationally more flexible and thus easier to select, double constrained peptides whose N- and C-terminus are both constrained by inclusion within a scaffold protein often showed high affinity binding to its target (Colas et al, 1996; Fabbrizio, 1999). To find double constrained peptide aptamers to DmEB1, a Y2H screen was performed in the same manner as the screen described for the single constrained peptide aptamers, except for the prey plasmid. The prey plasmid encoded a peptide where fixed SxIP flanked by random amino acid sequences was further flanked by TrxA sequence. The construct thus expressed an SxIP peptide library (called "Trx-SxIP") as an internal fusion of TrxA. The whole Trx-SxIP was fused to the C-terminus of GAL4-AD.

Prior to the screen, the quality of the Trx-SxIP prey plasmid library was verified as previously described. The encoded peptides appeared to be composed of amino acid mixture without any amino acids dominating and each of the peptides was unique. I examined 10 random sequences and majority of them (6) were as designed, another 3 sequences were shorter but they still encoded SxIP and only 1 sequence had a stop codon, thus resulting in the peptide being singly constained (Figure 3.24). Hence the Trx-SxIP library was of a good quality.

To test whether amino acids encoding the Trx-SxIP library were random at each position in the Trx-SxIP library, a chi-squared test was performed. Amino acid occurrence at each position was scored for the 9 peptides (the peptide with the stop codon was excluded) and compared to the expected number of each amino acid, which was calculated taking into account the number of codons by which each of the amino acids can be encoded using NNK (Figure 3.25). The amino acids on all 13

```
1   FKYLMSYIPYWCIWRW
2   RSIVWSVIPINWLAGR
3   NACYYSWIPLWQRLWI
4   RTVSCSYIPLRDSWR
5   ERMGFSFIPLSRWGLR
6   TAMILSTIPMGGT-SW
7   VGRQKSRIPLSCAATR
8   RPRVSSRIPWNAVDWE
9    GDYASLIPKDVTYVP
10   EWGLSQIPVSVYYVS
```

Figure 3.24 Amino acid sequences of peptides encoded in Trx-SxIP prey plasmid library

Yeast were cotransformed with linearised prey vector and DNA encoding Trx-SxIP library (encoding random peptides with fixed SxIP displayed from Trx scaffold) flanked by sequences corresponding to fragments of 5' and 3' on linearised prey vector for gap repair. Transformants were plated on media selective for the prey plasmid but not activation of reporters. The region embracing the insert site on the prey plasmid was amplified by PCR from 10 clones picked at random and sequenced. Fixed sequence is denoted with asterisks, bold indicates variable sequence.

	position																Average amino acid occurrence	
	-5	-4	-3	-2	-1	S	x	I	P	+1	+2	+3	+4	+5	+6	+7	expected	observed
Ala	0	1	0	0	1	0	0	0	0	0	0	1	1	2	0	0	0.56	0.46
Arg	3	1	2	0	0	0	2	0	0	0	1	1	1	0	2	3	0.84	1.23
Asn	1	0	0	0	0	0	0	0	0	0	2	0	0	0	0	0	0.28	0.23
Asp	0	0	1	0	0	0	0	0	0	0	1	1	0	1	0	0	0.28	0.31
Cys	0	0	1	0	1	0	0	0	0	0	0	2	0	0	0	0	0.28	0.31
Glu	1	1	0	0	0	0	0	0	0	0	0	0	0	0	0	1	0.28	0.23
Gln	0	0	0	1	0	0	1	0	0	0	0	1	0	0	0	0	0.28	0.23
Gly	0	2	0	2	0	0	0	0	0	0	0	0	0	1	1	0	0.56	0.46
His	0	0	0	0	0	0	0	0	0	0	0	0	0	0	0	0	0.28	0.00
Ile	0	0	1	0	0	0	0	9	0	1	0	0	1	0	0	1	0.28	0.31
Leu	0	0	0	1	1	0	1	0	0	4	0	0	1	1	1	0	0.84	0.77
Lys	0	1	0	0	1	0	0	0	0	1	0	0	0	0	0	0	0.28	0.23
Met	0	0	1	0	1	0	0	0	0	0	0	0	0	0	0	0	0.28	0.15
Phe	1	0	0	0	1	0	1	0	0	0	0	0	0	0	0	0	0.28	0.23
Pro	0	1	0	0	0	0	0	0	9	0	0	0	0	0	0	1	0.56	0.15
Ser	0	1	0	1	1	9	0	0	0	0	3	0	1	0	0	1	0.84	0.62
Thr	0	1	0	0	0	0	0	0	0	0	0	0	1	0	1	0	0.56	0.23
Trp	0	0	1	0	1	0	1	0	0	1	2	1	1	2	2	1	0.28	1.00
Val	1	0	1	2	0	0	1	0	0	1	0	2	1	0	2	0	0.56	0.85
Tyr	0	0	1	2	1	0	2	0	0	1	0	0	1	2	0	0	0.28	0.77
*	0	0	0	0	0	0	0	0	0	0	0	0	0	0	0	0	0.28	0.00
Different from expected	-	-	-	-	-	n/a	-	n/a	n/a	-	±	-	-	±	-	-		

Figure 3.25 The frequencies of amino acids at each position encoded by unselected prey plasmid clones from Trx-SxIP library. Yeast carrying DmEB1 bait were cotransformed with Trx-SxIP prey plasmid library and plated on non-selective media. Prey plasmid inserts of randomly picked clones were sequenced and occurrence of amino acids at subsequent positions in these sequences was scored. The observed amino acid occurrence excludes the fixed amino acids (shadowed). Each position was tested using chi-squared test for statistical differences from the frequency expected from random DNA sequences. No significant differences were observed. "–", $p \geq 0.05$. "±", $0.01 \leq p < 0.05$.

positions arose randomly ($p > 0.05$) (Figure 3.25). Since 100% of the library encoded SxIP motif, only 10% of the library fragments contained a stop codon and amino acids were encoded at random at the subsequent positions within the Trx-SxIP library, the library was of good quality. A Y2H screen for peptides encoded in the Trx-SxIP library binding to DmEB1 was performed as previously. In total, ~1 million peptides were screened and 23 positive transformants were found.

3.4.2. Impact of constraining peptides from both sides on binding to DmEB1

To determine the amino acid sequence of double constrained Trx-SxIP peptides promoting binding to DmEB1, DNA inserts were amplified and sequenced from 23 yeast transformants that activated both reporter genes in Y2H (Figure 3.26). Five of the transformants encoded stop codons either within or shortly after the insert sequence and these peptides were excluded from further analysis. It appeared that the encoded peptides were rich in arginine and glycine and occurrence of some of the amino acids did not appear random at certain positions (Figure 3.27). To test whether the occurrence of particular amino acids at certain positions in the vicinity to SxIP was significantly different in selected peptides than peptides from unselected Trx-SxIP prey plasmid library, a chi-squared test was performed. I scored the amino acid occurrence at each position encoded by the 18 sequenced DNA fragments and compared them with the amino acids scored for the 10 random peptides from Trx-SxIP library. Since the occurrence of amino acids Gly at -5, Phe at -2, Arg and Lys at x, Arg and Val at 1, Trp at 2, Cys at 3, Gly at 4, Lys at 5 and Ser at 6 was significantly different in selected than unselected peptides ($p < 0.01$), I concluded that these amino acids promote binding of the constrained Trx-SxIP peptides to DmEB1 (Figure 3.28).

To verify whether occurrence of amino acids in the region flanking the SxIP and promoting binding to DmEB1 is different in the double constrained and the single constrained peptides (found in the SxIP library screen), I performed statistical analysis. Occurrence of amino acids Arg and Lys at position x, Arg and Val at +1, Trp at +2 and Gly at +4, which promote binding of both double constrained and the single constrained peptides to DmEB1 was not significantly different ($p > 0.08$). An exception was Phe at position -2 which appeared more frequently in double

Aptamer	Variable region
	* * *
T1	CGAFGSAIPRWN
T6	VKTGRSKIPVWGGRKH
T9	VSTFHSRIPVRADKRV
T10	GRVRGSKIPILMTKYC
T11	PSGVKSNIPRWVGWSK
T12	GRVRGSRIPLWMGFHN
T13	RQNNPSKIPVYTLRRD
T14	HRPGVSRIPRWL
T16	GSNGRSRIPRYTGKRK
T17	WFKFKSRIPVRLGGR
T20	RRSRIPRFQGGSGGG
T21	AGRLRSLIPRYCGC
T22	YTHMTSRIPIMRGSRV
T23	GGKFVSRIPRYVRNLS
T24	GRSSRSRIPRFCGFSS
T27	LRHGYSRIPASAPGWL
T28	SLVTGSLIPVATWRLG
T29	RFASNSRIPRWCGLS

Figure 3.26 Amino acid sequences of peptides encoded in Trx-SxIP prey plasmid library

Yeast were cotransformed with linearised prey vector and DNA encoding Trx-SxIP library (encoding random peptides with fixed SxIP displayed from Trx scaffold) flanked by sequences corresponding to fragments of 5' and 3' on linearised prey vector for gap repair. Transformants were plated on media selective for the prey plasmid and activation of reporters. The region embracing the insert site on the prey plasmid was amplified by PCR from clones and sequenced. Fixed sequence is denoted with asterisks, bold indicates variable sequence.

	position																Average amino acid occurrence	
	-5	-4	-3	-2	-1	S	x	I	P	+1	+2	+3	+4	+5	+6	+7	observed	expected
Ala	1	0	2	0	0	0	1	0	0	1	1	2	0	0	0	0	0.62	1.13
Arg	2	5	1	3	5	0	11	0	0	9	2	1	1	3	5	0	3.69	1.69
Asn	0	0	2	1	1	0	1	0	0	0	0	1	0	1	0	1	0.62	0.56
Asp	0	0	0	0	0	0	0	0	0	0	0	0	1	0	0	1	0.15	0.56
Cys	1	0	0	0	0	0	0	0	0	0	0	3	0	1	0	1	0.46	0.56
Glu	0	0	0	0	0	0	0	0	0	0	0	0	0	0	0	0	0.00	0.56
Gln	0	1	0	0	0	0	0	0	0	0	0	1	0	0	0	0	0.15	0.56
Gly	5	3	1	4	4	0	0	0	0	0	0	1	10	3	0	2	2.54	1.13
His	1	0	2	0	1	0	0	0	0	0	0	0	0	0	1	1	0.46	0.56
Ile	0	0	0	0	0	0	0	18	0	2	0	0	0	0	0	0	0.15	0.56
Leu	1	1	0	1	0	0	2	0	0	1	1	2	1	1	2	1	1.08	1.69
Lys	0	1	2	0	2	0	3	0	0	0	0	0	0	3	1	2	1.08	0.56
Met	0	0	0	1	0	0	0	0	0	0	1	2	0	0	0	0	0.31	0.56
Phe	0	2	0	4	0	0	0	0	0	0	2	0	0	2	0	0	0.77	0.56
Pro	1	0	1	0	1	0	0	0	18	0	0	0	1	0	0	0	0.31	1.13
Ser	1	3	1	2	0	18	0	0	0	0	1	0	0	1	4	2	1.15	1.69
Thr	0	1	2	1	1	0	0	0	0	0	0	3	1	0	0	0	0.69	1.13
Trp	1	0	0	0	0	0	0	0	0	0	6	0	1	1	1	0	0.77	0.56
Val	2	0	3	1	2	0	0	0	0	5	0	2	0	0	0	2	1.31	1.13
Tyr	1	0	0	0	1	0	0	0	0	0	4	0	0	0	1	0	0.54	0.56
*	0	0	0	0	0	0	0	0	0	0	0	0	0	0	0	0	0.00	0.56
Different from expected	-	-	-	+	-	n/a	+	n/a	n/a	+	+	-	+	-	-	-		

Figure 3.27 The frequency of amino acids at each position encoded by prey plasmid clones selected from Trx-SxIP library interacting with DmEB1 bait.

Yeast carrying DmEB1 bait were cotransformed with Trx-SxIP prey plasmid library and selected for bait-prey interaction. Prey plasmid inserts were sequenced and occurrence of amino acids at subsequent positions in these sequences was scored. The observed amino acid occurrence excludes the fixed amino acids (shadowed). Each position was tested using chi-squared test for statistical differences from the frequency expected from random DNA sequences. Occurrence of amino acids at some positions (-2, x, +1, +2 and +4) was not random. "+", p-value ≤0.01; "-", p-value ≥0.05.

Position	-5	-4	-3	-2	-1	S	x	I	P	+1	+2	+3	+4	+5	+6	+7
amino acid letter code	G V R	G R S	V	F G R	G R		R K			R V	W Y	C T	G	K R	S R	G

Figure 3.28 Amino acids promoting binding of double constrained peptide aptamers to DmEB1
Peptides interacting with DmEB1 were selected from Trx-SxIP prey plasmid library in Y2H. Occurrence of amino acids at subsequent positions (-5 to +7) in these peptide aptamers was scored. The frequencies of amino acids at each position were compared between these peptide aptamers and peptides from Trx-SxIP prey plasmid library not selected for DmEB1 binding. Some amino acids occurred more frequently in peptide aptamers than in unselected peptides ($p < 0.01$) and are marked with yellow background. Amino acids occurring most frequently in double constrained peptide aptamers to DmEB1 are presented.

constrained peptides than in the single constrained ones ($p < 0.0001$). I concluded that Phe at position -2 is more important for the binding of double constrained than the single constrained peptides to DmEB1. The rate of finding the double constrained DmEB1 interactors was 5 times lower than the single constrained interactors (18 in 1 million vs. 500 in 5 million). This can be explained by the double constrained peptides being less conformationally diverse than the single constrained peptides (Colas et al, 1996).

3.4.3. Identifying strongest double constrained peptide aptamers to DmEB1

To identify yeast clones carrying Trx-SxIP peptides with strongest binding to DmEB1, I measured β-galactosidase activity in liquid as described in 3.1.6. Yeast carrying Trx-SxIP peptides T6, T11, T13, T14 and T16 (Figure 3.26 and 3.29) produced most β-galactosidase. Then, I excluded the possibility that a random mutation in yeast, plasmid or TrxA caused expression from the reporters in transformants carrying peptides T6, T11, T13, T14 and T16, as described in 3.1.7. To more precisely compare the strength of aptamers T6, T11, T13, T14 and T16 interaction with DmEB1, I measured β-galactosidase activity in liquid in three independent replicas. I found that aptamers T6, T14 and T16 interact strongest with DmEB1 (Figure 3.30).

3.5. Screening for single constrained peptide aptamers to HsEB1 or HsEB3

3.5.1. Certain amino acid residues flanking SxIP promote peptide binding to HsEB1 or HsEB3

Although highly homologous to human EB1, human EB3 was shown to be upregulated in brain as well as in muscle tissues in late stages of muscle differentiation (Nakagawa et al, 2000; Straube & Merdes, 2007). The regulation of the cytoskeleton by EB1 and EB3 may be tissue-specific and dictated by recruitment of different MAPs by EB1 or EB3.

To find peptide aptamers interacting by SxIP with HsEB1 or HsEB3, I screened the SxIP prey plasmid library by Y2H. First, bait plasmids were constructed

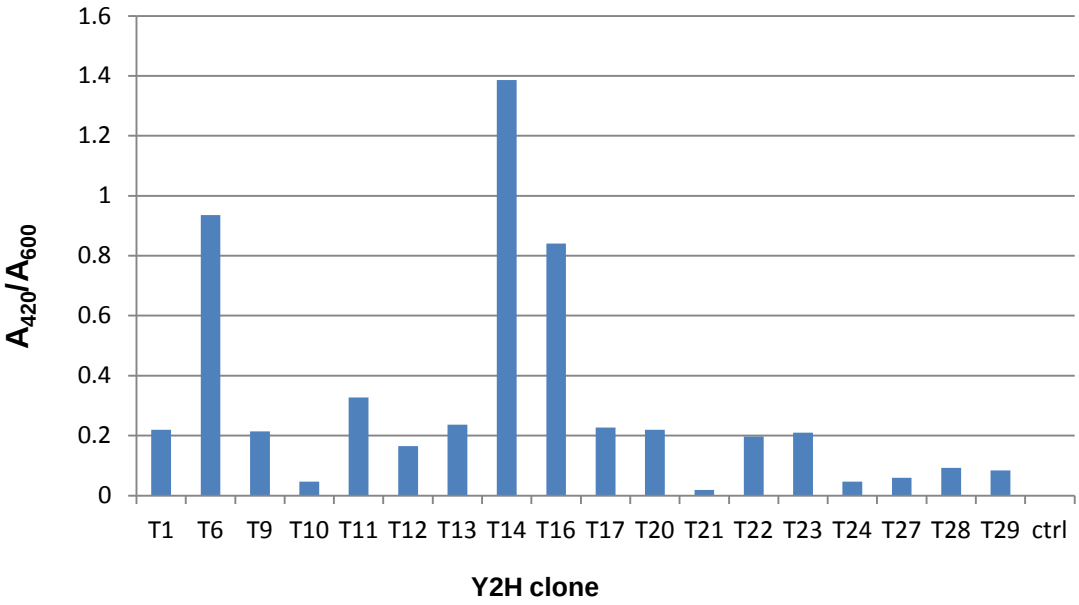

Figure 3.29 Strength of two-hybrid interactions between DmEB1 and double constrained peptide aptamers

The expression of the reporter gene *LacZ* was measured by a quantitative assay for β-galactosidase activity and normalised for the cell density (A_{420}/A_{600}). The empty bait plasmid was used as a control (ctrl). The numbers correspond to a Trx-SxIP clone;"T", Thioredoxin.

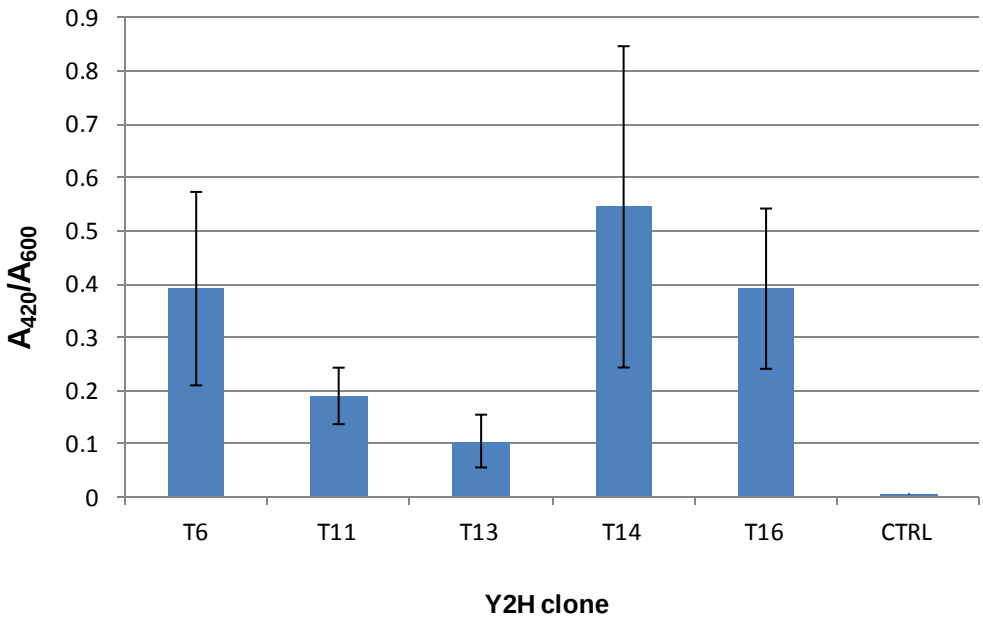

Figure 3.30 Strength of two-hybrid interactions of the strongest double constrained aptamers with DmEB1.
The expression of the reporter gene *LacZ* was measured by a quantitative assay for β-galactosidase activity and normalised for the cell density (A_{420}/A_{600}). The empty bait plasmid was used as a control (ctrl). The bars represent standard error of the mean (SEM; n=3); numbers correspond to a Trx-SxIP clone;"T", Thioredoxin.

as previously described containing either full length HsEB1 or HsEB3 coding DNA. In total, ~2 million peptides were screened for binding to HsEB1 and ~2 million peptides for binding to HsEB3. I found that 47 yeast HsEB1 interactors and 58 HsEB3 interactors that activate both reporter genes. Amino acids flanking SxIP which promote peptide interaction with HsEB1 or HsEB3 were determined as previously by sequencing the DNA encoding the variable peptide aptamer regions. These regions were arginine-rich and some of the amino acids appeared not random at certain positions (Figure 3.31 and 3.32).

To test whether the occurrence of particular amino acids at certain positions in the vicinity to SxIP was significantly different in selected peptides for HsEB1 or HsEB3 than unselected peptides encoded in the SxIP library, the chi-squared test was performed. I scored the amino acid occurrence at each position encoded by the 47 or 58 sequenced DNA fragments for HsEB1 or HsEB3, respectively (Figure 3.33 and 3.34). I compared them with the amino acids scored for the 39 peptides from the unselected SxIP library. As previously, by chi-squared test, I analysed whether occurrence of the most abundant amino acids in the region flanking SxIP was significantly different in peptides selected for HsEB1 or HsEB3 than the unselected peptides encoded in the SxIP library. The occurrence of the amino acids Arg at -1, Arg and Lys at x, Arg and Val at +1, Leu at +2, Lys at +3, Lys and Arg at +4 and Arg at +5 was significantly different in peptides selected for HsEB1 binding than in the unselected peptides ($p < 0.01$) (Figure 3.35). In peptides selected for binding to HsEB3 the occurrence of amino acids Arg at positions -5, -4 and -2, Lys and Arg at positions -1 and x, Arg and Val at +1, Trp and Arg at +2, Ile and Val at +3, Gly at +4, Arg at +5, Lys at +6 and Arg and Lys at +7 was significantly different than occurrence of these amino acids in random peptides encoded in the library ($p < 0.01$) (Figure 3.36).

I concluded that these amino acids promote binding of the SxIP-containing peptides to HsEB1 or HsEB3.

3.5.2. Peptide aptamers suggest sequence preferences for binding to HsEB1, HsEB3 or DmEB1

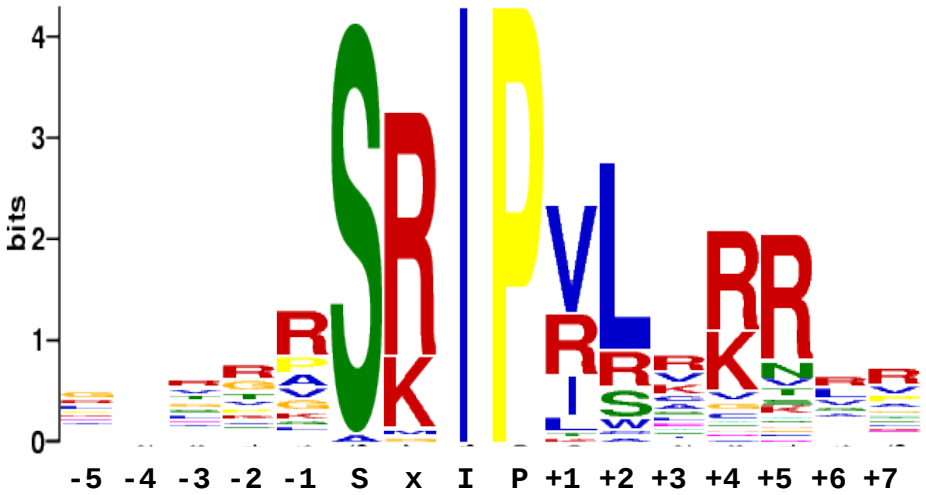

Figure 3.31 Sequence bias within SxIP motif and flanking region promoting binding to HsEB1

Amino acids of peptide aptamers selected from SxIP library for interaction with HsEB1. Peptide aptamers selected from SxIP library revealed that some amino acids flanking SxIP are overrepresented and promote interaction with HsEB1. The total height of each stack indicates the "information content" at that position (measured in bits). The height of symbols within the stack reflects the relative frequency of the corresponding amino acid at that position. The subsequent positions within the sequences are labeled -5 to +7. The figures were generated using www.meme.nbcr.net server by submitting 16 amino acid long sequences in fasta format.

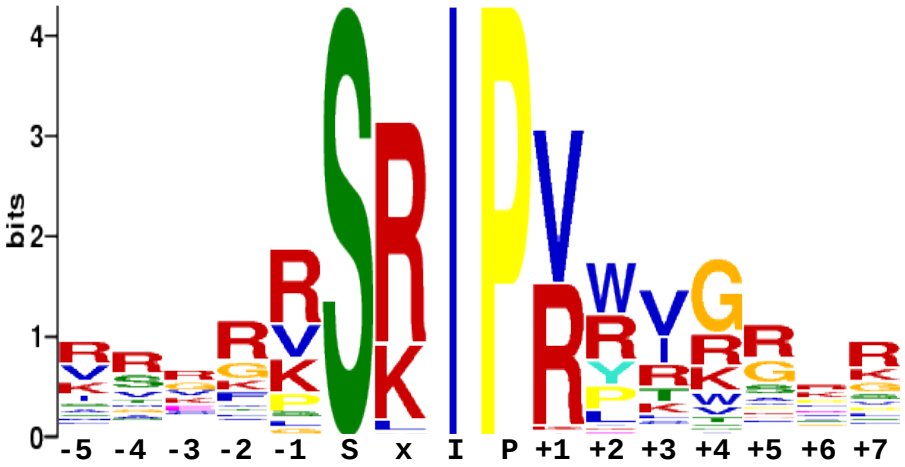

Figure 3.32 Sequence bias within SxIP motif and flanking region promoting binding to HsEB3

Amino acids of peptide aptamers selected from SxIP library for interaction with HsEB3. Peptide aptamers selected from SxIP library revealed that some amino acids flanking SxIP are overrepresented and promote interaction with HsEB3. The total height of each stack indicates the "information content" at that position (measured in bits). The height of symbols within the stack reflects the relative frequency of the corresponding amino acid at that position. The subsequent positions within the sequences are labeled -5 to +7. The figures were generated using www.meme.nbcr.net server by submitting 16 amino acid long sequences in fasta format.

	position																	Average amino acid occurrence	
	-5	-4	-3	-2	-1	S	x	I	P	+1	+2	+3	+4	+5	+6	+7	+8	observed	expected
Ala	3	1	3	3	5	1	0	0	0	0	1	4	1	0	5	4	0	2.38	2.94
Arg	5	5	7	10	17	0	35	0	0	13	6	9	22	28	8	11	0	13.54	4.41
Asn	2	1	2	1	0	0	0	0	0	0	0	1	0	4	1	1	0	1.00	1.47
Asp	0	2	0	0	0	0	0	0	0	0	0	0	1	1	1	2	0	0.54	1.47
Cys	0	4	0	1	0	0	0	0	0	0	1	4	2	0	2	0	1	1.15	1.47
Glu	3	1	3	1	1	0	0	0	0	0	0	3	0	0	1	0	0	1.00	1.47
Gln	2	1	2	0	2	0	0	0	0	0	0	2	0	1	4	1	0	1.15	1.47
Gly	8	3	5	7	4	0	1	0	0	0	0	0	2	1	2	3	0	2.77	2.94
His	2	0	0	0	1	0	0	0	0	0	0	0	1	1	0	1	0	0.46	1.47
Ile	1	2	1	1	0	0	0	47	0	8	0	2	0	0	2	1	1	1.46	1.47
Leu	5	4	4	1	2	0	0	0	0	3	32	3	0	0	8	2	0	4.92	4.41
Lys	4	2	2	4	3	0	10	0	0	1	0	7	14	2	1	2	0	4.00	1.47
Met	1	4	1	1	0	0	1	0	0	0	0	0	0	0	0	1	0	0.69	1.47
Phe	0	2	1	1	0	0	0	0	0	0	0	0	0	1	1	0	0	0.46	1.47
Pro	4	2	2	4	6	0	0	0	47	0	0	0	0	0	2	5	0	1.92	2.94
Ser	2	1	4	2	1	46	0	0	0	0	5	3	1	2	2	2	1	2.00	4.41
Thr	1	3	5	5	1	0	0	0	0	1	0	1	0	2	1	2	0	1.69	2.94
Trp	1	1	0	0	0	0	0	0	0	0	2	0	0	0	1	1	0	0.46	1.47
Val	2	5	5	4	4	0	0	0	0	21	0	6	2	2	5	6	0	4.77	2.94
Tyr	1	3	0	1	0	0	0	0	0	0	0	2	1	1	0	2	1	0.92	1.47
*	0	0	0	0	0	0	0	0	0	0	0	0	0	1	0	0	43	0.08	1.47
Different from expected	-	-	-	±	+	n/a	+	n/a	n/a	+	+	+	+	+	-	-	n/a		

Figure 3.33 The frequency of amino acids at each position encoded by prey plasmid clones selected from SxIP library interacting with HsEB1 bait.

Yeast carrying HsEB1 bait were cotransformed with SxIP prey plasmid library and selected for bait-prey interaction. Prey plasmid inserts were sequenced and occurrence of amino acids at subsequent positions in these sequences was scored. The observed amino acid occurrence excludes the fixed amino acids (shadowed). Each position was tested using chi-squared test for statistical differences from the frequency expected from random DNA sequences. Occurrence of amino acids at some positions (-2 to +4) was not random. "+", $p \leq 0.01$, "±"; $0.01 < p < 0.05$, "-"; $p \geq 0.05$.

	position																	Average amino acid occurrence	
	-5	-4	-3	-2	-1	S	x	I	P	+1	+2	+3	+4	+5	+6	+7	+8	observed	expected
Ala	3	4	2	2	1	0	0	0	0	0	1	0	0	4	4	1	0	1.69	3.63
Arg	14	15	12	22	23	0	41	0	0	29	15	8	11	18	7	17	0	17.85	5.44
Asn	1	2	0	1	0	0	0	0	0	0	0	0	1	2	1	0	0	0.62	1.81
Asp	1	0	1	0	0	0	0	0	0	0	1	0	0	1	4	1	1	0.77	1.81
Cys	0	1	4	0	0	0	0	0	0	0	0	2	0	1	1	1	1	0.85	1.81
Glu	1	1	5	1	0	0	0	0	0	0	0	0	0	0	1	0	0	0.69	1.81
Gln	2	1	1	0	0	0	0	0	0	0	0	1	2	0	2	2	0	0.85	1.81
Gly	1	3	8	8	2	0	0	0	0	0	0	1	24	11	3	6	0	5.15	3.63
His	0	1	2	1	0	0	0	0	0	0	0	0	0	2	1	0	0	0.54	1.81
Ile	6	3	0	0	0	0	0	58	0	1	0	13	0	1	1	1	0	2.00	1.81
Leu	0	1	4	3	2	0	2	0	0	0	5	2	0	0	4	4	0	2.08	5.44
Lys	7	1	5	6	12	0	12	0	0	1	1	6	9	3	10	7	0	6.15	1.81
Met	3	3	1	1	0	0	3	0	0	0	1	1	1	0	0	2	0	1.23	1.81
Phe	3	1	1	5	0	0	0	0	0	0	0	1	1	2	0	2	0	1.23	1.81
Pro	1	1	2	1	6	0	0	0	58	0	8	0	0	2	6	3	0	2.31	3.63
Ser	3	9	2	1	2	58	0	0	0	0	0	0	0	6	3	5	0	2.38	5.44
Thr	2	4	1	3	0	0	0	0	0	0	0	5	2	0	1	1	0	1.46	3.63
Trp	1	1	1	1	0	0	0	0	0	0	17	0	4	2	4	0	0	2.38	1.81
Val	9	5	6	2	10	0	0	0	0	27	0	18	3	2	3	3	0	6.77	3.63
Tyr	0	1	0	0	0	0	0	0	0	0	9	0	0	1	1	1	0	1.00	1.81
*	0	0	0	0	0	0	0	0	0	0	0	0	0	0	1	1	56	0.15	1.81
Different from expected	+	±	+	+	+	n/a	+	n/a	n/a	+	+	+	+	+	+	+	n/a		

Figure 3.34 The frequency of amino acids at each position encoded by prey plasmid clones selected from SxIP library interacting with HsEB3 bait.

Yeast carrying HsEB3 bait were cotransformed with SxIP prey plasmid library and selected for bait-prey interaction. Prey plasmid inserts were sequenced and occurrence of amino acids at subsequent positions in these sequences was scored. The observed amino acid occurrence excludes the fixed amino acids (shadowed). Each position was tested using chi-squared test for statistical differences from the frequency expected from random DNA sequences. Occurrence of amino acids at all positions (-5 to +7) was not random. "+", $p \leq 0.01$, "±"; $0.01 < p < 0.05$, "-"; $p \geq 0.05$.

Position	-5	-4	-3	-2	-1	S	x	I	P	+1	+2	+3	+4	+5	+6	+7
amino acid letter code	R L G	R V	R V	R G	R		R K			R V	L R	K R	K R	R	R L	R V

Figure 3.35 Amino acids promoting binding of peptide aptamers to HsEB1
Peptides interacting with HsEB1 were selected from SxIP prey plasmid library in Y2H. Occurrence of amino acids at subsequent positions (-5 to +7) in these peptide aptamers was scored. The frequencies of amino acids at each position were compared between these peptide aptamers and peptides from SxIP prey plasmid library not selected for HsEB1 binding. Some amino acids occurred more frequently in peptide aptamers than in unselected peptides ($p < 0.01$) and are marked with yellow background. Amino acids occurring most frequently in peptide aptamers to DmEB1 are presented.

Position	-5	-4	-3	-2	-1	S	x	I	P	+1	+2	+3	+4	+5	+6	+7
amino acid letter code	R V	R S	R G	R G	K R V		R K			R V	W R	I V R	G R	R G	K R	R K

Figure 3.36 Amino acids promoting binding of peptide aptamers to HsEB3
Peptides interacting with HsEB3 were selected from SxIP prey plasmid library in Y2H. Occurrence of amino acids at subsequent positions (-5 to +7) in these peptide aptamers was scored. The frequencies of amino acids at each position were compared between these peptide aptamers and peptides from SxIP prey plasmid library not selected for HsEB3 binding. Some amino acids occurred more frequently in peptide aptamers than in unselected peptides ($p < 0.01$) and are marked with yellow background. Amino acids occurring most frequently in peptide aptamers to DmEB3 are presented.

The sequence analyses of the peptide aptamers to HsEB1, HsEB3 or DmEB1 revealed that amino acids at certain positions flanking SxIP promote binding to these EB proteins. I further compared the sequences to find amino acids that are enriched in peptide aptamers to one EB protein, not to the other.

I found that different amino acids are preferred for binding to different EB proteins at certain positions downstream of SxIP (Figure 3.37). For example, Leu at position +2 is preferred for binding HsEB1 but Trp at this position is preferred for binding HsEB3 (Figure 3.37 A). More differences between HsEB1 peptide aptamers and HsEB3 peptide aptamers were detected at positions +3, +4 and +6 and they were all statistically different ($p < 0.01$). Also different amino acids are enriched at certain positions among DmEB1 peptide aptamers compared to HsEB1 or HsEB3 peptide aptamers (Figure 3.37 B and C).

These results suggest for the first time that even though similar sequences promote binding to HsEB1 and HsEB3, there are some differences between binding preferences of these two proteins. These differences between HsEB1 and HsEB3 may suggest different binding partners and indicate their biological roles distinct from each other.

3.6. Discussion

In this work I showed that peptide aptamers can be used to establish sequence determinants required for strong DmEB1 binding. This work also showed how the screen for peptide aptamers can be accelerated.

Although screening peptide libraries of random amino acid composition has been extensively used in search for peptide aptamers, a fixed motif flanked by random amino acid sequences was used for the first time in this work. This novel method not only saves the time required to perform a large-scale screen but it also allows selecting peptide aptamers which disrupt a very specific interaction. Indeed, I found ~500 single constrained interactors after screening ~5 million peptides. It can be estimated that ~20^3 times more peptides would have to be screened if the amino acids for SxIP motif were not fixed to find the same number of interactors. This new method could significantly change the peptide aptamer field as screening for peptide aptamers becomes considerably more effective.

A)

amino acid letter code		S	x	I	P	+1	+2	+3	+4	+5	+6	+7
	HsEB1					R V	**L**	K	K **R**	R		
	HsEB3					R V	R **W**	**I** V	**G**	R	**K**	R K

B)

amino acid letter code		S	x	I	P	+1	+2	+3	+4	+5	+6	+7
	HsEB1					R V	**L**	**K**	**K** R	R		
	DmEB1					R V	W	V	**G**	R		**G**

C)

amino acid letter code		S	x	I	P	+1	+2	+3	+4	+5	+6	+7
	HsEB3					R V	R W	**I** V	G	R	K	R K
	DmEB1					R V	W	V	G	R		**G**

Figure 3.37 Certain amino acids that follow on from SxIP promote specific binding to HsEB1, HsEB3 or DmEB1
Presented amino acids are overrepresented in peptide aptamers binding to HsEB1, HsEB3 or DmEB1, as determined by comparison to non-selected (random) peptides from SxIP library. Occurrence of amino acids overrepresented in peptide aptamers to (A) HsEB1 or HsEB3, (B) HsEB1 or DmEB1 and (C) HsEB3 or DmEB3 was analysed using chi-squared test. Yellow background highlights residues whose frequencies are significantly different between a pair of EB1 homologues ($p < 0.01$).

I also compared the frequency of peptide interactors found in a screen for single- and double constrained peptides displayed from TrxA protein scaffold. I found that the likelihood of finding a single constrained peptide aptamer is ~6-fold higher than finding a double constrained peptide aptamer binding to the same protein (18 peptide aptamers found after screening ~1 million of Trx-SxIP peptides). Although the frequency may vary greatly between the different protein targets and when screening peptide libraries of completely random sequences, this study gave experimental evidence that the chance of finding double constrained peptide aptamers is lower than finding the single constrained ones.

While the double constrained peptide aptamers reported by other research groups very often showed target binding affinity in nanomolar range and the single constrained fell in a mid-millimolar range (Colas et al, 1996; Fabbrizio, 1999; Oldenburg et al, 1992). Also, it was shown that a peptide-protein binding affinity was improved 1000-fold by displaying an originally singly-constrained peptide from the double-constraining TrxA scaffold (Cohen et al, 1998). However, I demonstrated that single constrained peptide aptamers can bind its target strongly since aptamer Perfect interaction with DmEB1 fell in a high nM range (K_d of ~300 nM). Nevertheless, it would be interesting to doubly-constrain this peptide to investigate how it affects its binding strength.

In this study I also showed that amino acids promoting binding of a peptide to DmEB1 can be revealed using peptide aptamers combined with statistical analysis. Peptides binding to DmEB1 were selected from a pool of peptides with fixed SxIP and flanked with random amino acids. Then, by statistical methods, I compared amino acid sequences of these DmEB1 interactors with random peptides encoded in the SxIP library. This comparison uncovered amino acids at certain positions which occurred more frequently in peptides interacting with DmEB1 than in peptides encoded in the library, thus promoting binding.

By finding amino acids which promote DmEB1 binding, I was able to generate a synthetic peptide aptamer, aptamer Perfect, resulting from combining these amino acids in one sequence. By performing a quantitative assay, indirectly evaluating a peptide-DmEB1 interaction, I showed that this synthetic peptide aptamer bound strongly to DmEB1. Thus the amino acids at specific positions which

were each shown to promote binding to DmEB1, also promote strong binding when they act in concert. This study showed that peptide aptamers can be designed to generate a very strongly interacting peptide aptamer if required. Also, considering that SxIP sequence occurs frequently in proteins but only some of them bind EB1, my study may be used to predict whether a MAP binds to EB1 (Jiang et al, 2012).

Additionally, using the aptamer Perfect as the basis for the design of a peptide library, I investigated whether other amino acids than the observed in the natural interactors (Ser/Thr-x-Ile/Leu-Pro) would allow for binding to DmEB1. I showed that additionally to the known amino acid variants, Cys and Gly can occupy X1, Arg, Met, Phe, Val position X3, Ala and Leu position X4 and almost all amino acids were found at X2. This finding shows that composition of SxIP motif is variant and interaction with DmEB1 is not purely dictated by Ser/Thr-x-Ile/Leu-Pro.

Since it was shown that dimerisation of an SxIP motif-containing fragment of MACF enhanced its accumulation at the plus end, I investigated what effect has oligomerisation of peptide aptamers on binding to DmEB1 (Buey et al, 2012). This study showed that binding of some peptides to DmEB1 can be improved by oligomerisation but not always. Importantly, more than two consecutive repeats significantly reduced peptide aptamer binding to DmEB1.

To investigate sequence determinants for binding to human EBs, HsEB1 or HsEB3, I performed the same screen and analysis as for DmEB1. I showed that some amino acids in the region flanking SxIP promote specific binding to HsEB1 or HsEB3. These binding preferences to HsEB1 or HsEB3 may characterise their biological roles distinct from each other. This suggestion is in agreement with previous studies demonstrating different expression patterns of HsEB1 or HsEB3 in some of the tissues (Geraldo et al, 2008; Zhang et al, 2009). The regulation of the cytoskeleton by HsEB1 or HsEB3 may be tissue-specific and dictated by recruitment of different MAPs by HsEB1 or HsEB3. Knowing this amino acid specificity it may be possible to classify *in silico* different EB-interacting MAPs to those preferentially interacting with HsEB1 or HsEB3.

I next decided to investigate whether some of the peptide aptamers can bind DmEB1 in cells, where other endogenous proteins are present, and outcompete natural SxIP-containing interactors from DmEB1 binding. I also tested what effect

inhibition of DmEB1 has on a multicellular organism by expressing in Drosophila some of the peptide aptamers I found. This work is presented in the next chapter.

CHAPTER 4

Disrupting DmEB1 functions in Drosophila using peptide aptamers

4.1. Peptide aptamers in Drosophila S2 cells

4.1.1. Expressing peptide aptamers in Drosophila S2 cells

Since I planned to express peptide aptamers in Drosophila, I tested whether single and double constrained peptide aptamers which bound most strongly to DmEB1 in yeast colocalise with DmEB1 in Drosophila S2 cells, hence in the presence of other proteins.

DNA encoding each of these peptide aptamers was cloned into a GFP C-terminus fusion vector (Materials and methods) under control of actin 5C promoter and Drosophila S2 cells were transfected with these plasmids. Drosophila S2 cells were transfected with a plasmid expressing GFP for a negative control (Figure 4.1). Localisation of peptide aptamers with respect to DmEB1 and microtubules was assessed by immunostaining using GFP, DmEB1 and tubulin antibodies.

All the peptide aptamers I tested, 37, 188, 312, 356, 380, Perfect, T13, T14 and T16, colocalised with DmEB1 at the microtubule plus ends in interphase cells and did not affect microtubule array (Figure 4.2 and 4.3). Visual examination indicated that aptamers 37, Perfect, T14 and T16 colocalised more strongly than aptamers 188, 312, 356, 380 and T13. Also in the mitotic cells, all the peptide aptamers displayed colocalisation with DmEB1 at the centrosomes, microtubule tips and on the interpolar microtubule bundles (Figure 4.4).

Colocalisation of aptamers 37, 188, 312, 356, 380, Perfect, T13, T14 and T16 to DmEB1 confirms specific binding of these peptide aptamers to DmEB1 in cells.

4.1.2. Expressing oligomerised peptide aptamers in Drosophila S2 cells

It was shown that dimerisation of human MACF fragment containing SxIP motif enhances its accumulation at the polymerising microtubule plus ends in mammalian cultured cells (Honnappa et al, 2009). I aimed to test if oligomerised aptamer 37 or Perfect colocalise to DmEB1 and whether their accumulation at the microtubule plus ends is enhanced relative to the monomeric aptamer forms.

DNA encoding each of the peptide aptamers was cloned into a GFP C-terminus fusion vector under control of actin 5C promoter and localisation of these

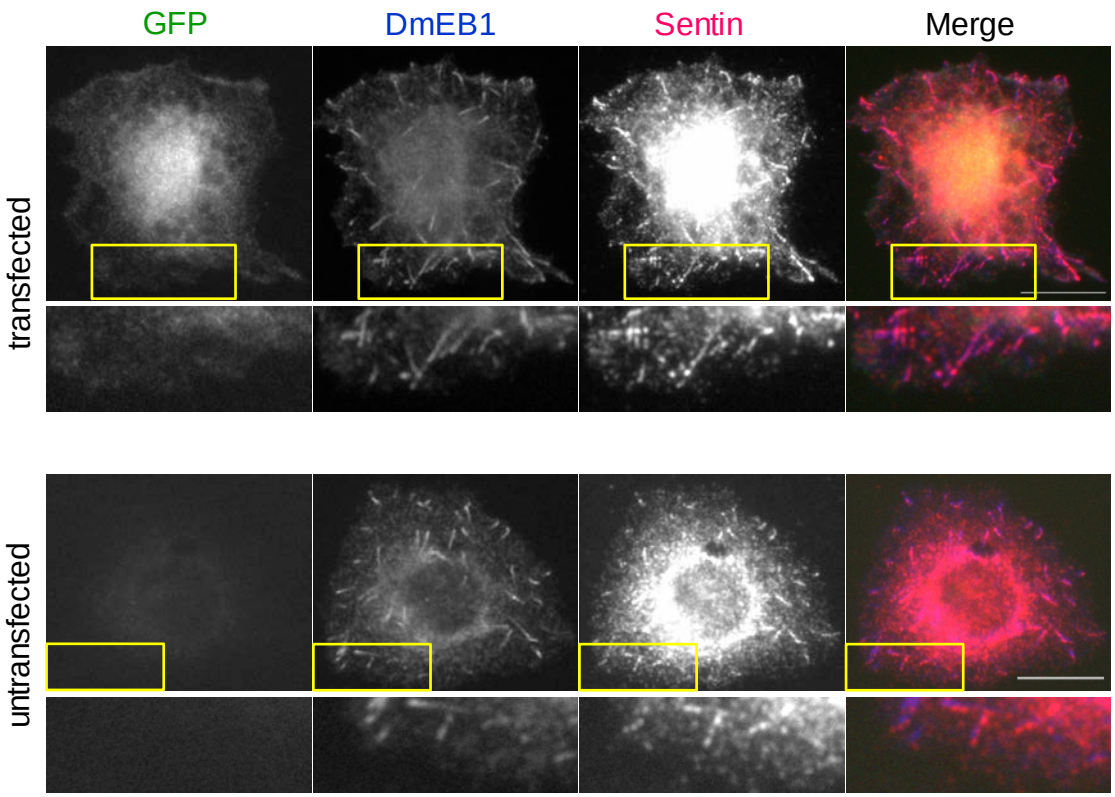

Figure 4.1 Expression of GFP aptamer scaffold in Drosophila S2 cells
Drosophila S2 cells were transfected with plasmid encoding GFP protein scaffold. GFP, DmEB1 and Sentin signals were visualised by immunostaining with anti-GFP, anti-DmEB1 and anti-Sentin antibodies. GFP did not colocalise with DmEB1 (second column, top panel) at the microtubule plus ends but was diffused inside the cells (first column, top panel) . Sentin immunostaining was not affected in cells expressing GFP (third column). A typical transfected (top panel) and untransfected (bottom panel) cell on the same slide are shown for comparison. The fourth column shows merged images from the three preceding columns. Bars, 10 µm. The yellow boxes indicate the areas that are magnified in the images below.

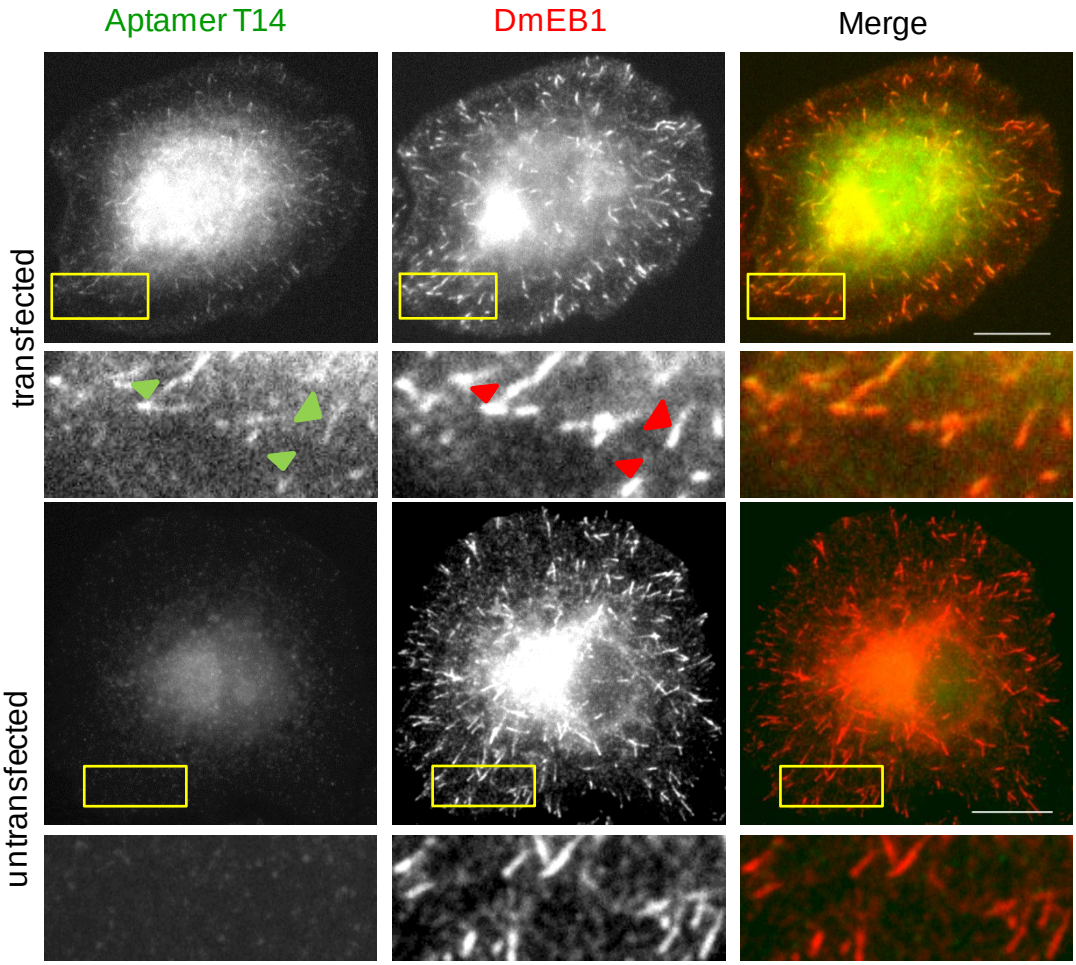

Figure 4.2 Peptide aptamers can colocalise to DmEB1 in interphase of Drosophila S2 cells

Aptamer T14 (green arrowheads) colocalises with DmEB1 (red arrowheads) at microtubule plus ends. Drosophila S2 cells were transfected with plasmid encoding double constrained peptide aptamer T14 displayed from GFP protein scaffold. GFP and DmEB1 signals were visualised by immunostaining with anti-GFP and anti-DmEB1 antibodies. The third column shows merged images from the two preceding columns. A typical transfected (top panel) and untransfected (bottom panel) cell on the same slide are shown for comparison. Bar=10 µm. The yellow boxes indicate the areas that are magnified in the images below.

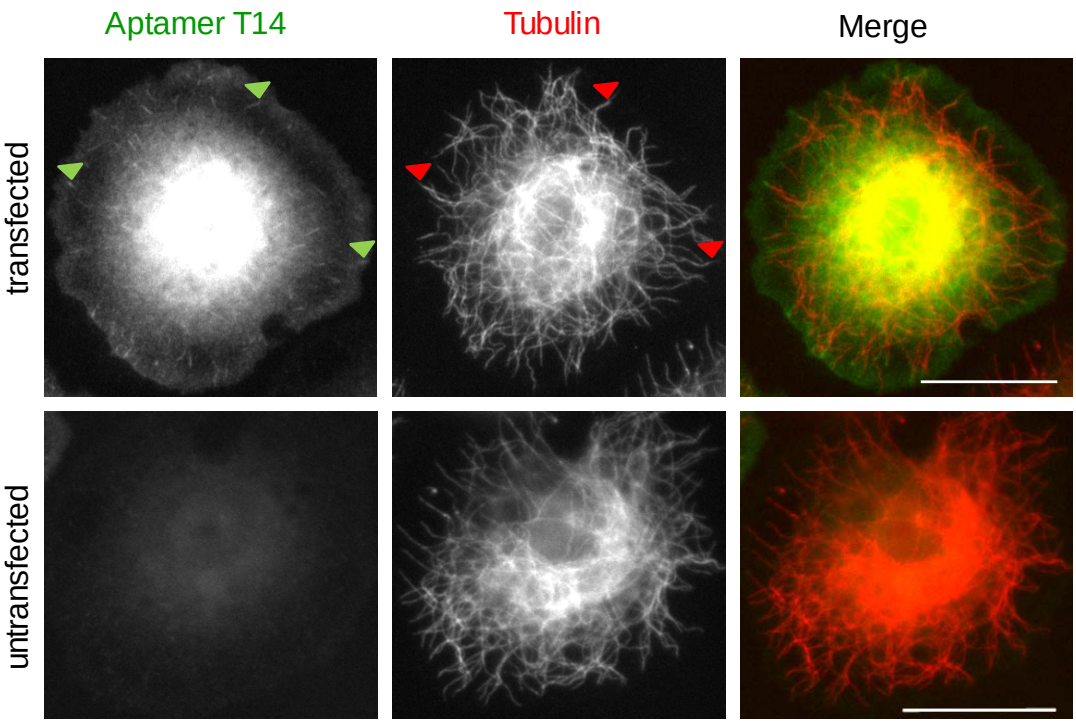

Figure 4.3 Peptide aptamers can colocalise to microtubule plus ends in Drosophila S2 cells and do not affect microtubule array
Aptamer T14 (green arrowheads) colocalises with microtubule plus ends (red arrowheads). Drosophila S2 cells were transfected with plasmid encoding double constrained peptide aptamer T14 displayed from GFP protein scaffold. GFP and DmEB1 signals were visualised by immunostaining with anti-GFP and anti-DmEB1 antibodies. The third column shows merged images from the two preceding columns. A typical transfected (top panel) and untransfected (bottom panel) cell on the same slide are shown for comparison. Bar=10 μm.

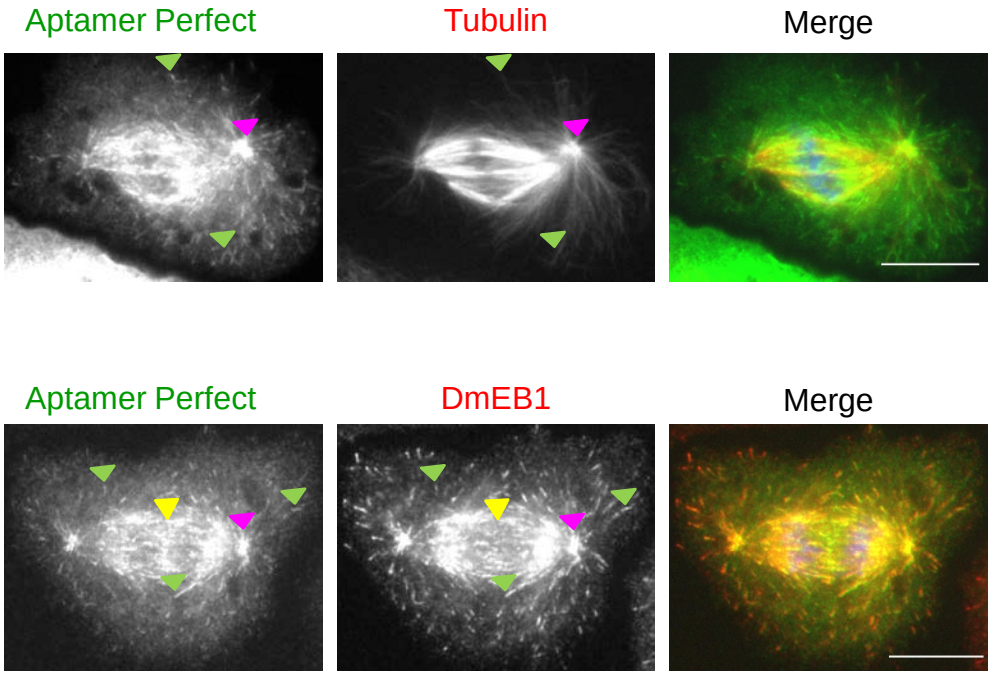

Figure 4.4 Localisation of peptide aptamers in mitotic cells
Drosophila S2 cells were transfected with plasmid encoding single constrained peptide aptamer Perfect displayed from GFP protein scaffold. GFP, tubulin and DmEB1 signals were visualised by immunostaining with anti-GFP, anti-γ-tubulin and anti-DmEB1 antibodies. The third column shows merged images from the two preceding columns. Peptide aptamer Perfect colocalised with DmEB1 at the centrosomes (purple arrowheads) and microtubule tips (green arrowheads) in metaphase (top panel). Additionally, the aptamer colocalised with the the interpolar microtubule bundles (yellow arrowheads) that separated each chromosomal mass in anaphase (bottom panel). The aptamer expression did not affect the spindle architecture. Bars, 10 μm.

peptide aptamers with respect to DmEB1 and microtubules was assessed by immunostaining, as previously.

Aptamer 37 dimer colocalised with DmEB1 in interphase cells (Figure 4.5) and did not affect microtubule organisation (Figure 4.6). However, although aptamers, 37 tetramer, Perfect dimer, Perfect tetramer or Perfect septamer, colocalised with DmEB1, localisation of DmEB1 was different in cells transfected than in the cells untransfected with the aptamers. In addition to the microtubule plus end localisation, DmEB1 localised along the microtubules and the microtubules sometimes bundled (Figure 4.7 and 4.8).

Colocalisation of the oligomerised peptide aptamers to DmEB1 confirmed their specific binding to DmEB1 in presence of endogenous proteins. However, some peptide aptamers, Perfect dimer, tetramer, septamer or aptamer 37 tetramer, affected DmEB1 localisation in the cells possibly by binding many DmEB1 molecules simultaneously and forming a higher-order structure.

4.1.3. Sentin localisation in Drosophila S2 cells expressing peptide aptamers

Sentin is one of the proteins which are recruited to microtubule plus ends by DmEB1 via SxIP (Li et al, 2011). To test whether peptide aptamers can compete with endogenous proteins for binding to DmEB1, I investigated localisation of Sentin in cultured cells expressing peptide aptamers.

Drosophila S2 cells were transfected with plasmids encoding GFP C-terminus-fused peptide aptamers under the control of actin 5C promoter and immunostained for GFP, DmEB1 and Sentin. For a control, cells were transfected with a plasmid expressing the GFP only.

By visual examination, Sentin immunostaining level at the microtubule plus ends was reduced in cells expressing peptide aptamers, Perfect, 37, T14 or T16 (Figure 4.9). To assess the extent to which peptide aptamers reduced Sentin levels at the microtubule plus ends, ~50 transfected and ~50 untransfected cells on the same slides were visually examined. The cells transfected and untransfected were scored for the comet-like staining typical for Sentin. The number of cells with typical Sentin staining was ~5% upon expression of aptamers Perfect, 37, T14 or T16 while in the untransfected cells ~90% of cells have the typical Sentin staining (Figure 4.10). To

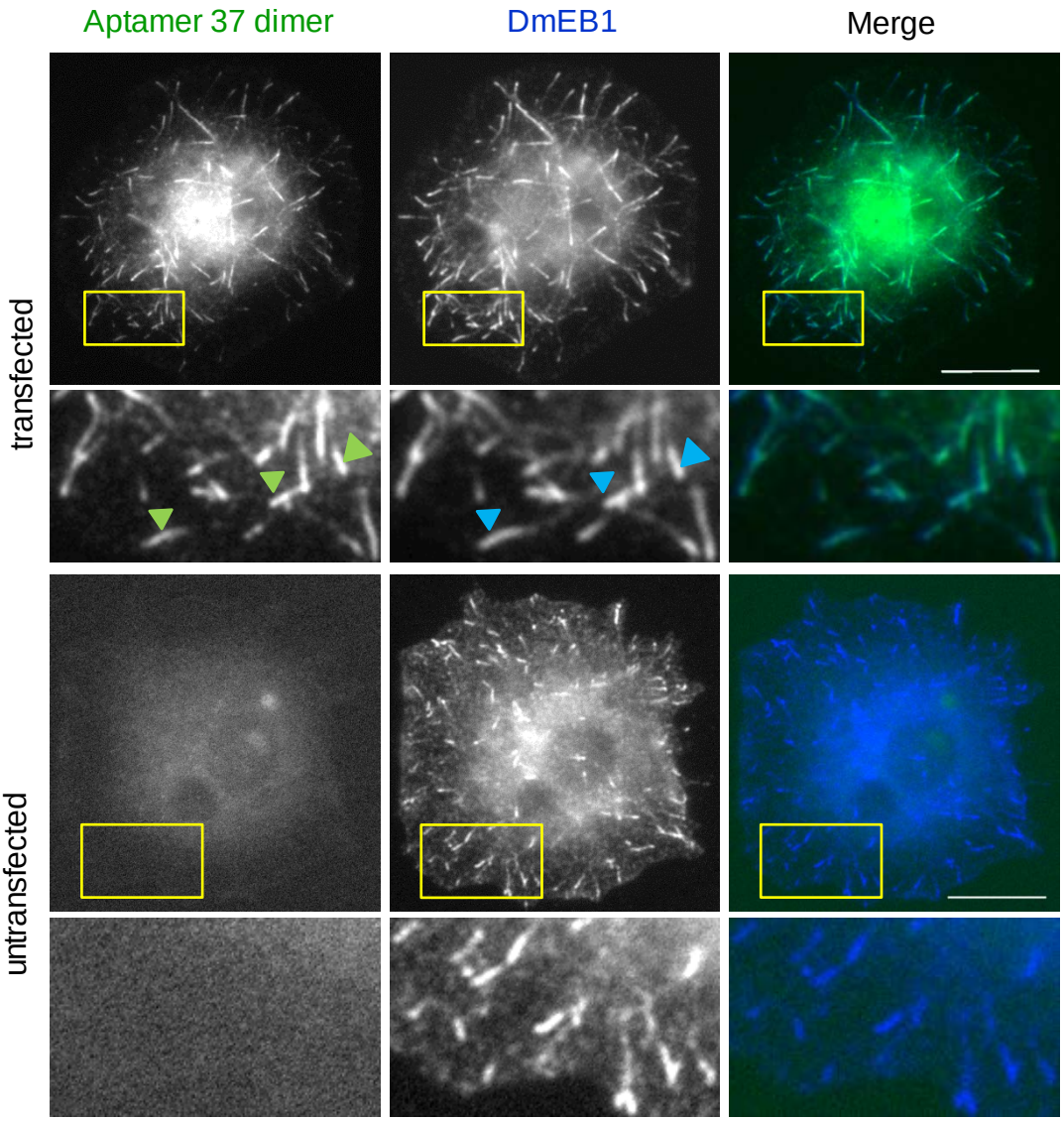

Figure 4.5 Peptide aptamer 37 dimer can colocalise to DmEB1 in interphase of Drosophila S2 cells.
Drosophila S2 cells were transfected with plasmid encoding single constrained aptamer 37 dimer displayed from GFP protein scaffold. GFP and DmEB1 signals were visualised by immunostaining with anti-GFP and anti-DmEB1 antibodies. The third column shows merged images from the two preceding columns. Peptide aptamer 37 dimer (green arrowheads) colocalised with DmEB1 (blue arrowheads) at the microtubule plus ends The aptamer expression did not affect the spindle architecture. A typical transfected (top panel) and untransfected (bottom panel) cell on the same slide are shown for comparison. Bar=10 µm. The yellow boxes indicate the areas that are magnified in the images below.

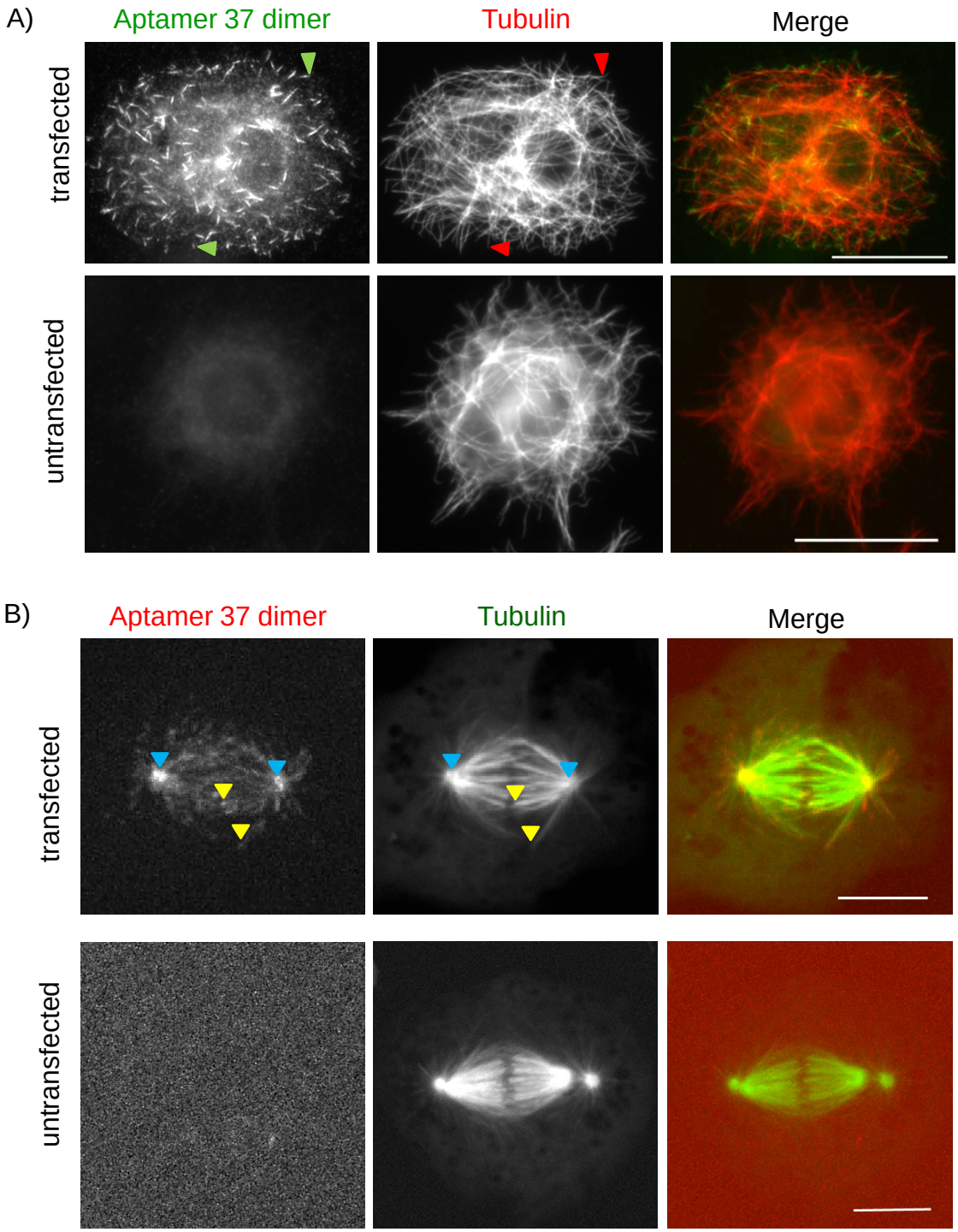

Figure 4.6 Microtubule array in Drosophila S2 cells expressing aptamer 37 dimer

Drosophila S2 cells were transfected with plasmid encoding single constrained peptide aptamer 37 dimer. (A) The aptamer was displayed from GFP protein scaffold. GFP and tubulin signals were visualised by immunostaining with anti-GFP, anti-γ-tubulin antibodies. Aptamer 37 dimer (green arrowheads) colocalises with microtubule plus ends (red arrowheads)

in interphase cells and does not affect the microtubule array. (B) The aptamer was displayed from mRFP protein scaffold in Drosophila S2 cells stably expressing GFP-tubulin. GFP and mRFP signals were visualised by laser excitation upon life imaging. Peptide aptamer 37 dimer colocalised with microtubule plus ends (yellow arrowheads) and to the centrosomes (blue arrowheads) in metaphase cells. The microtubule array was not affected in cells transfected with the peptide aptamer.
A typical transfected (top panel) and untransfected (bottom panel) cell on the same slide are shown for comparison. The third column shows merged images from the two preceding columns. Bars, 10 µm.

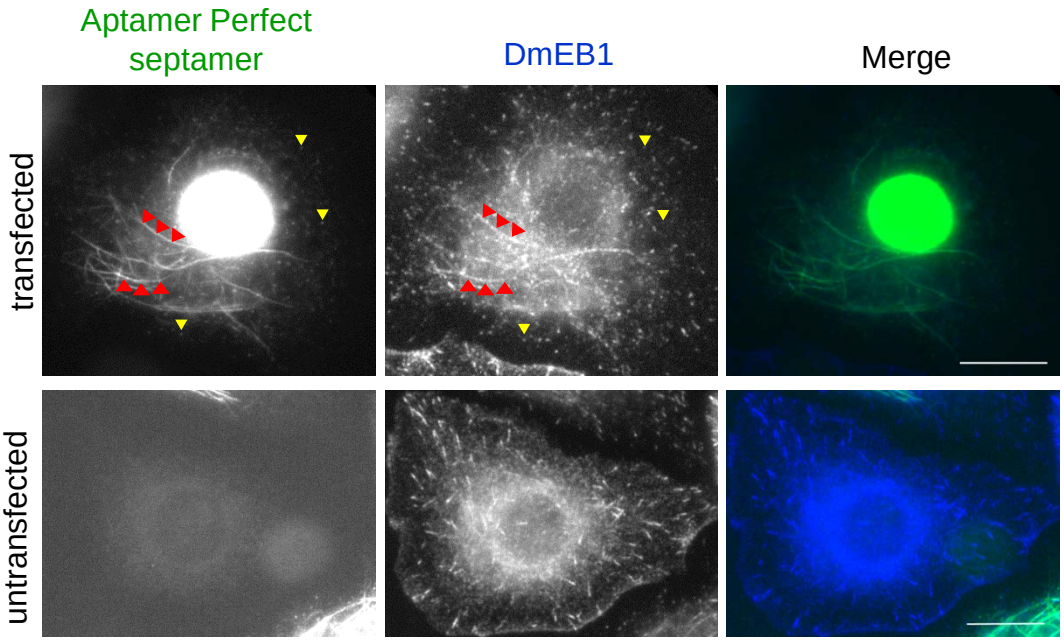

Figure 4.7 Localisation of aptamer Perfect septamer in Drosophila S2 cells

Drosophila S2 cells were transfected with plasmid encoding aptamer Perfect septamer displayed from GFP protein scaffold. GFP and DmEB1 signals were visualised by immunostaining with anti-GFP and anti-DmEB1 antibodies. The third column shows merged images from the two preceding columns. The peptide aptamer colocalised with DmEB1. Staining for the aptamer and DmEB1 revealed long bundles (red arrowheads) and comets (yellow arrowheads). The images show interphase cells. A typical transfected (top panel) and untransfected (bottom panel) cell on the same slide are shown for comparison. Bar=10 μm.

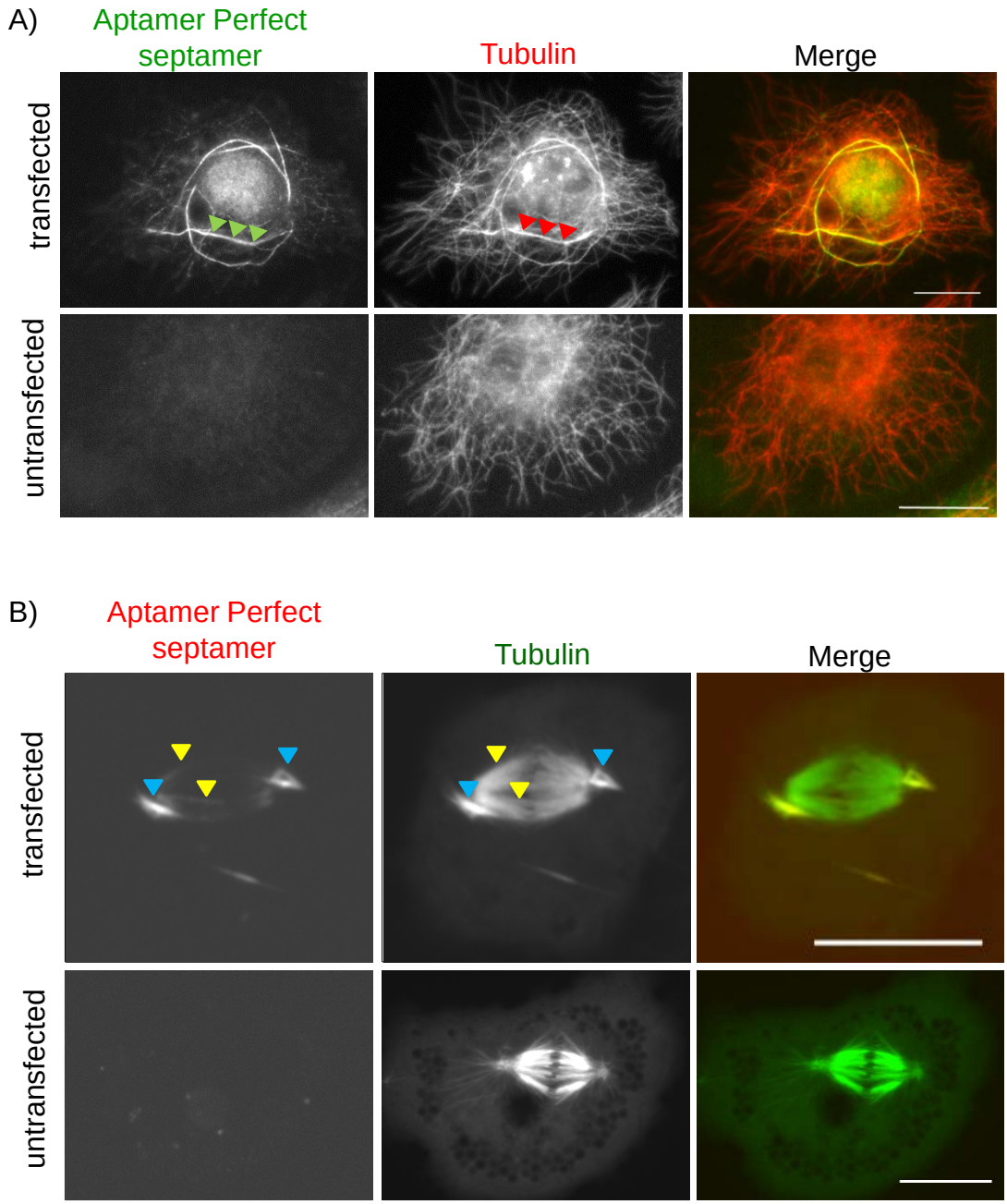

Figure 4.8 Microtubule array in Drosophila S2 cells expressing aptamer Perfect septamer

Drosophila S2 cells were transfected with plasmid encoding single constrained aptamer Perfect septamer. (A) The aptamer was displayed from GFP protein scaffold. GFP and tubulin signals were visualised by immunostaining with anti-GFP, anti-γ-tubulin antibodies. In interphase cells, in addition to the microtubule plus end localisation, aptamer Perfect septamer localised along the microtubules (green arrowheads) and microtubules sometimes bundled (red arrowheads). (B) The aptamer was displayed from mRFP protein scaffold in Drosophila S2 cells stably expressing GFP-tubulin. GFP and mRFP signals were visualised by laser excitation

upon life imaging. In mitotic metaphase cells transfected with the peptide aptamer, astral microtubules collapsed forming a blob (blue arrowheads, second panel). Peptide aptamer colocalised with the microtubules (yellow arrowheads) and with the blob at the centrosome (blue arrowheads, first panel). A typical transfected (top panel) and untransfected (bottom panel) cell on the same slide are shown for comparison. The third column shows merged images from the two preceding columns. Bars, 10 µm.

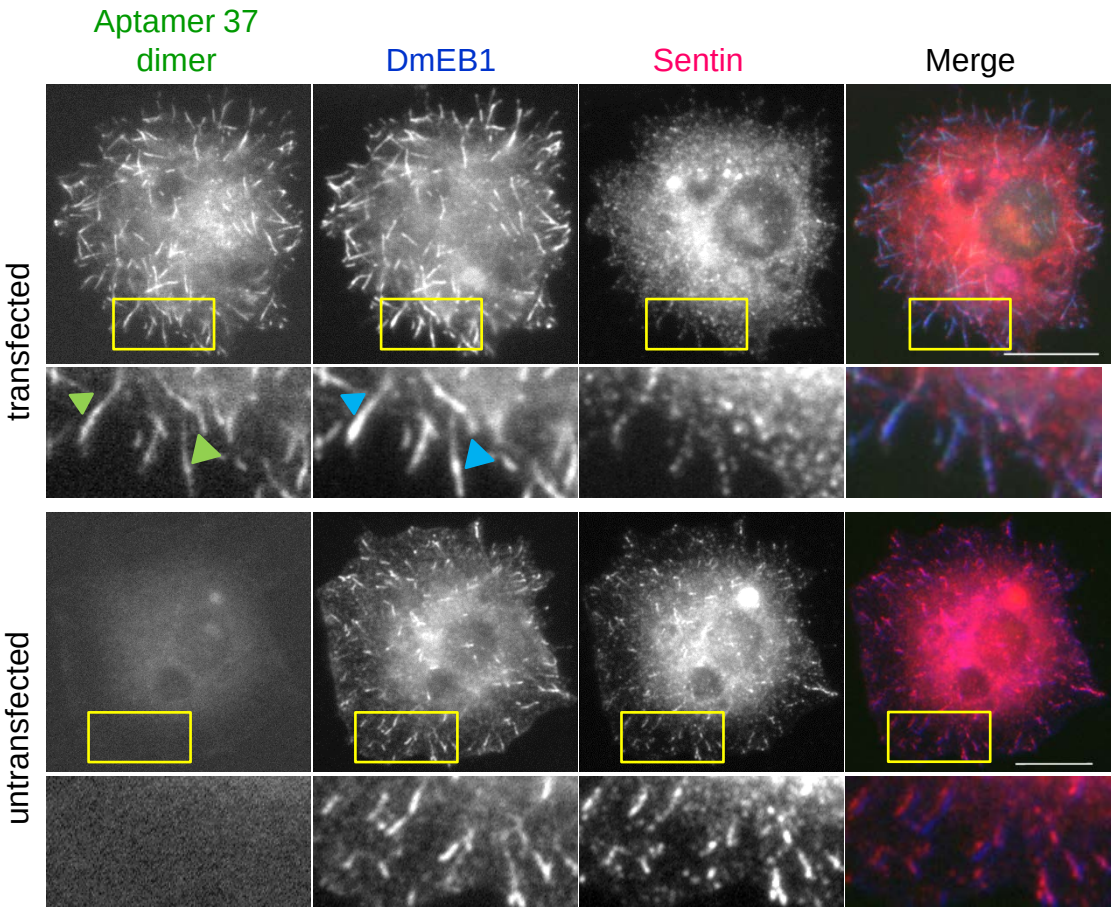

Figure 4.9 Sentin accumulation in Drosophila S2 cells expressing aptamer 37 dimer

Drosophila S2 cells were transfected with plasmid encoding aptamer 37 dimer displayed from GFP protein scaffold. GFP, DmEB1 and Sentin signals were visualised by immunostaining with anti-GFP, anti-DmEB1 and anti-Sentin antibodies. By visual examination, Sentin immunostaining level (third column) was reduced in cells expressing peptide aptamer (top panel) comparing to the cells not expressing the aptamer (bottom panel). The peptide aptamer (green arrowheads) colocalised to DmEB1 (blue arrowheads) at the microtubule plus ends. DmEB1 localisation was not affected in the cell expressing the aptamer compared to the cell not expressing the aptamer. A typical transfected (top panel) and untransfected (bottom panel) cell on the same slide are shown for comparison. The fourth column shows merged images from the three preceding columns. Bars, 10 µm. The yellow boxes indicate the areas that are magnified in the images below.

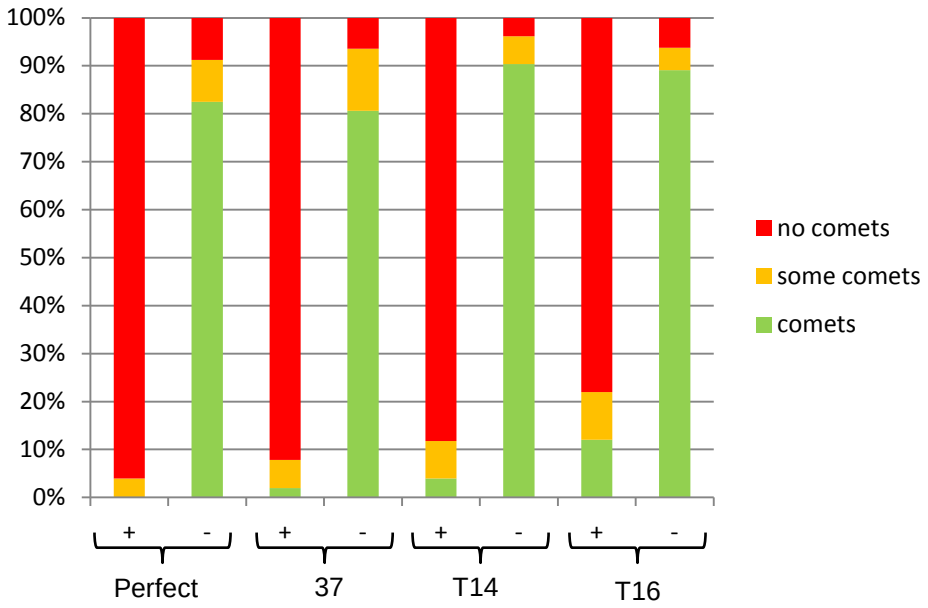

Figure 4.10 Sentin immunostaining (comets) at the microtubule plus ends in Drosophila S2 cells expressing peptide aptamers

Drosophila S2 cells were transfected with plasmids encoding aptamer Perfect, 37, T14 or T16 displayed from GFP protein scaffold. GFP , Sentin and tubulin signals were visualised by immunostaining with anti-GFP, anti-Sentin and anti-γ-tubulin antibodies. By visual examination, Sentin immunostaining level at the microtubule plus ends was reduced in cells expressing aptamers Perfect, 37, T14 or T16. To assess Sentin immunostaining signal at the microtubule plus ends, > 50 transfected and > 50 untransfected cells on the same slides were visually examined. The cells transfected and untransfected were scored for the comet-like staining typical for Sentin. ”+”; transfected cells,”-”; untransfected cells.

more quantitatively assess Sentin delocalisation, Sentin signal at the microtubules plus ends was measured in cells transfected with plasmids encoding GFP-fused aptamers or GFP only for a control. The transfected and the untransfected Drosophila S2 cells on the same slide were imaged for each of the peptide aptamers using the same exposure time. The microtubule plus end signals for DmEB1 or Sentin were calculated using S-B formula, where S is a total pixel intensity for a particular plus-end signal and B is a total pixel intensity of the equivalent area for the local background (Dzhindzhev, 2005). A hand-drawn DmEB1 area surrounding the comet was used to measure both DmEB1 and Sentin immunostaining intensities, and the local background area of the same size as the area of the comet was selected next to each comet. Three comets were measured in ten separate cells.

While Sentin signal intensity was significantly reduced in cells transfected with a plasmid expressing GFP fused aptamers Perfect, 37, 37 dimer, T14 or T16 compared with untransfected cells, the Sentin signal was not significantly reduced in cells expressing GFP alone (Figure 4.11 A). I concluded that aptamers caused Sentin displacement from the microtubule plus ends. To compare between the experiments carried out in different days, I calculated Sentin signal intensity in the transfected cells relative to the untransfected cells (Figure 4.11 B). Sentin signal was strongly reduced in cells expressing all the peptide aptamers (by at least 50%) (Figure 4.11 B). In conclusion, peptide aptamers compete with endogenous proteins for binding to DmEB1.

4.1.4. Spindle length in Drosophila S2 cells expressing peptide aptamers

Since some peptide aptamers displace Sentin from the microtubule plus ends, I investigated if expression of peptide aptamers in Drosophila S2 cells can cause shorter spindles, a phenotype specific to Sentin loss (Li et al, 2011).

Drosophila S2 cell line stably expressing GFP-fused tubulin was transfected with plasmids expressing aptamers 37, 37 dimer, T14 or T16 fused to the C-terminus of monomeric red fluorescent protein (mRFP). Cells transfected with a plasmid expressing mRFP only were included for control. A minimum of 10 metaphase spindles in transfected and untransfected cells each were imaged from the same cell

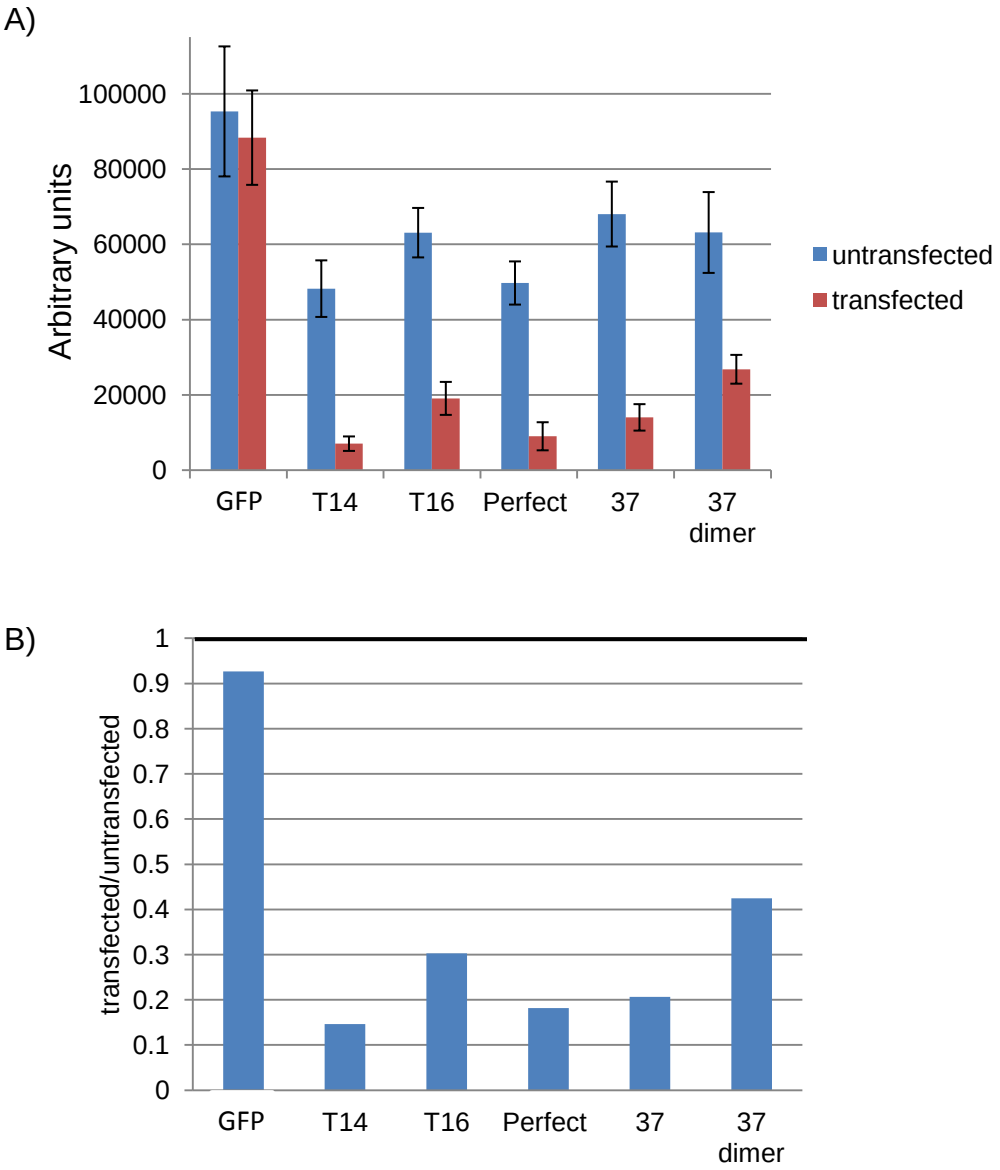

Figure 4.11 Sentin signal at the microtubule plus ends in Drosophila S2 cells expressing peptide aptamers

Drosophila S2 cells were transfected with plasmids encoding aptamer T14, T16, Perfect, 37 or 37 dimer displayed from GFP protein scaffold. GFP , Sentin and tubulin signals were visualised by immunostaining with anti-GFP, anti-Sentin and anti-γ-tubulin antibodies. (A) To assess Sentin immunostaining signal at the microtubule plus ends, Sentin signal was measured using Volocity by hand-drawing DmEB1 area surrounding the comet and the local background area of the same size as the area of the comet was selected next to each comet. Three comets each were measured in ten separate cells. (B) Sentin signal at the microtubule plus ends in cells transfected relative to untransfected. Error bars are SEM ; for control Drosophila S2 cells were transfected with plasmid encoding GFP scaffold only.

cultures. Spindle length was measured as a distance between the points where the microtubules focused.

Spindle lengths in cells transfected with peptide aptamers were not significantly different from spindles in untransfected cells ($p > 0.01$) (Figure 4.12). Even though the metaphase spindles were shorter in the Drosophila S2 cells expressing aptamer 37 dimer in the initial experiment, increasing the sample number did not reproduce significant differences. I concluded that peptide aptamers, 37, 37 dimer, T14 and T16, did not significantly affect spindle lengths.

4.1.5. CLIP-190 localisation in Drosophila S2 cells expressing peptide aptamers

CAP-Gly or SxIP motifs are commonly used to recruit proteins to microtubule plus ends in an EB1 dependent manner. However, he CAP-Gly and SxIP binding sites on EB1 partially overlap (Slep, 2010). I investigated whether CLIP-190, which is recruited to microtubules by CAP-Gly but it also has SxIP, can be outcompeted from the microtubule plus ends by peptide aptamers.

Drosophila S2 cells were transfected with plasmids encoding peptide aptamers fused to the C-terminus of GFP and the localisation of CLIP-190, DmEB1 and aptamers was assessed by immunostaining as previously. Cells transfected with each of the peptide aptamers and untransfected cells on the same slides were visually examined. Consistently with the previous results, all the peptide aptamers colocalised with DmEB1. CLIP-190 colocalised to DmEB1 in cells transfected with aptamers 37, Perfect, T14 or T16 and in the untransfected cells (Figure 4.13). For a quantitative assessment of CLIP-190 accumulation at the microtubule plus ends, CLIP-190 fluorescence signal was measured in cells transfected or untransfected with DNA encoding peptide aptamers following the same method as for Sentin (4.1.3).

CLIP-190 signal intensity was not significantly different in cells expressing aptamers 37, T14 or T16 compared to the cells not expressing these peptide aptamers (Figure 4.14 A). However, a significant decrease of CLIP-190 signal was observed in cells expressing aptamer Perfect (Figure 4.14 A). The ratio of Sentin signal from

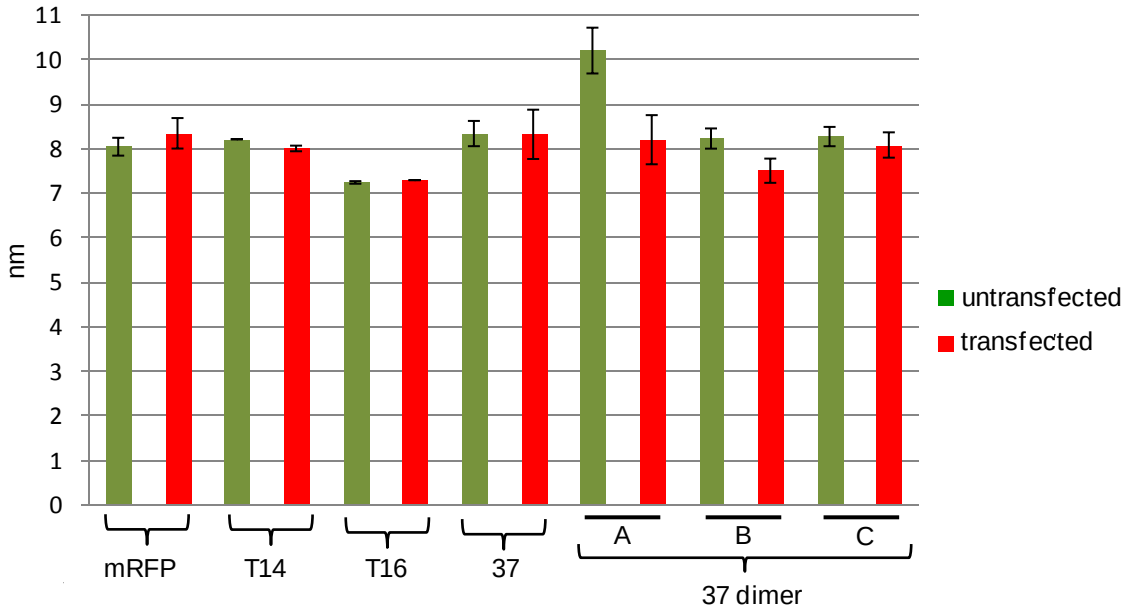

Figure 4.12 Spindle length in Drosophila S2 cells expressing peptide aptamers

Drosophila S2 cells stably expressing GFP-tubulin were transfected with plasmids encoding aptamer T14, T16, 37 or 37 dimer displayed from mRFP protein scaffold. GFP and mRFP signals were visualised by laser excitation upon life imaging. The spindle length was measured as a distance between the points where microtubules focused. Three separate experiments for aptamer 37 dimer, A, B and C, were performed, increasing the sample number in experiment B and C (at least 25 spindles in each transfected and untransfected cells were examined in each experiment). Error bars are SEM.

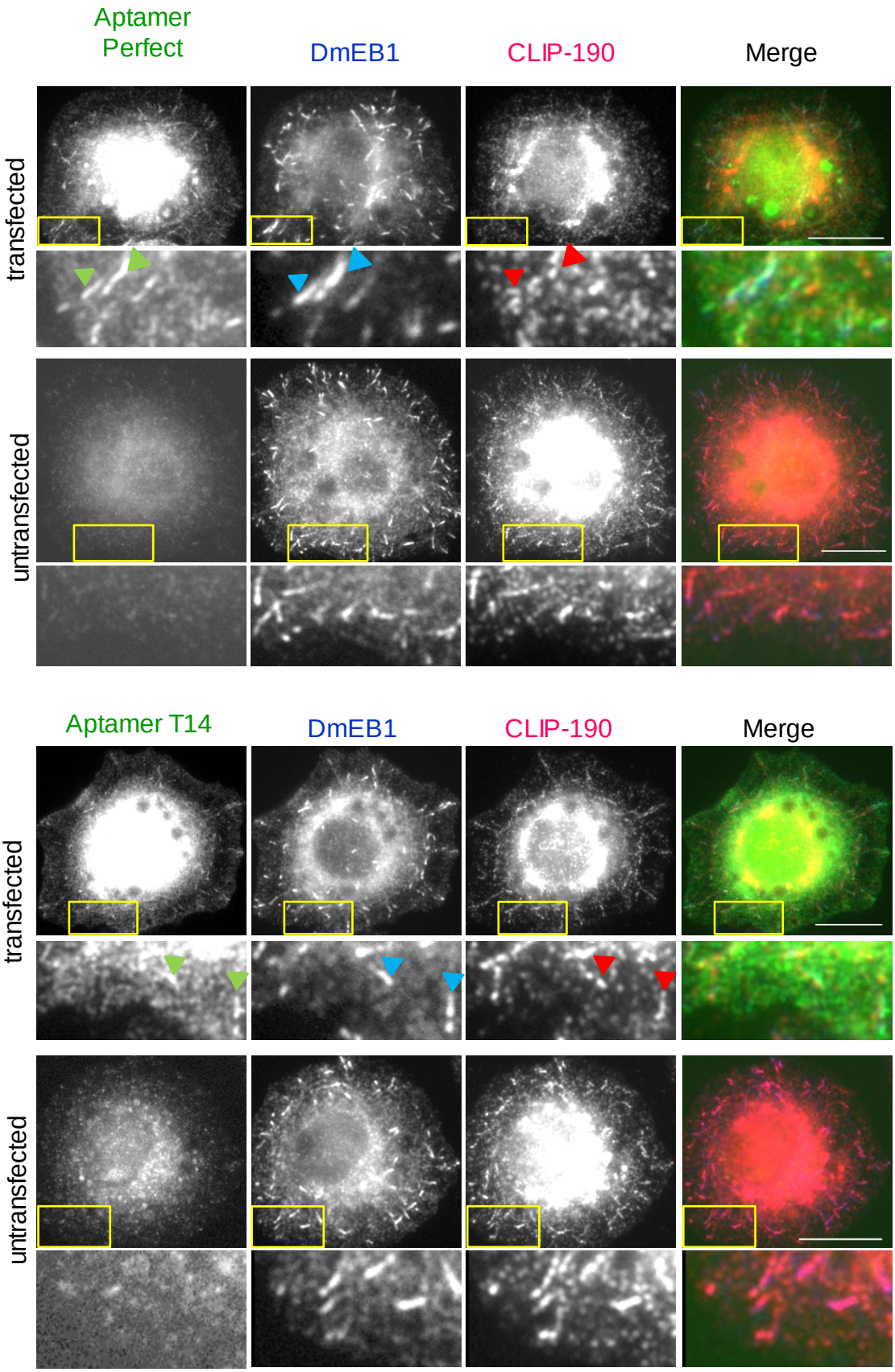

Figure 4.13 CLIP-190 accumulation in Drosophila S2 cells expressing aptamer Perfect or T14

Drosophila S2 cells were transfected with plasmid encoding aptamer Perfect or

T14 displayed from GFP protein scaffold. GFP, DmEB1 and CLIP-190 signals were visualised by immunostaining with anti-GFP, anti-DmEB1 and anti-CLIP-190 antibodies. By visual examination, CLIP-190 immunostaining level (third column) was reduced in cells expressing peptide aptamers (top panels) compating to the cells not expressing the aptamer (bottom panels). The peptide aptamer (green arrowheads) colocalised to DmEB1 (blue arrowheads) and CLIP-190 (red arrowheads) at the microtubule plus ends. DmEB1 localisation was not affected in the cell expressing the aptamer compared to the cell not expressing the aptamer. A typical transfected (top panels) and untransfected (bottom panels) cells on the same slide are shown for comparison. The fourth column shows merged images from the three preceding columns. Bars, 10 µm. The yellow boxes indicate the areas that are magnified in the images below.

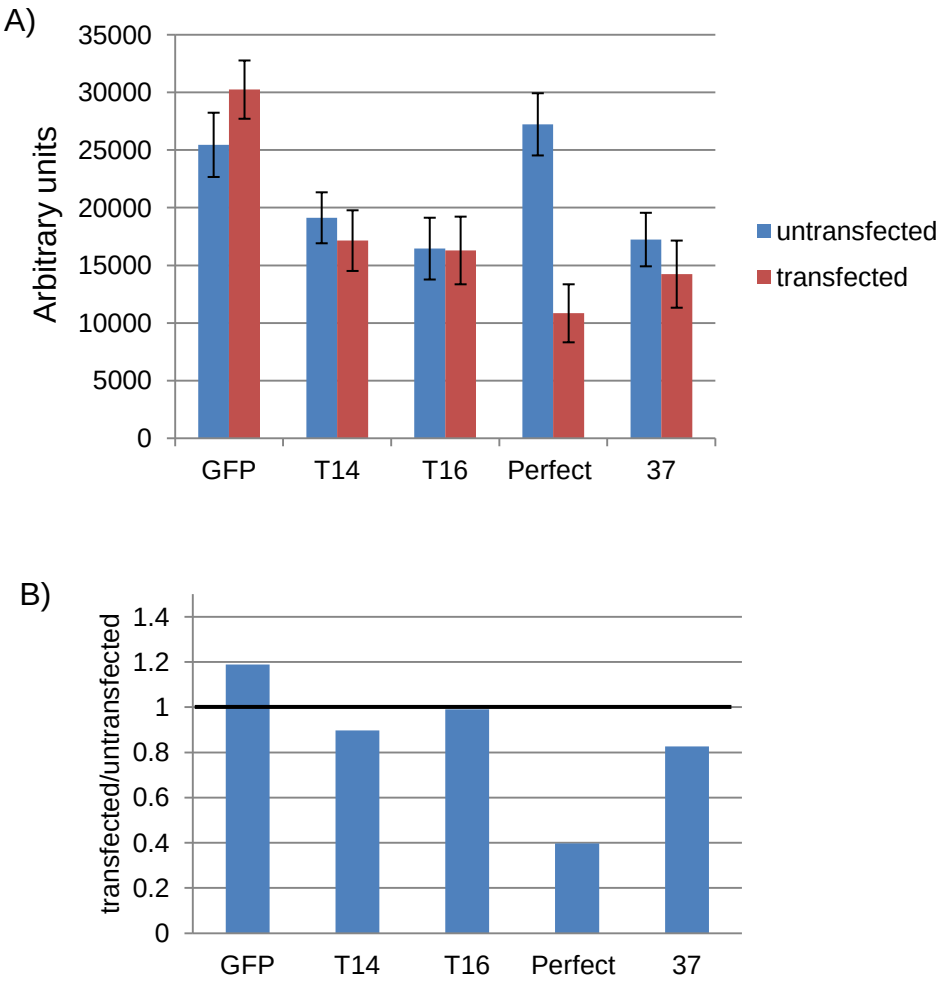

Figure 4.14 CLIP-190 signal at the microtubule plus ends in Drosophila S2 cells expressing peptide aptamers
Drosophila S2 cells were transfected with plasmids encoding aptamer T14, T16, Perfect, 37 or 37 dimer displayed from GFP protein scaffold. GFP, DmEB1 and CLIP-190 signals were visualised by immunostaining with anti-GFP, anti-DmEB1 and anti-CLIP-190 antibodies. (A) To assess CLIP-190 immunostaining signal at the microtubule plus ends, CLIP-190 signal was measured using Volocity by hand-drawing DmEB1 area surrounding the comet. The local background area of the same size as the area of the comet was also selected next to each comet. Three comets each were measured in ten separate cells. (B) CLIP-190 signal at the microtubule plus ends in cells transfected relative to untransfected. Error bars are SEM ; for control Drosophila S2 cells were transfected with plasmid encoding GFP scaffold only.

cells transfected to untransfected with aptamer Perfect was reduced by half comparing to other aptamers (Figure 4.14 B).

I concluded that aptamer Perfect, but not peptide aptamers 37, T14 or T16, can compete with CLIP-190 for the binding site on DmEB1.

4.2. Sequence requirements of aptamer Perfect to bind DmEB1

4.2.1. Interaction of Jumbled and SRAA peptide with DmEB1 in Y2H

To investigate the sequence requirements of aptamer Perfect to bind DmEB1, I addressed two questions. Is binding of aptamer Perfect to DmEB1 sequence specific or is it the overall amino acid composition that causes binding of aptamer Perfect to DmEB1? Is the amino acid sequence flanking the SxIP in aptamer Perfect sufficient for DmEB1 binding?

I tested binding of two peptides derived from the aptamer Perfect whose sequences were modified. In the first one, a “Jumbled” peptide, the amino acids order of the aptamer Perfect was changed in the region following SRIP (Figure 4.15). The second prey plasmid encoded “SRAA” peptide which resembled aptamer Perfect, except for the hydrophobic Ile-Pro which were replaced with polar Ala-Ala (Figure 4.16).

To test whether Jumbled or SRAA peptide bound to DmEB1 in Y2H, two prey plasmids encoding these peptides were constructed by gap repair as previously (chapter 3). I cotransformed yeast carrying DmEB1 bait plasmid with prey plasmid encoding peptide Jumbled or SRAA. For negative control, yeast carrying DmEB1 bait plasmid were cotransformed with empty prey plasmid and for the positive control yeast were cotransformed with prey plasmid encoding aptamer Perfect. Interactions between DmEB1 and SRAA or Jumbled peptide were assessed quantitatively. It showed that neither of the two peptides interacts with DmEB1 in Y2H assay (Figure 4.16).

Interaction of aptamer Perfect with DmEB1 depends on specific amino acids at specific positions in the region following SxIP and the SxIP motif, which are both essential for binding of aptamer Perfect to DmEB1.

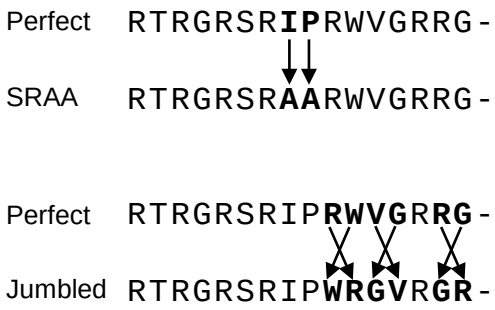

Figure 4.15 SRAA and Jumbled peptide sequences
Sequence of aptamer Perfect, that consists of the most frequently presented amino acid at each position in aptamers for DmEB1, was either shuffled following SRIP (Jumbled peptide) or the Ile-Pro in SxIP was substituted with Ala-Ala (SRAA peptide).

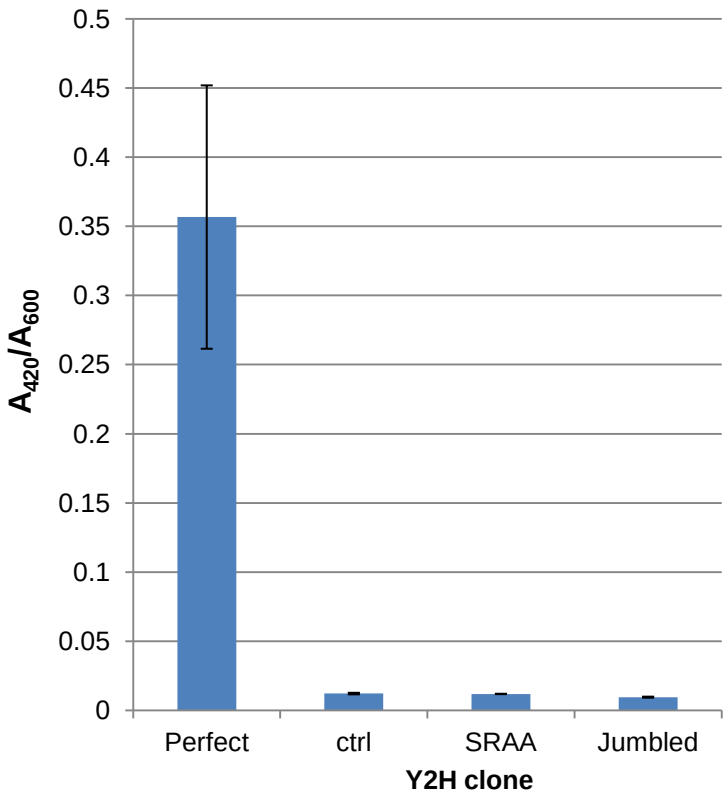

Figure 4.16 Strength of two-hybrid interactions of peptide SRAA or Jumbled with DmEB1.
Interaction strength was measured between DmEB1 and peptides whose sequence was derived from aptamer Perfect sequence: SRAA, where SxIP was replaced with SRAA; and Jumbled, where some amino acids in region flanking SxIP were shuffled. The expression of the reporter gene *LacZ* was measured by a quantitative assay for β-galactosidase activity and normalised for the cell density (A_{420}/A_{600}). The empty bait plasmid and aptamer Perfect were used as controls. The bars represent standard error of the mean (SEM; n=3).

4.2.2. Expression of Jumbled and SRAA peptide in Drosophila S2 cells

Although peptide Jumbled or SRAA did not bind to DmEB1 in yeast, I tested whether they colocalised with DmEB1 or outcompeted Sentin from the microtubule plus ends in Drosophila S2 cells.

I cloned DNA encoding Jumbled or SRAA peptide into a GFP C-terminus fusion vector under control of actin 5C promoter. Drosophila S2 cells were transfected with these plasmids or a plasmid encoding GFP only for control and localisation of peptide Jumbled or SRAA with respect to Sentin, DmEB1 and microtubule was assessed by immunostaining as previously.

Visual examination of cells transfected with plasmid for Jumbled or SRAA peptide showed that these peptides were diffused inside the cells and did not colocalise with DmEB1 at the microtubule plus ends, the same as in the untransfected cells (Figure 4.17 and 4.18). The level of Sentin accumulation at the microtubule plus ends in cells transfected with plasmid encoding SRAA or Jumbled peptide was indistinguishable from the untransfected cells (Figure 4.17 and 4.18). To assess quantitatively whether Sentin accumulation at the microtubule plus ends changed upon expression of peptide Jumbled or SRAA, I measured Sentin signal at the microtubule plus ends as previously. The Sentin signal was not significantly reduced in cells transfected with plasmid encoding for peptide SRAA comparing to the untransfected cells (Figure 4.19). However, a slight reduction of Sentin signal was observed in cells transfected with plasmid encoding for peptide Jumbled (Figure 4.19).

SxIP is critical for binding of aptamer Perfect to DmEB1. Partially jumbling amino acids flanking SxIP of aptamer Perfect abolished its interaction with DmEB1 in Y2H and, when judged by eye, peptide Jumbled did not colocalise to DmEB1 at the microtubule plus ends in Drosophila S2 cells. However, measurements of Sentin signal at the microtubule plus ends show a small difference between cells expressing and not expressing peptide Jumbled, suggesting that this peptide weakly displaces Sentin. Since the statistical difference for Sentin signal between cells expressing and not expressing peptide Jumbled was marginal ($p = \sim 0.02$), increasing the sample number would show whether they are different.

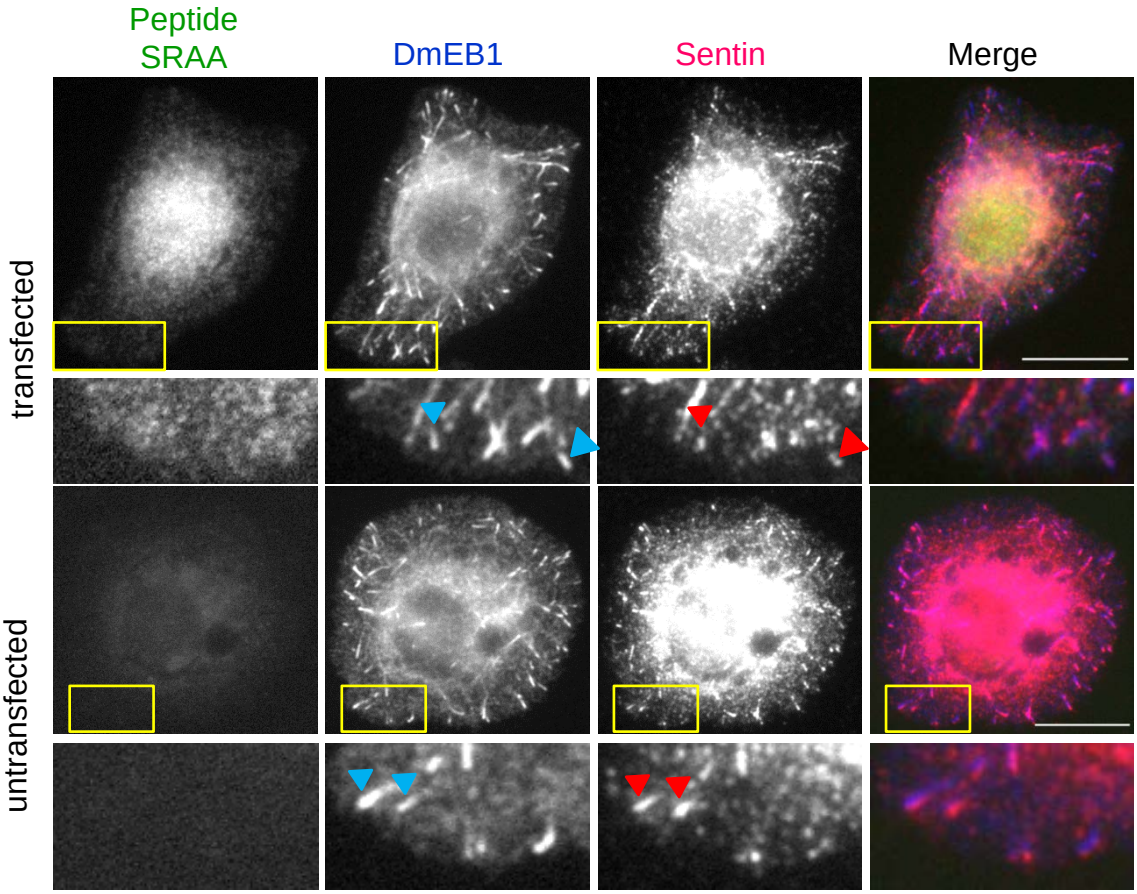

Figure 4.17 Sentin accumulation in Drosophila S2 cells expressing peptide SRAA

Drosophila S2 cells were transfected with plasmid encoding peptide SRAA displayed from GFP protein scaffold. GFP, DmEB1 and Sentin signals were visualised by immunostaining with anti-GFP, anti-DmEB1 and anti-Sentin antibodies. By visual examination, Sentin immunostaining level (third column) was not affected in cells expressing SRAA peptide (top panel). SRAA peptide (first column, top panel) was diffused inside the cell. DmEB1 (blue arrowheads) colocalised to Sentin (red arrowheads) at the microtubule plus ends. DmEB1 or Sentin localisation was not affected in the cell expressing the peptide compared to the cell not expressing the aptamer. A typical transfected (top panel) and untransfected (bottom panel) cell on the same slide are shown for comparison. The fourth column shows merged images from the three preceding columns. Bars, 10 µm. The yellow boxes indicate the areas that are magnified in the images below.

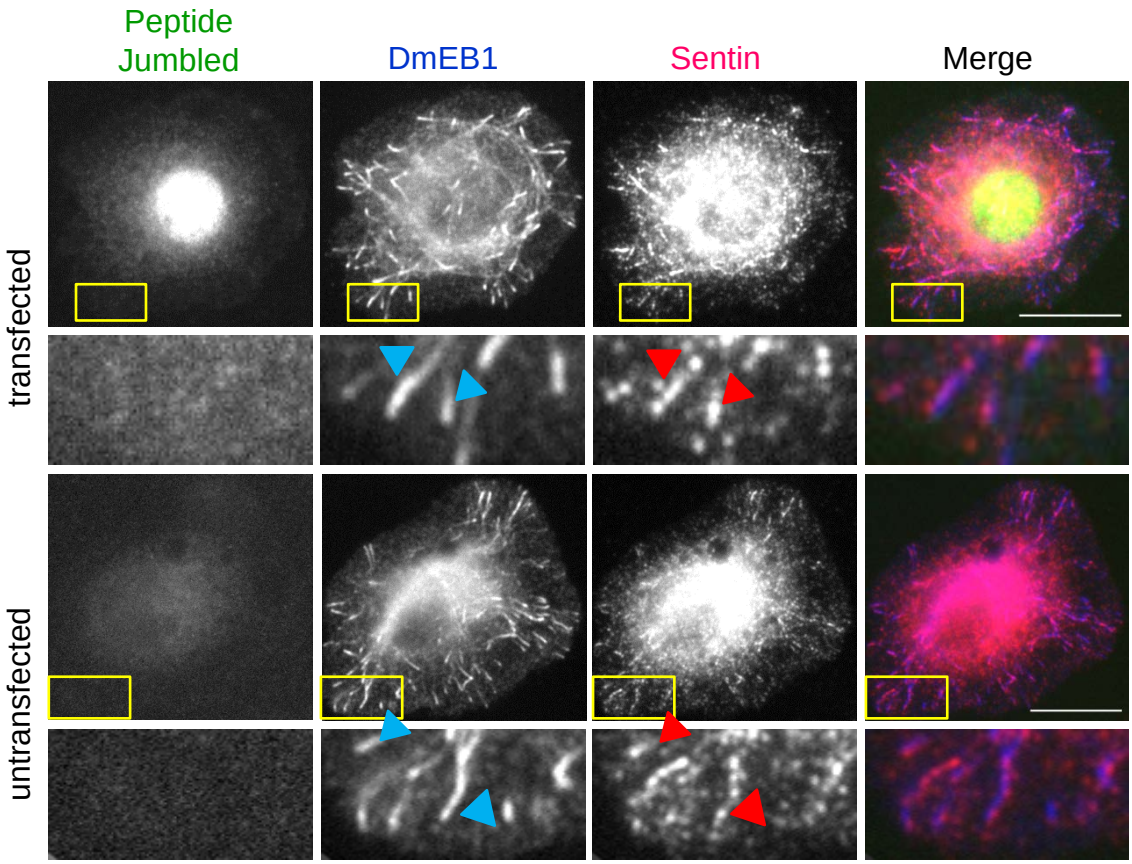

Figure 4.18 Sentin accumulation in Drosophila S2 cells expressing peptide Jumbled

Drosophila S2 cells were transfected with plasmid encoding peptide Jumbled displayed from GFP protein scaffold. GFP, DmEB1 and Sentin signals were visualised by immunostaining with anti-GFP, anti-DmEB1 and anti-Sentin antibodies. By visual examination, Sentin immunostaining level (third column) was not affected in cells expressing Jumbled peptide (top panel). Jumbled peptide (first column, top panel) was diffused inside the cell. DmEB1 (blue arrowheads) colocalised to Sentin (red arrowheads) at the microtubule plus ends. DmEB1 or Sentin localisation was not affected in the cell expressing the peptide compared to the cell not expressing the aptamer. A typical transfected (top panel) and untransfected (bottom panel) cell on the same slide are shown for comparison. The fourth column shows merged images from the three preceding columns. Bars, 10 µm. The yellow boxes indicate the areas that are magnified in the images below.

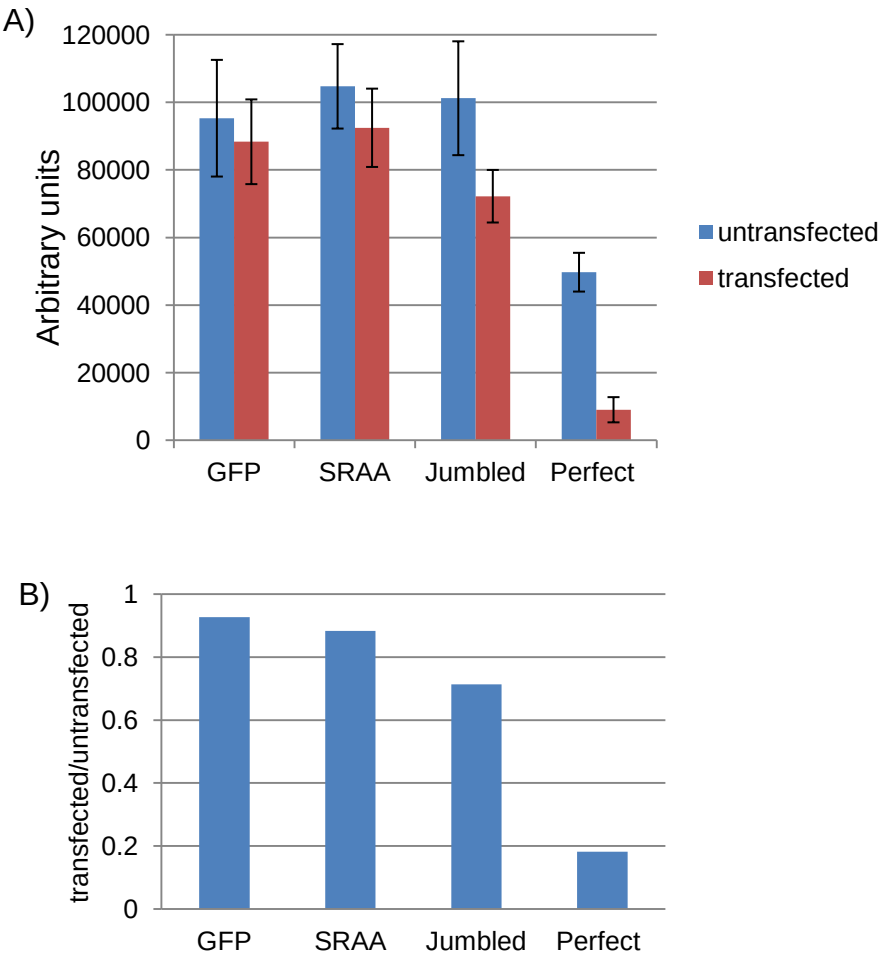

Figure 4.19 Sentin signal at the microtubule plus ends in Drosophila S2 cells expressing peptide SRAA or Jumbled
Drosophila S2 cells were transfected with plasmids encoding peptide SRAA or Jumbled displayed from GFP protein scafold. For control, cells were transfected with plasmid expressing GFP only or aptamer Perfect. GFP, DmEB1 and Sentin signals were visualised by immunostaining with anti-GFP, anti-DmEB1 and anti-Sentin antibodies. (A) To assess Sentin immunostaining signal at the microtubule plus ends, Sentin signal was measured using Volocity by hand-drawing DmEB1 area surrounding the comet. The local background area of the same size as the area of the comet was also selected next to each comet. Three comets each were measured in ten separate cells. (B) Sentin signal at the microtubule plus ends in cells transfected relative to untransfected. Error bars are SEM ; for control Drosophila S2 cells were transfected with plasmid encoding GFP scaffold only.

These results show that SxIP is critical for binding of aptamer Perfect to DmEB1 and particular amino acids at specific positions are important for the binding.

4.3. Expression of peptide aptamers in Drosophila

4.3.1. Ubiquitous aptamer expression reduces Drosophila viability

I aimed to test what effects has expression of peptide aptamers has on Drosophila. To express peptide aptamers in Drosophila, genes encoding these peptide aptamers were introduced into the Drosophila germline by P-element mediated transformation (done commercially). P-element mediated transformation is a powerful technique using transposable DNA that inserts itself randomly into genomic DNA of a Drosophila. The transformants were possible to select from the untransformed Drosophila because of an eye marker linked to the genes encoding the peptide aptamers.

To express peptide aptamers in Drosophila, I took an advantage of *GAL4*/UAS system which allows for a targeted gene expression. The system has two components which can be carried by different Drosophila lines, the *GAL4* gene specific to *S. cerevisiae* encoding GAL4, a transcription factor, and the UAS (upstream activating sequence) to which GAL4 binds and activates expression of a downstream gene (Duffy, 2002; Fischer et al, 1988). These can be brought together by genetic crossing to induce expression from a peptide aptamer gene downstream of the UAS. To ubiquitously express a peptide aptamer in a Drosophila, I introduced by genetic cross *GAL4* driven by actin 5C promoter into a Drosophila line carrying a peptide aptamer gene under UAS. For control, I introduced the *GAL4* driven by actin 5C promoter into wild-type Drosophila.

Drosophila expressing aptamer T14, 37, 37 dimer, Perfect or Perfect dimer were viable and formed a complete adult body. These Drosophila could recover into an upright position as quickly as the controls after they were turned upside down and walked normally. All the peptide aptamer Drosophila mutants were tested for viability. To quantify the Drosophila viability, a Drosophila line homozygous for a peptide aptamer gene under UAS was crossed with a Drosophila line heterozygous between chromosome carrying *GAL4* (under actin 5C promoter) and one without it.

This cross gave two types of progeny, first with *GAL4* and UAS-aptamer, allowing for expression of a peptide aptamer, and the second population which contained only the UAS-aptamer, so not expressing a peptide aptamer. A ratio was calculated of the Drosophila number representing two genotypes resulting from the cross. For all cases a relative number of adult Drosophila expressing aptamers was reduced with respect to the Drosophila not expressing the aptamers (Figure 4.20). The highest reduction (by ~80%) in viability had Drosophila expressing aptamer 37 or Perfect (Figure 4.20). Although less affected, the viability of Drosophila expressing aptamer T14, 37 dimer or Perfect dimer was also reduced (by ~60%) (Figure 4.20). The Drosophila were next tested for fertility by crossing single Drosophila expressing a peptide aptamer with wild-type Drosophila. Frequency of sterile Drosophila was not statistically significantly different comparing to the control ($p > 0.05$).

Expression of aptamers T14, 37, 37 dimer, Perfect or Perfect dimer did not affect adult Drosophila morphogenesis, fertility and locomotion. However, expressing these peptide aptamers significantly reduced Drosophila viability.

4.4. Discussion

In Drosophila S2 cells, DmEB1 is essential to maintain microtubules dynamic in interphase and it is required for accurate segregation of chromosomes by maintaining correct spindle architecture and dynamics in mitosis (Rogers, 2002). At the whole organism level, where residual amount of DmEB1 is produced, DmEB1 was shown to be essential during Drosophila development for neuromuscular functions and viability (Elliott et al, 2005). Not only being essential in Drosophila development, human EB1 is expressed in adult tissues, including tissues whose cells generally do not divide (Nakagawa et al, 2000). Consistently, DmEB1 is ubiquitously expressed in Drosophila adults, including head, abdomen and thorax (Elliott et al, 2005).

Since DmEB1 is essential for cell division, it is challenging to study its post-mitotic roles, particularly in a context of a multicellular organism. I aimed to develop a new tool to inhibit DmEB1 in adult Drosophila, also after the Drosophila came out of the pupae case. By inducing expression of peptide aptamers strongly bound to DmEB1 in specific tissues, I would be able to investigate what impact has microtubule regulation by DmEB1 in tissues of a multicellular organism.

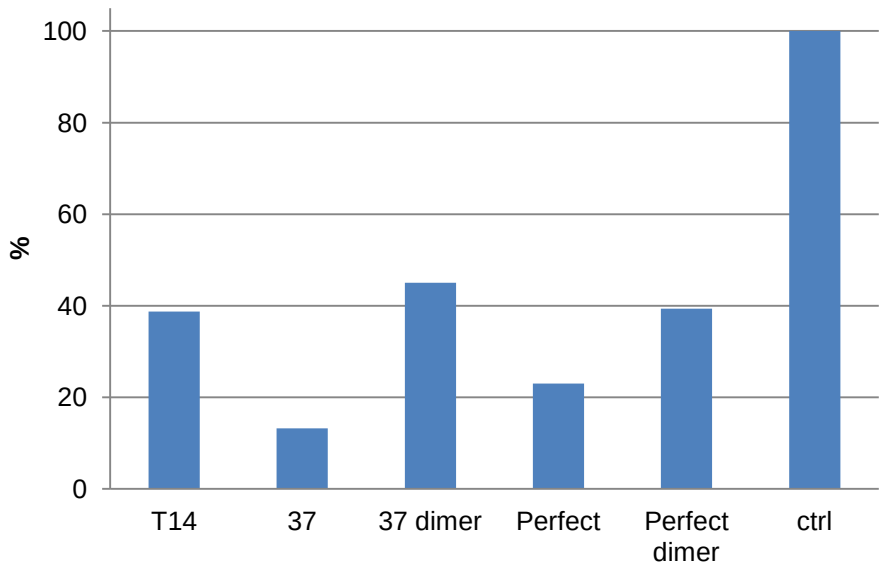

Figure 4.20 Viability of Drosophila expressing peptide aptamers
To quantify viability, Drosophila heterozygotes of *GAL4* (driven by actin 5C) and a wild-type chromosome (TM6C) were crossed with Drosophila homozygous for a peptide aptamer gene under UAS or wild-type flies for control. A relative number was calculated of the flies representing two genotypes resulting from the cross (first genotype with *GAL4* and UAS components and the second genotype which contained only the UAS component). $p = 0.02$ for aptamer Perfect and < 0.01 for the remaining peptide aptamers.

In the previous chapter, I described the use of peptide aptamers to dissect sequence determinants required for binding to DmEB1. I also found strong peptide aptamers to DmEB1. In this chapter, I showed that expressing these strong peptide aptamers in Drosophila S2 cells and in a multicellular organism of a Drosophila can be used to address biological questions.

Since I aimed to express some of peptide aptamers in a multicellular organism, it was essential for these peptide aptamers to target DmEB1 in presence of other endogenous Drosophila proteins. Drosophila S2 cells were used to investigate localisation of peptide aptamers. I showed that peptide aptamers colocalised with DmEB1 at the microtubule plus ends which was an important confirmation of their specific binding to DmEB1. Importantly, the single constrained peptide aptamers, which are considered to have lower proteolytic stability than the double constrained ones, were observed to colocalise with DmEB1, too, which confirms their presence and activity inside the cells.

This study showed that colocalisation of dimerised aptamer 37 with DmEB1 at the microtubule plus ends was more pronounced than localisation of the monomer. The finding is in agreement with a study which showed improved microtubule plus end localisation of a dimerised peptide derived from MACF (Buey et al, 2012). The other oligomerised peptide aptamers also colocalised with DmEB1 in cells, however, they sometimes changed the DmEB1 localisation. Apart from DmEB1 localising to the microtubule plus ends, it also bound along the microtubules and bundled them. It is possible that a single peptide aptamer molecule bound multiple DmEB1 and formed a higher-order structure.

Importantly, apart from binding to DmEB1, this work demonstrated that peptide aptamers also competed with endogenous proteins for binding to DmEB1. I showed that a level of a natural interactor protein at microtubule plus ends was significantly reduced in presence of all of the tested peptide aptamers. All the peptide aptamers interfered with binding to DmEB1 but none of these peptide aptamers could completely outcompete a natural interactor protein since residual amounts of Sentin were observed on some of the microtubule plus ends. This partial effectiveness of peptide aptamers may be a reason why expressing them did not

cause phenotype seen in cells depleted of that natural DmEB1 interactor (shorter spindles) (Li et al, 2011).

Since DmEB1 is one of several EB1 homologues in Drosophila (Hiro Ohkura, personal communication), it is possible that the other homologues can complement for DmEB1 when it is inactivated by peptide aptamers. I showed in chapter 3 that amino acids promoting binding of peptides containing SxIP to human EB1 or EB3, although similar, are different at some positions. The peptide aptamers which I expressed in Drosophila S2 cells may bind specifically, or stronger, to DmEB1 but not to other DmEBs, allowing these other DmEBs to recruit MAPs to microtubules. To ensure that other DmEBs do not compensate for DmEB1 inhibited by peptide aptamers, one could find and simultaneously express peptide aptamers to other DmEBs or a single peptide aptamer which binds different DmEB proteins. However, it would be necessary to first investigate what are similarities and differences of SxIP binding motifs targeted by such DmEB proteins to find a universal aptamer.

In this study, I also demonstrated that aptamer Perfect, a peptide aptamer designed by combining into one sequence amino acids which promoted binding at subsequent positions to DmEB1, colocalised with DmEB1 in Drosophila S2 cells. I also showed that this designed peptide aptamer displaced a natural DmEB1 interactor. Therefore, a synthetic peptide aptamer was generated which binds a target protein in the presence of endogenous proteins. For the first time, this work showed novel approach to finding a strong peptide aptamer which was achieved by a specific designing of the peptide which has high binding activity in presence of endogenous competitors.

I further showed that the amino acids flanking SxIP in this synthetic aptamer Perfect are not sufficient to trigger binding to DmEB1. The SxIP is crucial for binding of aptamer Perfect to DmEB1, as shown in Y2H and in Drosophila S2 cells. This finding is in agreement with another study where these Ile-Pro residues of a peptide derived from a human MAP when mutated to polar amino acids also eliminated binding of this peptide to EB1 (Honnappa et al, 2009). I also showed that the amino acid order in SxIP vicinity of aptamer Perfect is essential for interaction with DmEB1 in Y2H. Although in Drosophila S2 cells the variant of aptamer Perfect

with the changed amino acid order did not colocalise with DmEB1, this variant still weakly interfered with binding of a MAP to DmEB1. However, the interference was much less pronounced as when expressing the non-jumbled aptamer Perfect. Since the effect was subtle and statistical difference between cells expressing and not expressing jumbled aptamer Perfect was marginal ($p = \sim 0.02$), I would repeat this analysis. A similar study was performed to verify a peptide aptamer sequence specificity to its target where the amino acid sequence of a peptide aptamer was randomised (Warbrick, 2006). However, my approach used a less dramatic change of amino acids. Not only the amino acid order was changed within a much shorter region (7 vs. 16 amino acids) but also each amino acid was shifted by one position (Figure 4.15). In comparison, in Warbrick et al., 2006, amino acids were shifted from the original positions by as far as 7 amino acids. Therefore, I demonstrated that interaction of aptamer Perfect with DmEB1 is highly specific to the order of the amino acids in the peptide aptamer, further confirming that certain amino acids at very specific positions are important for the binding.

Expressing peptide aptamers in a multicellular organism has been done but it is not yet a common practice. Recently, peptide aptamers were expressed in Drosophila to demonstrate that disruption of a signalling pathway results in an abnormal wing development (Yeh et al, 2013). In this chapter, I demonstrated that the peptide aptamers I found, and the synthetic aptamer Perfect, can be also used for a protein function studies. Expressing peptide aptamers in Drosophila significantly reduced their viability (by up to 80%). Although it is most likely that this reduction in viability was caused by aptamers which disrupted recruitment of MAPs to microtubules by binding to DmEB1, one cannot exclude the possibility that these peptide aptamers targeted different proteins than DmEB1 when expressed in Drosophila. Also, assuming that these peptide aptamers inhibit DmEB1 function when expressed in Drosophila, they did not inhibit DmEB1 completely. It was previously shown that neuromuscular functions and viability were affected in mutant Drosophila expressing residual amounts of DmEB1 (Elliott et al, 2005). It would be interesting to investigate whether expressing peptide aptamers to DmEB1 in these mutant Drosophila would enhance the phenotype. Another interesting approach would be to introduce genes encoding a peptide aptamer to DmEB1 and a DmEB1

RNAi into the same Drosophila line. RNAi itself can only deplete messenger RNA and hence inhibit a protein expression, leaving the already produced protein intact. Expressing peptide aptamers in concert with RNAi could abolish the protein function. This method would be particularly valuable in differentiated cells. Since the already produced protein pool, carried from previous cells from which a tissue originates, in differentiated cells cannot be diluted by rounds of cell division, as in the mitotic cells, because differentiated cells no longer divide. Although peptide aptamers were not as effective in Drosophila as expected, they can be used to inactivate the residual DmEB1 in cells no longer expressing this protein because of RNAi. Peptide aptamers have never been used in Drosophila together with RNAi, thus it would be a novel and possibly a powerful tool to study protein functions in differentiated cells in Drosophila.

CHAPTER 5

Msps is important for neuromuscular functions

5.1. Single constrained peptide aptamers to Msps

5.1.1. Screening prey plasmid library for peptide aptamers to Msps

Msps is one of two unique MAPs which bind and track growing microtubule plus ends autonomously. In interphase cells, Msps has an antipausing activity on microtubules and in mitosis it is also responsible for keeping spindle integrity (Brittle & Ohkura, 2005; Cullen et al, 1999). Except for being abundant in the dividing cells, since it is essential for cell division, Msps is also highly expressed in brain (Charrasse et al, 1998; Gard & Kirschner, 1987). To identify post-mitotic roles of Msps in a context of a multicellular organism, I aimed to find peptide aptamers which bind to Msps. To perform Y2H screen, two bait plasmids were constructed by gap repair as previously. One bait plasmid contains N-terminal fragment of Msps including tubulin interaction region (amino acids 1-550) and the other contains C-terminal fragment of Msps including D-TACC interaction region (amino acids 1543-2042). For positive controls of Y2H, two prey plasmids were made including either full length D-TACC or α-tubulin.

Y2H prey plasmid library encoding completely random, single constrained peptides with 16 residues was constructed next and its quality was verified as previously described. The sequences were heterogeneous mixture of nucleotides encoding peptides composed of amino acid mixture without any amino acids dominating and each of the peptides was unique (Figure 5.1 and 5.2). Five out of the ten transformants contained a prey plasmid encoding 16 amino acids followed by the stop codon, as designed (Figure 5.2). A premature stop codon was present in four transformants, but three of them were still reasonably long (Figure 5.2). There was no stop codon after the 16^{th} amino acid in one transformant making the insert longer than it was designed (Figure 5.2). A chi-squared test was performed to test whether amino acids encoding the library occurred at random at each position in the library, as previously described (Figure 5.3). Amino acids occurrence on all 16 positions was random ($p > 0.05$). Since 90% of the random peptide fragments were of good composition and acceptable lengths and amino acids were encoded at random at the

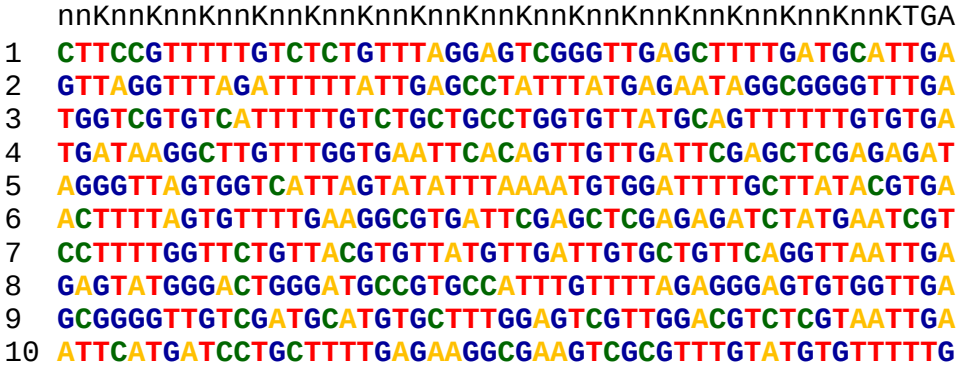

Figure 5.1 The composition of the unselected NNK prey plasmid library
Yeast were cotransformed with linearised prey vector and DNA encoding random peptides flanked by sequences corresponding to fragments of 5' and 3' on linearised prey vector for gap repair. Transformants were plated on media selective for the prey plasmid but not activation of reporters. The region embracing the insert site on the prey plasmid was amplified by PCR from clones picked at random and sequenced. The sequences were a heterogeneous mixture of nucleotides. K = G/T, n = A/T/C/G

1 **LPFLSLFRSRVELLMH**-
2 **VRFRFLLSLFMRIGGV**-
3 **WSCHFCLLPGVMQFFV**-
4 --GLFGEFTVVDSSSRD
5 **RVSGH**-YI-NVDFAYT-
6 **TFSVLKA**-FELERSMNR
7 **PFGSVTCYVDCAVQVN**-
8 **EYGTGMPCHLF**-RECG-
9 **AGLSMHVLWSRWTSRN**-
10 **IHDPAFEKAKSRLYVFL**

Figure 5.2 The composition of the unselected NNK prey plasmid library
Yeast were cotransformed with linearised prey vector and DNA encoding random peptides flanked by sequences corresponding to fragments of 5' and 3' on linearised prey vector for gap repair. Transformants were plated on media selective for the prey plasmid but not activation of reporters. The region embracing the insert site on the prey plasmid was amplified by PCR from clones picked at random and sequenced. Bold indicates translated sequence.

	position																	Average amino acid occurrence	
	1	2	3	4	5	6	7	8	9	10	11	12	13	14	15	16	17	observed	expected
Ala	1	0	0	0	1	0	1	0	1	0	0	1	0	1	0	0	0	0.38	0.63
Arg	1	1	0	1	0	0	0	1	0	1	1	2	2	0	1	1	1	0.81	0.94
Asn	0	0	0	0	0	0	0	0	0	1	0	0	0	0	0	3	0	0.25	0.31
Asp	0	0	1	0	0	0	0	0	0	1	0	2	0	0	0	0	1	0.31	0.31
Cys	0	0	1	0	0	1	1	1	0	0	1	0	0	0	1	0	0	0.38	0.31
Glu	1	0	0	0	0	0	2	0	0	1	0	2	0	1	0	0	0	0.44	0.31
Gln	0	0	0	0	0	0	0	0	0	0	0	0	1	1	0	0	0	0.13	0.31
Gly	0	1	3	1	1	1	0	0	0	1	0	0	0	1	1	1	0	0.69	0.63
His	0	1	0	1	1	1	0	0	1	0	0	0	0	0	0	1	0	0.38	0.31
Ile	1	0	0	0	0	0	0	1	0	0	0	0	1	0	0	0	0	0.19	0.31
Leu	1	0	1	2	1	2	2	2	1	1	1	0	2	1	0	0	1	1.13	0.94
Lys	0	0	0	0	0	1	0	1	0	1	0	0	0	0	0	0	0	0.19	0.31
Met	0	0	0	0	1	1	0	0	0	0	1	1	0	0	2	0	0	0.38	0.31
Phe	0	2	2	0	3	1	1	1	1	1	1	0	1	1	1	1	0	1.06	0.31
Pro	1	1	0	1	0	0	1	0	1	0	0	0	0	0	0	0	0	0.31	0.63
Ser	0	1	2	2	1	0	0	1	1	1	1	0	1	3	1	0	0	0.94	0.94
Thr	1	0	0	1	0	1	0	0	1	0	0	0	1	0	0	1	0	0.38	0.63
Trp	1	0	0	0	0	0	0	0	1	0	0	1	0	0	0	0	0	0.19	0.31
Val	1	1	0	1	1	0	1	0	1	1	4	0	1	0	2	2	0	1.00	0.63
Tyr	0	1	0	0	0	0	1	1	0	0	0	0	0	1	1	0	0	0.31	0.31
*	1	1	0	0	0	1	0	1	1	0	0	1	0	0	0	0	7	0.81	0.31
Different from expected	-	-	-	-	±	-	-	-	-	-	-	-	-	-	-	±	n/a		

Figure 5.3 The frequencies of amino acids at each position encoded by unselected prey plasmid clones from NNK library.
Yeast carrying bait plasmid were cotransformed with NNK prey plasmid library and plated on non-selective media. Prey plasmid inserts of randomly picked clones were sequenced and occurrence of amino acids at subsequent positions in these sequences was scored. Each position was tested using chi-squared test for statistical differences from the frequency expected from random DNA sequences. No significant differences were observed. "–", $p \geq 0.05$. "±", $0.01 \leq p < 0.05$.

subsequent positions within the library, I concluded that the library was of good quality.

Y2H was performed as previously described. In total, ~40 million peptides were screened for binding to Msps N-terminus. Only one transformant which activated both reporter genes was found, but later it was shown to be a false positive as expression of reporter was not dependent on aptamer. Two transformants, C2 and C28, which showed activation of both reporter genes, were found after screening ~6 million peptides for Msps C-terminus.

5.1.2. Peptide aptamers to Msps C-terminus

To determine the amino acid sequences encoded in the variable region on prey plasmids in transformants C2 and C28, these DNA fragments were amplified from yeast colonies and sequenced. While C2 was a 16 amino acid peptide as designed, C28 was 24 amino acids long due to a frameshift resulting in a delayed stop codon (Figure 5.4 A).

To exclude that expression from the *lacZ* reporter gene in transformants C2 and C28 was caused by a spontaneous mutation in plasmid or yeast, the DNA encoding the peptides was amplified and inserted back into a prey plasmid in yeast transformation as described. Both yeast carrying Msps C-terminus and cotransformed with C2 or C28 showed expression of the reporter gene. However, one of C28 transformants tested failed to express from the reporter gene. The DNA encoding the variable peptide region of this white transformant was sequenced. A missense mutation of the first base was found in the DNA encoding the variable peptide region of the prey plasmid, changing Phe to Ile (Figure 5.4 B). To exclude the possibility that C2 and C28 peptides fused to the *GAL4* activation domain induce expression of *lacZ* on their own, rather than by interaction with the bait, it would be necessary to cotransform yeast carrying empty bait vector with each of the prey plasmids.

I found two true interactors of Msps C-terminus, which are hereafter called aptamer C2 and C28. I also showed that the first amino acid of aptamer C28, phenylalanine, is important for the C28 interaction with the C-terminus of Msps.

A)

C2 IREDVLEFVAAVLIRAREIYES*

C28 FWAWFMVAYALQMHPK*

B)

peptide name	DNA sequence of a peptide encoded on a prey	Amino acid sequence of a peptide encoded on a prey	Interaction with Msps C-terminus
C28	TTTTGGGCGTGGTTTATGGT GGCTTATGCGCTGCAGATGC ATCCTAAGTGAT	FWAWFMVAYALQMHPK*	+
C28 mutant	ATTTGGGCGTGGTTTATGGT GGCTTATGCGCTGCAGATGC ATCCTAAGTGAT	IWAWFMVAYALQMHPK*	-

Figure 5.4 The amino acid sequences of the peptides found in Y2H for Msps interactors
(A) Two peptides were found in Y2H screen for interactors of Msps C-terminus, C2 and C28. (B) A point mutation in peptide C28, changing phenylalanine to isoleucine, showed that this phenylalanine is essential for interaction of C28 with Msps. Asterisks indicate stop codons. The sequence mutation resulting in amino acid substitution is highlighted in yellow.

5.2. Expression of peptide aptamers in Drosophila S2 cells

5.2.1. Peptide aptamers to Msps are diffused in Drosophila S2 cells

Since I aimed to express aptamers C2 and C28 in Drosophila, I tested whether they colocalise with Msps in presence of endogenous proteins by expressing them in Drosophila S2 cells. I expected that if peptide aptamers interact with Msps inside the cells, these peptide aptamers will colocalise with Msps. Drosophila S2 cells were transfected with a plasmid expressing GFP-fused aptamer C2 or C28 under control of actin 5C promoter. For negative control, Drosophila S2 cells were transfected with a plasmid expressing GFP only. Localisation of the aptamers was assessed by immunostaining using a GFP and a tubulin antibody. Both of the aptamers were diffused inside the cells (Figure 5.5). Microtubule array was unchanged in cells expressing the aptamers (Figure 5.5).

While Msps binds to microtubules, aptamers C2 or C28 did not colocalise with microtubules. Instead, the aptamers were uniformly diffused inside the cells. However, it cannot be excluded that these peptide aptamers interacted with the cytoplasmic pool of Msps.

5.3. Expression of peptide aptamers in Drosophila

5.3.1. Peptide aptamers have no effect on Drosophila

Although aptamers C2 and C28 did not colocalise with microtubule plus ends in cultured cells, I investigated whether their expression has an effect on a developing Drosophila. Genes encoding the peptide aptamers were introduced commercially into the Drosophila genome by P-element-mediated transformation as previously.

Taking advantage of the GAL4/UAS system, expression was induced by bringing the two components together, an aptamer gene under UAS and GAL4 under actin 5C promoter, in a genetic cross. For negative control, I introduced the GAL4 driven by actin 5C promoter into wild-type Drosophila.

Drosophila expressing aptamers C2 or C28 were viable and formed a complete adult body. The frequency of the Drosophila expressing the aptamers was not significantly different from the control Drosophila. To test whether expressing an

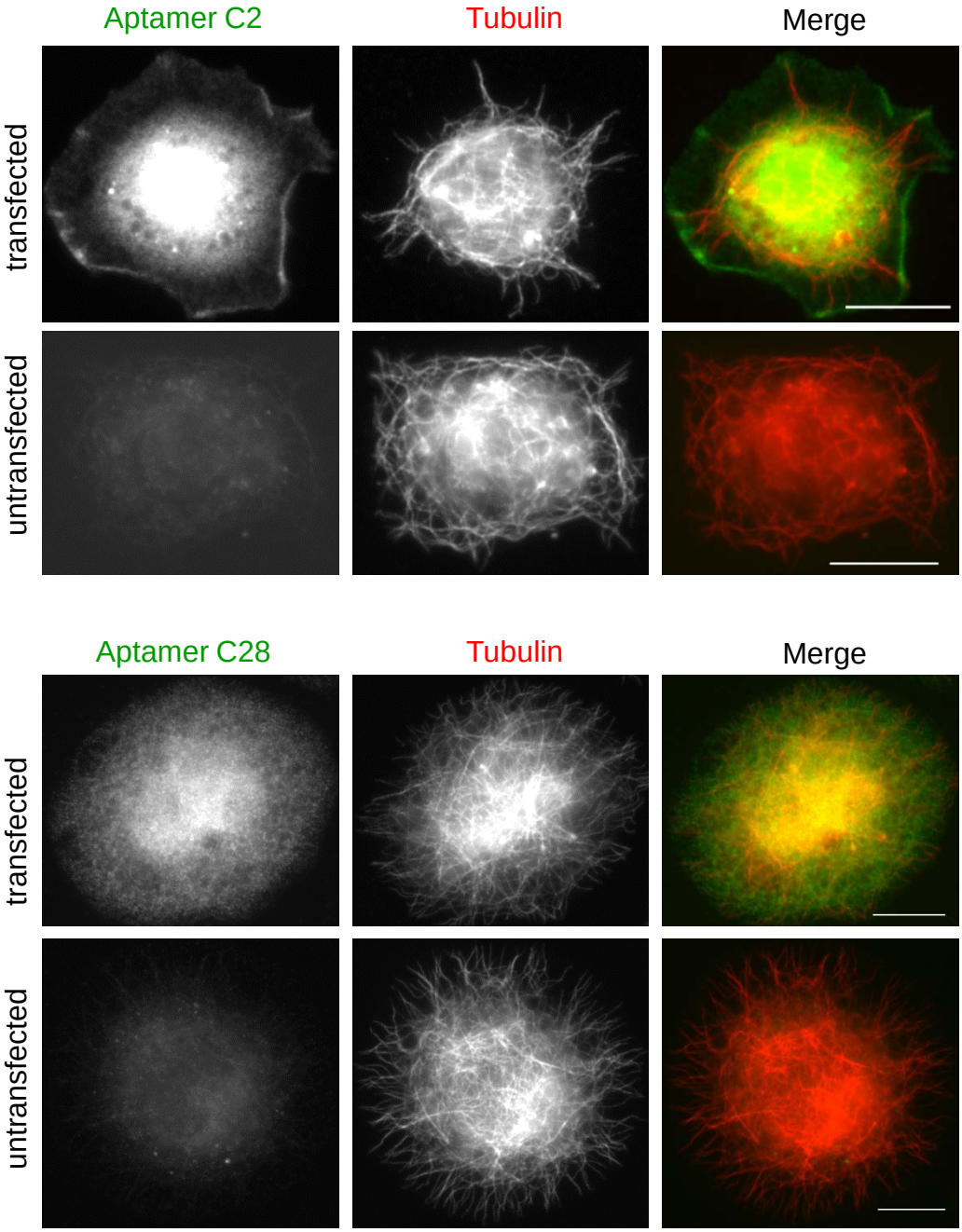

Figure 5.5 Peptide aptamers C2 and C28 are diffused in Drosophila S2 cells and do not affect microtubule array

Drosophila S2 cells were transfected with plasmid encoding peptide aptamer C2 or C28 displayed from GFP protein scaffold. GFP and tubulin signals were visualised by immunostaining with anti-GFP and anti-γ-tubulin antibodies. The third column shows merged images from the two preceding columns. The peptide aptamers were diffused inside the cells and they did not affect microtubule array. A typical transfected (top panel) and untransfected (bottom panel) cell on the same slide are shown for comparison. Bar=10 μm.

aptamer has an effect on Drosophila locomotion, the Drosophila were knocked upside-down. These Drosophila could recover into an upright position as quickly as the controls and they also walked normally. To test for fertility, single Drosophila expressing aptamer C2 or C28 were crossed with wild-type Drosophila. The frequency of fertile Drosophila expressing either of the peptide aptamers was not significantly different from the control Drosophila ($p > 0.05$).

Summarising, expression of aptamers C2 or C28 has no detectable effect on Drosophila viability, morphogenesis, locomotion or fertility.

5.4. Msps has neuromuscular functions in Drosophila

5.4.1. A temperature-sensitive msps mutant was generated

Since expression of peptide aptamers in Drosophila did not inactivate Msps, I investigated whether amino acid change equivalent to temperature-sensitive mutation in *msps* plant homologue, *mor1*, would result in *msps* temperature-sensitive Drosophila (Figure 5.6).

Transgenic *msps [E190K]* Drosophila were generated commercially by P-element-mediated transformation as previously. The plasmid used for the transformation was made by Brittle et al, 2005, and encoded a mutant gene under the control of the native *msps* promoter. The *[E190K]* mutation was generated by site-directed mutagenesis (Brittle & Ohkura, 2005).

To test if transgenic *msps [E190K]* Drosophila in the *msps* null background (as described in Figure 2.1) are temperature-sensitive, these Drosophila were grown at the permissive (18°C) or restrictive (25°C) temperature. The mutant larvae were able to pupate at both temperatures. The mutant Drosophila grown at the restrictive temperature died at early pupae. The *msps [E190K]* mutants in the *msps* null background grown at the permissive temperature came out of pupae case and looked normal. The *msps [E190K]* Drosophila in the *msps* null background were tested for fertility by crossing single Drosophila with the wild-type Drosophila. Crosses were set up at the permissive or at the restrictive temperature. The *msps [E190K]* female Drosophila were sterile at both temperatures. ~50% of male mutant Drosophila kept at permissive or restrictive temperature were fertile.

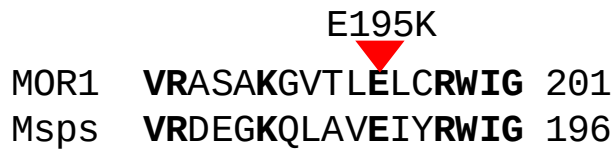

Figure 5.6 Point mutation in MOR1 and Msps causes their temperature-sensitivity.
Amino acid sequence comparison of TOG1 fragments from MOR1 and Msps. Mutation at position 195 in MOR1 and 190 in Msps (indicated by red arrowhead) leading to substitution of glutamic acid to lysine renders the proteins temperature-sensitive. Residues in bold indicate sequence identity.

I concluded that Drosophila carrying *msps [E190K]* in the *msps* null background are temperature-sensitive and hereafter called *msps*^{ts} Drosophila.

5.4.2. Msps is essential for maintenance of neuromuscular functions but not survival of adult Drosophila

To test if *msps* has a role in maintenance of adult functions, adult Drosophila carrying *msps*^{ts} were grown at the permissive temperature and then, within 24 hours after coming out of pupae, they were shifted to the restrictive temperature. Wild-type Drosophila in the *msps* null background were used for control. Drosophila were tested daily for 13 days after temperature shift for their ability to climb up the wall of the vial. The vials, one with the mutant and the other with the wild-type Drosophila, were recorded daily side by side. The *msps*^{ts} Drosophila climbed up the vial visibly slower than the control Drosophila or not at all after four days following the shift to the restrictive temperature (Figure 5.7). After nine days most of the mutant Drosophila kept at restrictive temperature did not climb up the vial (Figure 5.7). Therefore *msps* has a role in maintenance of neuromuscular functions of adult Drosophila.

From day one after coming out of the pupae case, some of the mutant Drosophila had abnormally spread wings or held their wing(s) out and up and moved them in an uncoordinated way. To assess their flying abilities, flight tests were performed similar to that described by Benzer et al. (1973) with modification of the cylinder, which was lined with a moist tissue paper to reduce static electricity (Benzer, 1973). *msps*^{ts} mutants, or wild-type Drosophila for the control, were grown at the permissive temperature and shifted to the restrictive temperature within 24 hours after they came out of pupae case or were kept at the permissive temperature. Drosophila were assessed for flying abilities daily by releasing them individually into a cylinder through a funnel (Figure 5.8 A). The approximate height where a Drosophila landed in the cylinder was recorded. Next, statistical analyses showed that *msps*^{ts} Drosophila, regardless the temperature, were significantly different from the wild-type Drosophila ($p < 0.01$). The median values for the flight of the mutant Drosophila were lower than for the wild-type Drosophila (Figure 5.8 B). No significant differences were found between mutant or wild-type Drosophila grown at

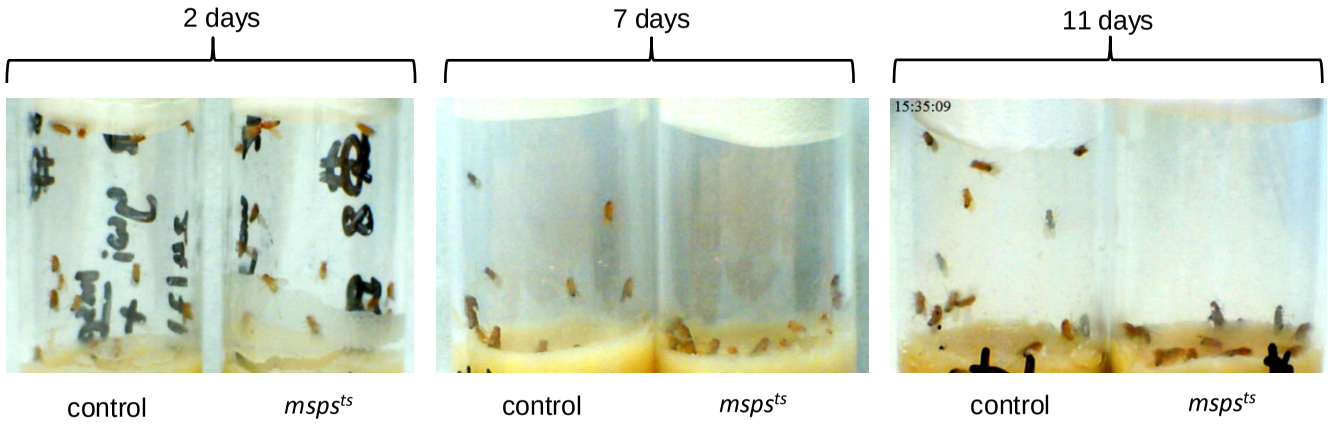

Figure 5.7 Temperature shifts of adult *msps*^{ts} Drosophila

Adult *msps*^{ts} Drosophila grown at the permissive temperature were shifted to the restrictive temperature within 24 hours after coming out of pupae case. Wild-type Drosophila in the *msps* null background were used for control. Vials were tapped and the snapshot was taken after 3 seconds. Drosophila were tested daily for 13 days after temperature shift for their ability to climb up the wall of the vial. The *msps*^{ts} Drosophila climbed up the vial visibly slower than the control Drosophila or not at all after four to nine days following the shift to the restrictive temperature and the difference was striking following nine days at restrictive temperature.

A)

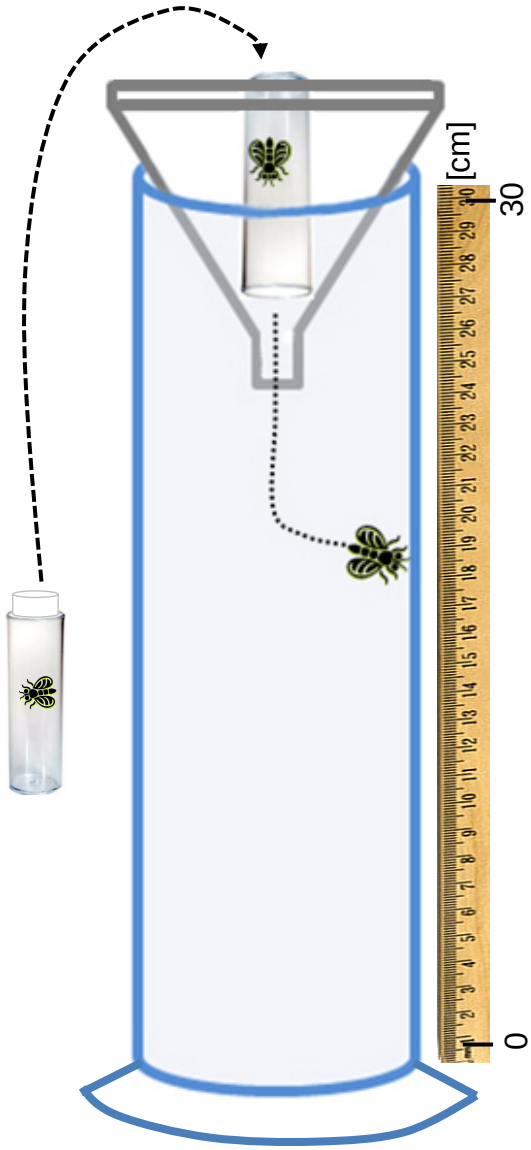

B)

	Median [cm]	
Day	*msps*^{ts}	wild-type
1	0	27
2	0	25
3	4	24
4	0	28
5	0	26
6	18	27
7	0	26
8	18	26
9	4	28
11	0	26
12	0	26

Figure 5.8 Flying of *msps*^{ts} Drosophila is compromised
Adult *msps*^{ts} Drosophila grown at the permissive temperature were shifted to the restrictive temperature within 24 hours after coming out of pupae case. Wild-type Drosophila in the *msps* null background were used for control. (A) Drosophila were assessed for flying abilities daily by releasing them individually into a cylinder through a funnel, gently tapping avial. An approximate height where a Drosophila landed in the cylinder was recorded. (B) The median values (in centimetres) were calculated.

permissive temperature from the mutant Drosophila grown at restrictive temperature ($p > 0.01$).

Hence the *msps [E190K]* mutation has a negative effect on neuromuscular abilities of Drosophila in both permissive and restrictive temperature. These results showed that *msps* is important for maintenance of neuromuscular functions in adult Drosophila.

5.4.3. Msps is essential for neuromuscular functions in developing Drosophila pupae

To test if Msps affects development of Drosophila pupae, Drosophila were crossed at permissive temperature to obtain $msps^{ts}$ progeny. Pupae were picked up each day (1-24, 24-48, 48-72, 72-96, 96-120 and 120-144 hour) after pupation and transferred to the restrictive temperature. For the control, a vial of the mutant pupae was kept at the permissive temperature.

Almost all, 97%, of 100 tested $msps^{ts}$ pupae shifted to 25°C earlier than 72 hours after pupation failed to emerge from the pupae (Figure 5.9). Dissection of pupae indicated that a complete adult body was formed inside the pupae case and limited leg movement was observed in some. Half of $msps^{ts}$ Drosophila shifted to 25°C four days after pupation came out from pupae (22 out of 44) but almost all of them, 18 Drosophila, were unable to walk (Figure 5.9). Two mutant adults (~10%) which emerged moved in an uncoordinated way and it took them significantly longer than the wild-type Drosophila to correct their body positions once pushed upside down. A large majority, 10 out of 13 (~80%), of $msps^{ts}$ Drosophila shifted to the restrictive temperature from five days after pupation emerged from pupae (Figure 5.9). While half of them could walk normally, the other half was uncoordinated and they failed to recover their correct body position promptly once upside down. All nine control Drosophila kept at 18°C throughout the development emerged from pupae and seven (~80%) of them were fully coordinated (Figure 5.9).

Therefore Msps is important for neuromuscular functions in developing Drosophila. The time period of 0 – 4 days (at 18°C) after pupation is critical for the majority of Drosophila to emerge and move normally.

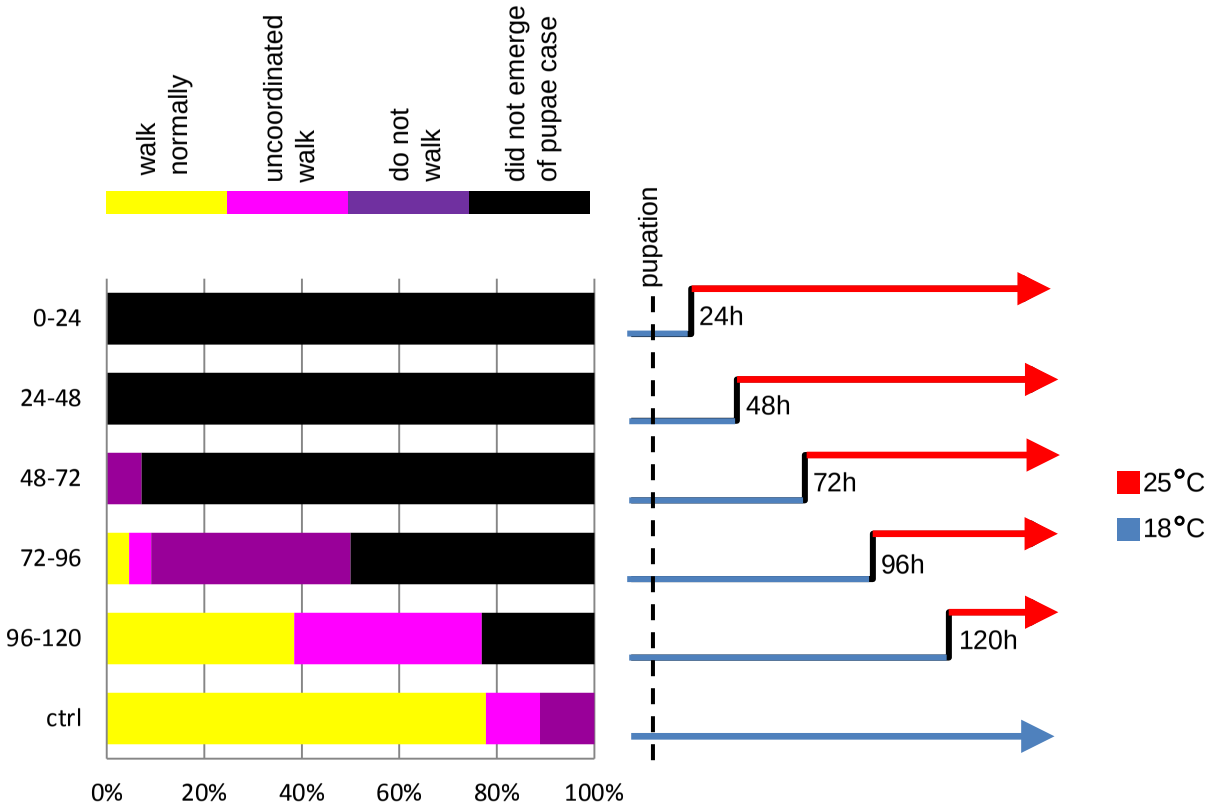

Figure 5.9 Temperature shift-up of *msps*^{ts} Drosophila pupae

msps^{ts} Drosophila pupae grown at permissive temperature (18 ℃) were picked up daily (0-24, 24-48, 48-72, 72-96 and 96-120 hours) after pupation and shifted to restrictive temperature (25 ℃). For control, pupae were kept at permissive temperature. Shifting Drosophila to the restrictive temperature earlier than 96 hours post pupation had severe effect on their walking abilities.

To narrow down the time period when *msps* is particularly important in developing pupae, $msps^{ts}$ larvae grown at 18°C were shifted to 25°C at pupation (Figure 5.10). Following incubations of half, one, one and a half or two days (0-12, 12-24, 24-36 and 36-48 hours) at restrictive temperature, the pupae were shifted back to the permissive temperature. The vast majority (23 out of 28) of the $msps^{ts}$ Drosophila developing at the restrictive temperature for 12 hours from pupation emerged from pupae and 17 of them were fully coordinated (Figure 5.10). The remaining 6 of mutants had significant coordination problems. Less than 50% (41 out of 86) of the mutants developing at the restrictive temperature for 24 hours from pupation emerged from pupae but 37 of them did not walk at all (Figure 5.10). A complete adult body was formed inside the pupae case and limited leg movement was observed.

Therefore, msps is critical for neuromuscular functions in developing Drosophila pupae in the time period from 12 to 48 hours at 25°C from pupation.

5.5. Discussion

In this chapter, I described work aiming to inactivate Msps, another crucial regulator of microtubule dynamics. Similarly to DmEB1, I tried to identify peptide aptamers to disrupt protein interactions with Msps. Moreover, I generated a new tool, a *msps* temperature-sensitive Drosophila, allowing to study role of microtubule regulation by Msps in multicellular organism.

To find peptide aptamers to Msps, I used Msps fragments rather than the full length protein in Y2H. Firstly, Msps is a large protein (2050 amino acids) which could cause handling difficulties. Secondly, since the major interaction sites of Msps have been mapped (tubulin binding occurs via N-terminal TOG domains and D-TACC binding via the C-terminus), I targeted peptide aptamers to disrupt specific interactions (Lee et al, 2001; Slep & Vale, 2007). Two peptide aptamers to Msps C-terminus were found but I did not find any peptide aptamers binding to the N-terminus. A possible explanation for the difficulty in finding interactors of the N-terminus of Msps is the structure of TOG domains. The crystal structure of TOG domains shows that there are no clefts present where a small interactor, such as a

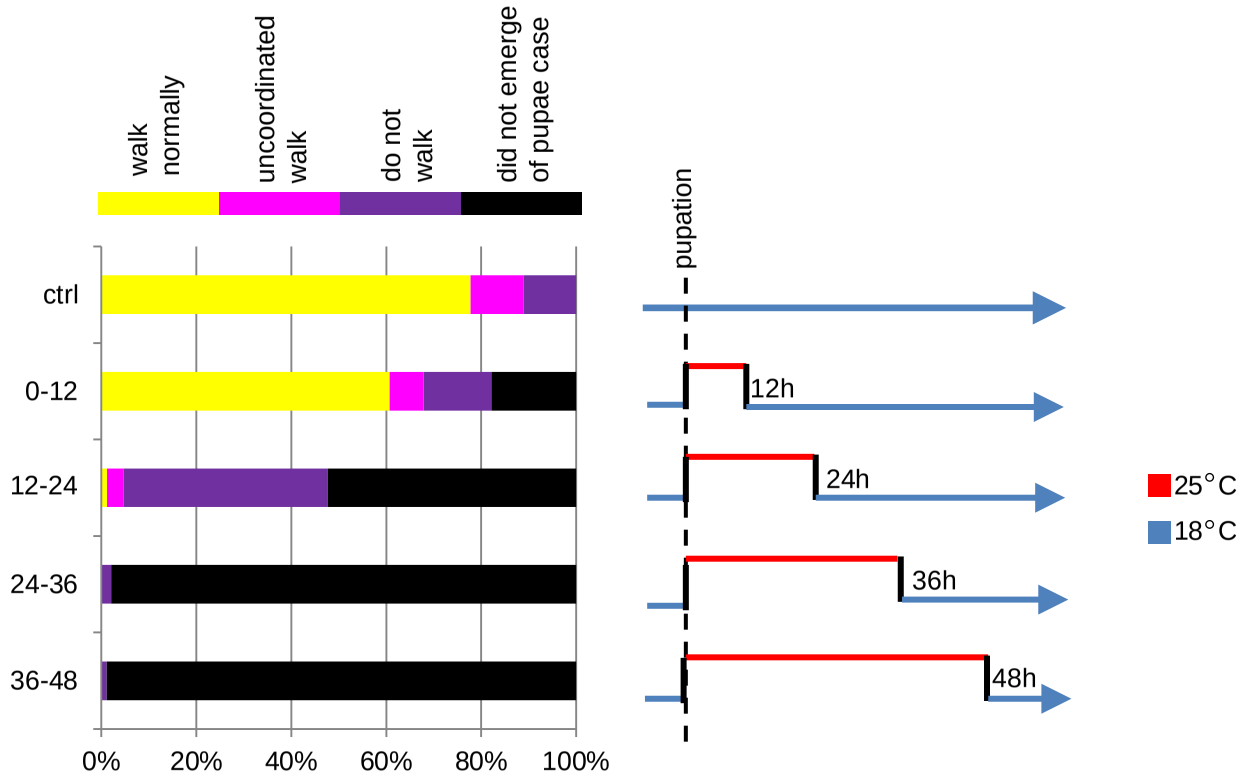

Figure 5.10 Temperature shift-down of *msps*^{ts} Drosophila pupae
msps^{ts} larvae grown at permissive temperature (18°C) were shifted to restrictive temperature (25°C) at pupation. Following incubations of half, one, one and a half or two days (0-12, 12-24, 24-36 and 36-48 hours) at 25°C, the pupae were shifted back to the permissive temperature. Shifting Drosophila to the restrictive temperature for more than 24 hours post-pupation had severe effect on their walking abilities.

peptide aptamer, could dock. Also, Msps binds to tubulin via multiple interfaces generated by TOGs arrayed in tandem.

Next, the two peptide aptamers were expressed in cultured cells to investigate their localisation. I expected that if a peptide aptamer interacts with Msps, I would see an aptamer localising along the microtubules, the same as localisation of Msps. Although these peptide aptamers were evenly diffused inside the cells and I did not see their colocalisation with microtubules, it is possible that they still interacted with the cytoplasmic pool of Msps. However, another possibility is that C2 and C28 peptides fused to the *GAL4* activation domain in two-hybrid screen induced expression of *lacZ* on their own. To exclude this possibility, it would be necessary to cotransform yeast carrying empty bait vector with each of the prey plasmids to see if they express from the reporter gene.

These peptide aptamers were further expressed in Drosophila. However, expression of aptamers did not have any strong effect on Drosophila viability, morphogenesis, locomotion or fertility.

Peptide aptamers did not inactivate Msps but a different tool was presented in this study. I showed that an amino acid change in *msps*, equivalent to a temperature-sensitive mutation in plant homologue, *mor1*, results in *msps* temperature-sensitive Drosophila.

Msps is required for cell division and it is not only highly expressed in proliferating tissues but also in brain, which is mostly composed of differentiated cells (Charrasse et al, 1998; Cullen et al, 1999; Gard & Kirschner, 1987). Similarly to DmEB1, studying the function of a protein which is necessary for cell division at a whole organism level is challenging. *msps* null mutant Drosophila are available but these mutants die around larvae-pupae transition (Cullen et al, 1999). The temperature-sensitive *msps* mutant Drosophila are an improvement in studies of Msps because these mutants will allow investigation of the roles of the protein in adult Drosophila.

Initially, I investigated whether *msps* affects adult Drosophila in different stages of adulthood. I showed that Msps has neuromuscular functions in developing Drosophila. Shifting *msps* temperature-sensitive Drosophila at the pupae stage to the restrictive temperature for different amounts of time caused neuromuscular defects

ranging from uncoordinated movement, through walking difficulties to various degrees as well as partial or complete failure of emergence from the pupae. I also investigated whether Msps has a role in Drosophila after their emergence from the pupae by shifting *msps* temperature-sensitive Drosophila to the restrictive temperature. These Drosophila, five days after the shift, climbed up the wall of a vial visibly more slowly than the control and some of them did not climb up the vial at all. I showed that Msps is important for maintenance of neuromuscular functions in these adult Drosophila. I further confirmed that *msps* has neuromuscular functions in adult Drosophila by flight tests, where *msps* temperature-sensitive Drosophila did not fly as well as the control Drosophila. Therefore, *msps* is important for neuromuscular functions in Drosophila pupae as well as in Drosophila that came out of pupae case.

However, I showed that the $msps^{ts}$ mutation is not fully functional at the permissive temperature since the Drosophila did not fly as well as the control Drosophila and they are also female sterile. It is important to be careful when $msps^{ts}$ Drosophila are used as a control. It would be interesting to find out whether the protein expression level is changed in the mutant Drosophila at both permissive and restrictive temperatures compared with the wild-type Drosophila.

Previously, *msps* deficient embryos were shown to be defective in axonal fascicle morphology (incorrect bundling, axons and fascicles were wavy) (Lowery et al, 2010). I would like to investigate whether the neuromuscular defects that I observed in the adult Drosophila were also caused by abnormal neuron morphology, possibly leading to defective pathfinding by neurons and consequently, wrong neurone-muscle connections. Also, it is interesting to test whether neuromuscular junctions formed correctly in *msps* mutant adult Drosophila. Further, I would like to examine the organisation of microtubules in neurons of adult mutant Drosophila. Generating a *msps* temperature-sensitive mutant Drosophila will allow investigation of the role of Msps in neurons of adult Drosophila for the first time.

CHAPTER 6

Conclusions

Microtubules are highly regulated by MAPs to perform variety of functions in different types of cells. The same MAPs can regulate microtubule dynamics and organisation both in mitosis and in post-mitotic cells. However, it is a challenge to study non-mitotic functions of proteins essential for cell division at a whole organism level. To overcome the problem, I developed new tools: a *msps* temperature-sensitive Drosophila to study roles of Msps and peptide aptamers to interfere with DmEB1 interactions.

In this thesis I described the isolation of aptamers to DmEB1 which is central in regulating microtubule dynamics by recruiting many proteins to growing microtubule plus ends. I biased aptamer libraries by introducing invariant SxIP into a randomised amino acid sequence which improved efficiency of screening. This resulted in finding many aptamers which provided vital information on sequence determinants for DmEB1 binding. Although the SxIP motif was identified essential for binding of many MAPs to EB1, based on being overrepresented in known EB1-binding fragments, it is not sufficient (Honnappa et al, 2009). Many proteins which have SxIP do not bind to EB1; the sequence flanking the motif has important stabilising effect on EB1-SxIP interaction (Buey et al, 2012). To find out what amino acids in the region flanking SxIP promote binding to HsEB1, a study was performed where each residue was systematically replaced in a MACF-derived fragment and tested for HsEB1 binding *in vivo* (Buey et al, 2012). The approach presented in this thesis was opposite; aptamers for EB proteins: DmEB1, HsEB1 and HsEB3 were selected *in vivo* from a pool of peptides with completely random amino acid composition in the region flanking SxIP. The results for HsEB1 sequence determinants are generally consistent between the two different studies but there are some differences in the pattern of sequence requirement. The differences may be due to different sequences used for testing: in my system a large pool of random sequences was used; the other study used a fragment of known HsEB1 interacting protein and changed amino acids systematically one by one. Also, the two studies were performed in different assay contexts, one was performed *in vivo* in yeast cells and the other study was carried out *in vitro* on a cellulose membrane. However, the sequence determinants found in either of the two screens do not strongly match any of the known EB1 interactor protein sequences; usually these are limited to only

some of amino acids determined in the screen laying in a basic amino acid environment. It is possible that too high SxIP-EB1 affinity is not advantageous inside the cells because it outcompetes other proteins from interacting with EB1. Also, considering that the SxIP protein family is large and still growing, these proteins have to have moderate affinities to EB1 for each of them being able to interact with EB1.

By comparing peptide interactors found in screen for HsEB1 or HsEB3, I showed that sequence requirements in region flanking SxIP is similar for the two proteins but there are also significant sequence differences at particular positions. This finding is consistent with studies reporting that mammalian EB1 and EB3 share functions and SxIP interactors but they also have diverse functions and interactors in myogenesis and neurogenesis (Geraldo et al, 2008; Zhang et al, 2009). The finding presented in this thesis provides an insight into a molecular level of these differences.

Findings presented in my study can be further applied if one wanted to improve an SxIP protein binding to EBs, for example to amplify the effects resulting from such interactions. Improving affinity of specific SxIP proteins to EBs could help addressing the question as to the role of this specific protein when in interaction with an EB. Such experiment could give a similar effect to overexpressing the protein but it would allow for a finer dissection of the protein role; providing an information of this protein's role in the context of interaction with an EB protein. Such an experimental setup would also have an advantage over protein overexpression as it would not increase the global protein level. Peptide aptamers for the EB proteins also give an idea whether a set of natural protein interactors would significantly differ between the EBs and what amino acid positions are the most likely source of such differences.

The aim of generating peptide aptamers binding to EBs was to learn about sequences that promote interaction with EB1 and its homologues. The other aim of using peptide aptamers in this study was to obtain new tools to interfere with DmEB1 or Msps functions at specific time and in specific tissues.

Although aptamers for DmEB1 colocalised with the microtubule plus ends, the same as DmEB1, and they displaced Sentin from the microtubule plus ends, they did not cause shorter mitotic spindles, a phenotype specific to Sentin depletion. It is

possible that the aptamer expression level was not sufficiently high to saturate the DmEB1 pool. Also, it cannot be excluded that these aptamers targeted other proteins inside the cells reverting the Sentin RNAi phenotype. One could investigate this possibility by using a peptide aptamer to pull down proteins from the cell lysates. Also, Drosophila DmEB1 deletion mutants reach pupae stage but fail to eclose or they eclose (escapers) but have serious neuromuscular defects (Elliott et al, 2005). However, expressing peptide aptamers in Drosophila causes less severe effects. Although I observed strong reduction in viability, neuromuscular functions were not obviously affected. Previous studies by Elliott et al (2005) showed that the source of neuromuscular defects in Drosophila DmEB1 deletion mutants are disrupted chordotonal mechanosensory organs which are mechanosensory stretch receptors. Sensory units of chordotonal organs comprise of one or more ciliated neurons and several supporting cells where DmEB1 is concentrated. In Drosophila DmEB1 deletion mutants neuronal cells in these organs are misaligned and stretched (Elliott et al, 2005). It would be interesting to look at the same organs in Drosophila expressing aptamers to investigate neuron morphology; whether aptamers cause a similar but possibly much less pronounced effect on chordotonal organs. Also, one could investigate at what stage of the development Drosophila die. However, to achieve the aim of utilising peptide aptamers for inhibiting DmEB1 function at specific time and tissue of Drosophila, it is necessary to improve its affinity for DmEB1 first. To improve binding of aptamer Perfect to DmEB1, I would perform another two-hybrid screen using prey plasmid library with fixed amino acids at these positions which were shown to promote the binding and leaving the rest of the positions random. It is also necessary to confirm the aptamer binding specificity inside the cells to ensure that it does not target different proteins. Additionally, I would introduce several genes for an aptamer in tandem to ensure saturation of aptamer-DmEB1 interaction.

To study post-mitotic roles of Msps, I generated *msps* temperature-sensitive Drosophila. Although *msps* null mutant Drosophila are available, these mutants die around larvae-pupae transition (Cullen et al, 1999). Thus $msps^{ts}$ Drosophila is a powerful tool to investigate the protein roles at the whole organism level. To investigate the effect of this temperature-sensitive mutation, it would be interesting

to look at its molecular nature first, for example, does the mutant Msps still bind to tubulin? If so, is affinity of this interaction affected? Also, is the mutant protein produced at the wild-type protein level? One could check these by performing a pull down and western blotting experiments.

In this thesis, I showed that Msps is crucial for development of neuromuscular functions in Drosophila pupae. However, further investigation is required to address the basis of these impairments. In this study, many of the Drosophila did not even eclose following pupae incubations at restrictive temperature. Since Msps is abundant in brain, I would first check if enough neurons were generated at pupae; neuroblasts continue dividing in brain and thorax until pupal stages, ceasing the division at ~120 hours from pupation (Maurange et al, 2008). To investigate this, one could count the mitotic index of neuroblasts in the mutant and the wild-type pupae at subsequent stages.

Msps is involved in axon guidance (Lowery et al, 2010). A study showed defects in axonal fascicle morphology in Drosophila embryos deficient of *msps*; axons and fascicles had incorrect pathfinding and axon bundling was abnormal (Lowery et al, 2010). Axonal guidance is an a very important process in Drosophila development because its body undergoes significant changes during metamorphosis and the neuronal network becomes significantly reorganized during the pupal period (Sánchez-Soriano et al, 2007). Many of the neurons which developed at larvae have to control their shape and size when at pupae. Microtubule dynamics is inherent to axon guidance as efficient microtubule rearrangements in the neuronal growth cones influence axon dynamics. Considering implication of Msps in embryonal axon morphology, one could predict its involvement in neuron rearrangements at pupae resulting in incorrect targeting of, for example, muscles and leading to walking impairments of $msps^{ts}$ Drosophila. One could investigate such possibility by pupae dissections and confocal imaging.

In summary, new tools were developed which allow study of the roles of Msps and DmEB1 in Drosophila. Also, this work revealed amino acid residues which promote binding and specificity to EB proteins. Finally, my new approach to generating tight peptide aptamers contributed to progress in the field of biotechnology.

References

Akhmanova A, Steinmetz MO (2008) Tracking the ends: a dynamic protein network controls the fate of microtubule tips. *Nature Reviews Molecular Cell Biology* **9:** 309-322

Al-Bassam J (2006) Stu2p binds tubulin and undergoes an open-to-closed conformational change. *The Journal of Cell Biology* **172:** 1009-1022

Al-Bassam J, Chang F (2011) Regulation of microtubule dynamics by TOG-domain proteins XMAP215/Dis1 and CLASP. *Trends in Cell Biology* **21:** 604-614

Al-Bassam J, Larsen NA, Hyman AA, Harrison SC (2007) Crystal Structure of a TOG Domain: Conserved Features of XMAP215/Dis1-Family TOG Domains and Implications for Tubulin Binding. *Structure* **15:** 355-362

Anders A, Sawin KE (2011) Microtubule stabilization in vivo by nucleation-incompetent -tubulin complex. *Journal of Cell Science* **124:** 1207-1213

Asakawa K, Toya M, Sato M, Kanai M, Kume K, Goshima T, Garcia MA, Hirata D, Toda T (2005) Mal3, the fission yeast EB1 homologue, cooperates with Bub1 spindle checkpoint to prevent monopolar attachment. *EMBO reports* **6:** 1194-1200

Ashburner M, Golic KG, Hawley RS (2005) *Drosophila: a laboratory handbook. Second edition*.

Askham JM, Vaughan KT, Goodson HV, Morrison EE (2002) Evidence That an Interaction between EB1 and p150Glued Is Required for the Formation and Maintenance of a Radial Microtubule Array Anchored at the Centrosome. *Molecular Biology of the Cell* **13:** 3627-3645

Ayaz P, Ye X, Huddleston P, Brautigam CA, Rice LM (2012) A TOG: -tubulin Complex Structure Reveals Conformation-Based Mechanisms for a Microtubule Polymerase. *Science* **337:** 857-860

Baines IC, Colas P (2006) Peptide aptamers as guides for small-molecule drug discovery. *Drug Discovery Today* **11:** 334-341

Barros TP (2005) Aurora A activates D-TACC-Msps complexes exclusively at centrosomes to stabilize centrosomal microtubules. *The Journal of Cell Biology* **170:** 1039-1046

Benzer S (1973) Genetic Dissection of Behavior. *Scientific American* **229:** 24-37

Berrueta L, Kraeft S-K, Tirnauer JS, Schuyler SC, Chen LB, Hill DE, Pellman D, Bierer BE (1998) The adenomatous polyposis coli-binding protein EB1 is associated with cytoplasmic and spindle microtubules. *Proceedings of the National Academy of Sciences* **95:** 10596-10601

Bieling P, Kandels-Lewis S, Telley IA, van Dijk J, Janke C, Surrey T (2008) CLIP-170 tracks growing microtubule ends by dynamically recognizing composite EB1/tubulin-binding sites. *The Journal of Cell Biology* **183:** 1223-1233

Bieling P, Laan L, Schek H, Munteanu EL, Sandblad L, Dogterom M, Brunner D, Surrey T (2007) Reconstitution of a microtubule plus-end tracking system in vitro. *Nature* **450:** 1100-1105

Bjelić S, De Groot CO, Schärer MA, Jaussi R, Bargsten K, Salzmann M, Frey D, Capitani G, Kammerer RA, Steinmetz MO (2012) Interaction of mammalian end binding proteins with CAP-Gly domains of CLIP-170 and p150glued. *Journal of Structural Biology* **177:** 160-167

Brittle AL, Ohkura H (2005) Mini spindles, the XMAP215 homologue, suppresses pausing of interphase microtubules in Drosophila. *EMBO J* **24:** 1387-1396

Brouhard GJ, Stear JH, Noetzel TL, Al-Bassam J, Kinoshita K, Harrison SC, Howard J, Hyman AA (2008) XMAP215 Is a Processive Microtubule Polymerase. *Cell* **132:** 79-88

Bryan J (1974) Microtubules. *BioScience* **24:** 701-711

Bu W (2003) Characterization of Functional Domains of Human EB1 Family Proteins. *Journal of Biological Chemistry* **278:** 49721-49731

Bu W, Su LK (2001) Regulation of microtubule assembly by human EB1 family proteins. *Oncogene* **20:** 3185-3192

Buey RM, Sen I, Kortt O, Mohan R, Gfeller D, Veprintsev D, Kretzschmar I, Scheuermann J, Neri D, Zoete V, Michielin O, de Pereda JM, Akhmanova A, Volkmer R, Steinmetz MO (2012) Sequence Determinants of a Microtubule Tip Localization Signal (MtLS). *Journal of Biological Chemistry* **287:** 28227-28242

Butz K, Denk C, Ullmann A, Scheffner M, Hoppe-Seyler F (2000) Induction of apoptosis in human papillomaviruspositive cancer cells by peptide aptamers targeting the viral E6 oncoprotein. *Proceedings of the National Academy of Sciences* **97:** 6693-6697

Cassimeris L, Gard D, Tran PT, Erickson HP (2001) XMAP215 is a long thin molecule that does not increase microtubule stiffness. *Journal of Cell Science* **114:** 3025-3033

Charrasse S, Schroeder M, Gauthier-Rouviere C, Ango F, Cassimeris L, Gard DL, Larroque C (1998) The TOGp protein is a new human microtubule-associated protein homologous to the Xenopus XMAP215. *Journal of Cell Science* **111:** 1371-1383

Choi YK, Liu P, Sze SK, Dai C, Qi RZ (2010) CDK5RAP2 stimulates microtubule nucleation by the -tubulin ring complex. *The Journal of Cell Biology* **191:** 1089-1095

Chrétien D, Metoz F, Verde F, Karsenti E, Wade R (1992) Lattice defects in microtubules: protofilament numbers vary within individual microtubules. *The Journal of Cell Biology* **117:** 1031-1040

Cohen BA, Colas P, Brent R (1998) An artificial cell-cycle inhibitor isolated from a combinatorial library. *Proceedings of the National Academy of Sciences* **95:** 14272-14277

Colas P (2008) The eleven-year switch of peptide aptamers. *Journal of Biology* **7:** 2

Colas P, Cohen B, Ferrigno PK, Silver PA, Brent R (2000) Targeted modification and transportation of cellular proteins. *Proceedings of the National Academy of Sciences* **97:** 13720-13725

Colas P, Cohen B, Jessen T, Grishina I, McCoy J, Brent R (1996) Genetic selection of peptide aptamers that recognize and inhibit cyclin-dependent kinase 2. *Nature* **380:** 548-550

Crawford M, Woodman R, Ferrigno PK (2003) Peptide aptamers: Tools for biology and drug discovery. *Briefings in Functional Genomics & Proteomics* **2:** 72-79

Cullen CF, Deák P, Glover DM, Ohkura H (1999) mini spindles: A Gene Encoding a Conserved Microtubule-Associated Protein Required for the Integrity of the Mitotic Spindle in Drosophila. *The Journal of Cell Biology* **146:** 1005-1018

Cullen CF, Ohkura H (2001) Msps protein is localized to acentrosomal poles to ensure bipolarity of Drosophila meiotic spindles. *Nat Cell Biol* **3:** 637-642

Currie JD, Stewman S, Schimizzi G, Slep KC, Ma A, Rogers SL (2011) The microtubule lattice and plus-end association of Drosophila Mini spindles is spatially regulated to fine-tune microtubule dynamics. *Molecular Biology of the Cell* **22:** 4343-4361

Davis JJ, Tkac J, Humphreys R, Buxton AT, Lee TA, Ko Ferrigno P (2009) Peptide Aptamers in Label-Free Protein Detection: 2. Chemical Optimization and Detection of Distinct Protein Isoforms. *Analytical Chemistry* **81:** 3314-3320

De Groot CO, Jelesarov I, Damberger FF, Bjelic S, Scharer MA, Bhavesh NS, Grigoriev I, Buey RM, Wuthrich K, Capitani G, Akhmanova A, Steinmetz MO (2009) Molecular Insights into Mammalian End-binding Protein Heterodimerization. *Journal of Biological Chemistry* **285:** 5802-5814

Desai A, Mitchison TJ (1997) MICROTUBULE POLYMERIZATION DYNAMICS. *Annual Review of Cell and Developmental Biology* **13:** 83-117

Dibenedetto S, Cluet D, Stebe PN, Baumle V, Leault J, Terreux R, Bickle M, de Chassey B, Mikaelian I, Colas P, Spichty M, Zoli M, Rudkin BB (2013) Calcineurin A vs NS5A-TP2/HDDC2: a case study of site-directed low-frequency random mutagenesis for dissecting target specificity of peptide aptamers. *Molecular & Cellular Proteomics*

Dimitrov A, Quesnoit M, Moutel S, Cantaloube I, Poüs C, Perez F (2008) Detection of GTP-Tubulin Conformation in Vivo Reveals a Role for GTP Remnants in Microtubule Rescues. *Science* **322:** 1353-1356

Dixit R, Barnett B, Lazarus JE, Tokito M, Goldman YE, Holzbaur ELF (2009) Microtubule plus-end tracking by CLIP-170 requires EB1. *Proceedings of the National Academy of Sciences* **106:** 492-497

Duffy JB (2002) GAL4 system in drosophila: A fly geneticist's swiss army knife. *genesis* **34:** 1-15

Dzhindzhev NS (2005) Distinct mechanisms govern the localisation of Drosophila CLIP-190 to unattached kinetochores and microtubule plus-ends. *Journal of Cell Science* **118:** 3781-3790

Elliott SL, Cullen CF, Wrobel N, Kernan MJ, Ohkura H (2005) EB1 Is Essential during Drosophila Development and Plays a Crucial Role in the Integrity of Chordotonal Mechanosensory Organs. *Molecular Biology of the Cell* **16:** 891-901

Erickson HP, Stoffler D (1996) Protofilaments and rings, two conformations of the tubulin family conserved from bacterial FtsZ to alpha/beta and gamma tubulin. *The Journal of Cell Biology* **135:** 5-8

Esparza JM, O'Toole E, Li L, Giddings TH, Jr., Kozak B, Albee AJ, Dutcher SK (2013) Katanin Localization Requires Triplet Microtubules in Chlamydomonas reinhardtii. *PLoS ONE* **8:** e53940

Estojak J, Brent R, Golemis EA (1995) Correlation of two-hybrid affinity data with in vitro measurements. *Molecular and cellular biology* **15:** 5820-5829

Fabbrizio E (1999) Inhibition of mammalian cell proliferation by genetically selected peptide aptamers that functionally antagonize E2F activity. *Oncogene*

Faivre-Moskalenko C, Dogterom M (2002) Dynamics of microtubule asters in microfabricated chambers: The role of catastrophes. *Proceedings of the National Academy of Sciences* **99:** 16788-16793

Fischer JA, Giniger E, Maniatis T, Ptashne M (1988) GAL4 activates transcription in Drosophila. *Nature* **332:** 853-856

Gard DL, Kirschner MW (1987) A microtubule-associated protein from Xenopus eggs that specifically promotes assembly at the plus-end. *The Journal of Cell Biology* **105:** 2203-2215

Gardner MK, Zanic M, Howard J (2013) Microtubule catastrophe and rescue. *Current Opinion in Cell Biology* **25:** 14-22

Geraldo S, Khanzada UK, Parsons M, Chilton JK, Gordon-Weeks PR (2008) Targeting of the F-actin-binding protein drebrin by the microtubule plus-tip protein EB3 is required for neuritogenesis. *Nature Cell Biology* **10:** 1181-1189

Geyer CR (2001) Peptide Aptamers: Dominant "Genetic" Agents for Forward and Reverse Analysis of Cellular Processes. In *Current Protocols in Molecular Biology*. John Wiley & Sons, Inc.

Geyer CR, Brent R (2000) [13] Selection of genetic agents from random peptide aptamer expression libraries. In *Methods in Enzymology*, Jeremy Thorner SDE, John NA (eds), Vol. Volume 328, pp 171-208. Academic Press

Goshima G, Nédélec F, Vale RD (2005) Mechanisms for focusing mitotic spindle poles by minus end–directed motor proteins. *The Journal of Cell Biology* **171:** 229-240

Groves MR, Hanlon N, Turowski P, Hemmings BA, Barford D (1999) The Structure of the Protein Phosphatase 2A PR65/A Subunit Reveals the Conformation of Its 15 Tandemly Repeated HEAT Motifs. *Cell* **96:** 99-110

Guthrie C, Fink G. (2004) Guide to Yeast Genetics and Molecular and Cell Biology. *Methods in Enzymology*. Elsevier Inc., Vol. 194, pp. 3-933.

Hall M, Misra S, Chaudhuri M, Chaudhuri G (2011) Peptide aptamer mimicking RAD51-binding domain of BRCA2 inhibits DNA damage repair and survival in Trypanosoma brucei. *Microbial Pathogenesis* **50:** 252-262

Hayashi I (2003) Crystal Structure of the Amino-terminal Microtubule-binding Domain of End-binding Protein 1 (EB1). *Journal of Biological Chemistry* **278:** 36430-36434

Heald R, Nogales E (2002) Microtubule dynamics. *Journal of Cell Science* **115:** 3-4

Holmfeldt P, Stenmark S, Gullberg M (2004) Differential functional interplay of TOGp/XMAP215 and the KinI kinesin MCAK during interphase and mitosis. *EMBO J* **23:** 627-637

Holmgren A (1989) Thioredoxin and glutaredoxin systems. *Journal of Biological Chemistry* **264:** 13963-13966

Honnappa S, Gouveia SM, Weisbrich A, Damberger FF, Bhavesh NS, Jawhari H, Grigoriev I, van Rijssel FJA, Buey RM, Lawera A, Jelesarov I, Winkler FK, Wüthrich K, Akhmanova A, Steinmetz MO (2009) An EB1-Binding Motif Acts as a Microtubule Tip Localization Signal. *Cell* **138:** 366-376

Honnappa S, John CM, Kostrewa D, Winkler FK, Steinmetz MO (2005) Structural insights into the EB1-APC interaction. *EMBO J* **24:** 261-269

Honnappa S, Okhrimenko O, Jaussi R, Jawhari H, Jelesarov I, Winkler FK, Steinmetz MO (2006) Key Interaction Modes of Dynamic +TIP Networks. *Molecular Cell* **23:** 663-671

Hoppe-Seyler F, Butz K (2000) Peptide aptamers: powerful new tools for molecular medicine. *J Mol Med* **78:** 426-430

Hoppe-Seyler F, Crnkovic-Mertens I, Denk C, Fitscher BA, Klevenz B, Tomai E, Butz K (2001) Peptide aptamers: new tools to study protein interactions. *The Journal of Steroid Biochemistry and Molecular Biology* **78:** 105-111

Hoppe-Seyler F, Crnkovic-Mertens I, Tomai E, Butz K (2004) Peptide aptamers: specific inhibitors of protein function. *Current molecular medicine* **4:** 529-538

Iimori M, Ozaki K, Chikashige Y, Habu T, Hiraoka Y, Maki T, Hayashi I, Obuse C, Matsumoto T (2012) A mutation of the fission yeast EB1 overcomes negative regulation by phosphorylation and stabilizes microtubules. *Experimental Cell Research* **318:** 262-275

Jiang K, Akhmanova A (2011) Microtubule tip-interacting proteins: a view from both ends. *Current Opinion in Cell Biology* **23:** 94-101

Jiang K, Toedt G, Montenegro Gouveia S, Davey Norman E, Hua S, van der Vaart B, Grigoriev I, Larsen J, Pedersen Lotte B, Bezstarosti K, Lince-Faria M, Demmers J, Steinmetz Michel O, Gibson Toby J, Akhmanova A (2012) A Proteome-wide Screen for Mammalian SxIP Motif-Containing Microtubule Plus-End Tracking Proteins. *Current Biology* **22:** 1800-1807

Kinoshita K, Noetzel TL, Pelletier L, Mechtler K, Drechsel DN, Schwager A, Lee M, Raff JW, Hyman AA (2005) Aurora A phosphorylation of TACC3/maskin is required for centrosome-dependent microtubule assembly in mitosis. *The Journal of Cell Biology* **170:** 1047-1055

Klevenz B, Butz K, Hoppe-Seyler F (2002) Peptide aptamers: exchange of the thioredoxin-A scaffold by alternative platform proteins and its influence on target protein binding. *CMLS, Cell Mol Life Sci* **59:** 1993-1998

Kobe B, Gleichmann T, Horne J, Jennings IG, Scotney PD, Teh T (1999) Turn up the HEAT. *Structure* **7:** R91-R97

Kollman JM, Merdes A, Mourey L, Agard DA (2011) Microtubule nucleation by γ-tubulin complexes. *Nature Reviews Molecular Cell Biology* **12:** 709-721

Kollman JM, Polka JK, Zelter A, Davis TN, Agard DA (2010) Microtubule nucleating γ-TuSC assembles structures with 13-fold microtubule-like symmetry. *Nature* **466:** 879-882

Kolonin MG, Finley RL (1998) Targeting cyclin-dependent kinases in Drosophila with peptide aptamers. *Proceedings of the National Academy of Sciences* **95:** 14266-14271

Komarova Y, De Groot CO, Grigoriev I, Gouveia SM, Munteanu EL, Schober JM, Honnappa S, Buey RM, Hoogenraad CC, Dogterom M, Borisy GG, Steinmetz MO, Akhmanova A (2009) Mammalian end binding proteins control persistent microtubule growth. *The Journal of Cell Biology* **184:** 691-706

Komarova Y, Lansbergen G, Galjart N, Grosveld F, Borisy GG, Akhmanova A (2005) EB1 and EB3 Control CLIP Dissociation from the Ends of Growing Microtubules. *Molecular Biology of the Cell* **16:** 5334-5345

Kumar P, Chimenti MS, Pemble H, Schönichen A, Thompson O, Jacobson MP, Wittmann T (2012) Multisite Phosphorylation Disrupts Arginine-Glutamate Salt Bridge Networks Required for Binding of Cytoplasmic Linker-associated Protein 2 (CLASP2) to End-binding Protein 1 (EB1). *Journal of Biological Chemistry* **287:** 17050-17064

Kumar P, Wittmann T (2012) +TIPs: SxIPping along microtubule ends. *Trends in Cell Biology* **22:** 418-428

Lansbergen G, Grigoriev I, Mimori-Kiyosue Y, Ohtsuka T, Higa S, Kitajima I, Demmers J, Galjart N, Houtsmuller AB, Grosveld F (2006) CLASPs Attach Microtubule Plus Ends to the Cell Cortex through a Complex with LL5β. *Developmental Cell* **11:** 21-32

LaVallie ER, DiBlasio EA, Kovacic S, Grant KL, Schendel PF, McCoy JM (1993) A Thioredoxin Gene Fusion Expression System That Circumvents Inclusion Body Formation in the E. coli Cytoplasm. *Nat Biotech* **11:** 187-193

Lee MJ, Gergely F, Jeffers K, Peak-Chew SY, Raff JW (2001) Msps/XMAP215 interacts with the centrosomal protein D-TACC to regulate microtubule behaviour. *Nat Cell Biol* **3:** 643-649

Leterrier C, Vacher H, Fache MP, d'Ortoli SA, Castets F, Autillo-Touati A, Dargent B (2011) End-binding proteins EB3 and EB1 link microtubules to ankyrin G in the axon initial segment. *Proceedings of the National Academy of Sciences* **108:** 8826-8831

Lewis SA, Tian G, Cowan NJ (1997) The α- and β-tubulin folding pathways. *Trends in Cell Biology* **7:** 479-484

Li S, Finley J, Liu Z-J, Qiu S-H, Chen H, Luan C-H, Carson M, Tsao J, Johnson D, Lin G, Zhao J, Thomas W, Nagy LA, Sha B, DeLucas LJ, Wang B-C, Luo M (2002) Crystal Structure of the Cytoskeleton-associated Protein Glycine-rich (CAP-Gly) Domain. *Journal of Biological Chemistry* **277:** 48596-48601

Li W, Miki T, Watanabe T, Kakeno M, Sugiyama I, Kaibuchi K, Goshima G (2011) EB1 promotes microtubule dynamics by recruiting Sentin in Drosophila cells. *The Journal of Cell Biology* **193:** 973-983

Li W, Moriwaki T, Tani T, Watanabe T, Kaibuchi K, Goshima G (2012a) Reconstitution of dynamic microtubules with Drosophila XMAP215, EB1, and Sentin. *The Journal of Cell Biology* **199:** 849-862

Li Z, Uzawa T, Tanaka T, Hida A, Ishibashi K, Katakura H, Kobatake E, Ito Y (2012b) In vitro selection of peptide aptamers with affinity to single-wall carbon nanotubes using a ribosome display. *Biotechnology Letters* **35:** 39-45

Ligon LA, Shelly SS, Tokito M, Holzbaur ELF (2003) The Microtubule Plus-End Proteins EB1 and Dynactin Have Differential Effects on Microtubule Polymerization. *Molecular Biology of the Cell* **14:** 1405-1417

Lodish H, Berk A, Kaiser C, Krieger M, Scott M, Bretscher A, Ploegh H, Matsudaira P (2007) *Molecular Cell Biology (Lodish, Molecular Cell Biology)*: W. H. Freeman.

Lowery LA, Lee H, Lu C, Murphy R, Obar RA, Zhai B, Schedl M, Van Vactor D, Zhan Y (2010) Parallel Genetic and Proteomic Screens Identify Msps as a CLASP-Abl Pathway Interactor in Drosophila. *Genetics* **185:** 1311-1325

Lu Z, Murray KS, Cleave VV, LaVallie ER, Stahl ML, McCoy JM (1995) Expression of Thioredoxin Random Peptide Libraries on the Escherichia coli Cell Surface as Functional Fusions to Flagellin: A System Designed for Exploring Protein-Protein Interactions. *Nat Biotech* **13:** 366-372

Mandelkow EM, Schultheiss R, Rapp R, Müller M, Mandelkow E (1986) On the surface lattice of microtubules: helix starts, protofilament number, seam, and handedness. *The Journal of Cell Biology* **102:** 1067-1073

Maurange C, Cheng L, Gould AP (2008) Temporal Transcription Factors and Their Targets Schedule the End of Neural Proliferation in Drosophila. *Cell* **133:** 891-902

Maurer SP, Bieling P, Cope J, Hoenger A, Surrey T (2011) GTPγS microtubules mimic the growing microtubule end structure recognized by end-binding proteins (EBs). *Proceedings of the National Academy of Sciences* **108:** 3988-3993

Maurer Sebastian P, Fourniol Franck J, Bohner G, Moores Carolyn A, Surrey T (2012) EBs Recognize a Nucleotide-Dependent Structural Cap at Growing Microtubule Ends. *Cell* **149:** 371-382

McKean PG, Vaughan S, Gull K (2001) The extended tubulin superfamily. *Journal of Cell Science* **114:** 2723-2733

Mena MA, Daugherty PS (2005) Automated design of degenerate codon libraries. *Protein Engineering Design and Selection* **18:** 559-561

Miller JH (1972) *Experiments in molecular genetics*, Cold Spring Harbor, N.Y.: Cold Spring Harbor Laboratory.

Mimori-Kiyosue Y, Shiina N, Tsukita S (2000) The dynamic behavior of the APC-binding protein EB1 on the distal ends of microtubules. *Current Biology* **10:** 865-868

Mishima M, Maesaki R, Kasa M, Watanabe T, Fukata M, Kaibuchi K, Hakoshima T (2007) Structural basis for tubulin recognition by cytoplasmic linker protein 170 and its autoinhibition. *Proceedings of the National Academy of Sciences* **104:** 10346-10351

Moudjou M, Bordes N, Paintrand M, Bornens M (1996) gamma-Tubulin in mammalian cells: the centrosomal and the cytosolic forms. *Journal of Cell Science* **109:** 875-887

Murray E, McKenna EO, Burch LR, Dillon J, Langridge-Smith P, Kolch W, Pitt A, Hupp TR (2007) Microarray-Formatted Clinical Biomarker Assay Development Using Peptide Aptamers to Anterior Gradient-2†. *Biochemistry* **46:** 13742-13751

Nakagawa H, Koyama K, Murata Y, Morito M, Akiyama T, Nakamura Y (2000) EB3, a novel member of the EB1 family preferentially expressed in the central nervous system, binds to a CNS-specific APC homologue. *Oncogene* **19:** 210-216

Nakata T, Niwa S, Okada Y, Perez F, Hirokawa N (2011) Preferential binding of a kinesin-1 motor to GTP-tubulin-rich microtubules underlies polarized vesicle transport. *The Journal of Cell Biology* **194:** 245-255

Niethammer P, Kronja I, Kandels-Lewis S, Rybina S, Bastiaens P, Karsenti E (2007) Discrete States of a Protein Interaction Network Govern Interphase and Mitotic Microtubule Dynamics. *PLoS Biol* **5:** e29

Ohkura H, Garcia MA, Toda T (2001) Dis1/TOG universal microtubule adaptors - one MAP for all? *Journal of Cell Science* **114:** 3805-3812

Oladipo A, Cowan A, Rodionov V (2007) Microtubule Motor Ncd Induces Sliding of Microtubules In Vivo. *Molecular Biology of the Cell* **18:** 3601-3606

Oldenburg KR, Loganathan D, Goldstein IJ, Schultz PG, Gallop MA (1992) Peptide ligands for a sugar-binding protein isolated from a random peptide library. *Proceedings of the National Academy of Sciences* **89:** 5393-5397

Pamonsinlapatham P, Hadj-Slimane R, Raynaud F, Bickle M, Corneloup C, Barthelaix A, Lepelletier Y, Mercier P, Schapira M, Samson J, Mathieu A-L, Hugo N, Moncorgé O,

Mikaelian I, Dufour S, Garbay C, Colas P (2008) A RasGAP SH3 Peptide Aptamer Inhibits RasGAP-Aurora Interaction and Induces Caspase-Independent Tumor Cell Death. *PLoS ONE* **3:** e2902

Panda D, Miller HP, Wilson L (1999) Rapid treadmilling of brain microtubules free of microtubule-associated proteins in vitro and its suppression by tau. *Proceedings of the National Academy of Sciences* **96:** 12459-12464

Patel K, Nogales E, Heald R (2012) Multiple domains of human CLASP contribute to microtubule dynamics and organization in vitro and in Xenopus egg extracts. *Cytoskeleton* **69:** 155-165

Piasecki BP, Silflow CD (2009) The UNI1 and UNI2 Genes Function in the Transition of Triplet to Doublet Microtubules between the Centriole and Cilium in Chlamydomonas. *Molecular Biology of the Cell* **20:** 368-378

Popov AV, Pozniakovsky A, Arnal I, Antony C, Ashford AJ, Kinoshita K, Tournebize R, Hyman AA, Karsenti E (2001) XMAP215 regulates microtubule dynamics through two distinct domains. *EMBO J* **20:** 397-410

Rogers SL (2002) Drosophila EB1 is important for proper assembly, dynamics, and positioning of the mitotic spindle. *The Journal of Cell Biology* **158:** 873-884

Sambrook J, Maniatis T, Fritsch EF (1989) *Molecular Cloning: A Laboratory Manual(2nd edition)*.

Sambrook J, Russell D (2001) *Molecular Cloning: A Laboratory Manual*: Cold Spring Harbor Laboratory Press.

Sánchez-Soriano N, Tear G, Whitington P, Prokop A (2007) Drosophila as a genetic and cellular model for studies on axonal growth. *Neural Development* **2:** 1-28

Schroder JM, Larsen J, Komarova Y, Akhmanova A, Thorsteinsson RI, Grigoriev I, Manguso R, Christensen ST, Pedersen SF, Geimer S, Pedersen LB (2011) EB1 and EB3 promote cilia biogenesis by several centrosome-related mechanisms. *Journal of Cell Science* **124:** 2539-2551

Schroer TA (2004) Dynactin. *Annual Review of Cell and Developmental Biology* **20:** 759-779

Seigneuric R, Gobbo J, Colas P, Garrido C (2011) Targeting cancer with peptide aptamers. *Oncotarget; Vol 2, No 7: July 2011*

Skube SB, Chaverri JM, Goodson HV (2010) Effect of GFP tags on the localization of EB1 and EB1 fragments in vivo. *Cytoskeleton* **67:** 1-12

Slep KC (2005) Structural determinants for EB1-mediated recruitment of APC and spectraplakins to the microtubule plus end. *The Journal of Cell Biology* **168:** 587-598

Slep Kevin C (2009) The role of TOG domains in microtubule plus end dynamics. *Biochemical Society Transactions* **37:** 1002

Slep KC (2010) Structural and mechanistic insights into microtubule end-binding proteins. *Current Opinion in Cell Biology* **22:** 88-95

Slep KC, Vale RD (2007) Structural Basis of Microtubule Plus End Tracking by XMAP215, CLIP-170, and EB1. *Molecular Cell* **27:** 976-991

Steinmetz MO, Akhmanova A (2008) Capturing protein tails by CAP-Gly domains. *Trends in Biochemical Sciences* **33:** 535-545

Straube A, Merdes A (2007) EB3 Regulates Microtubule Dynamics at the Cell Cortex and Is Required for Myoblast Elongation and Fusion. *Current Biology* **17:** 1318-1325

Su L-K, Burrell M, Hill DE, Gyuris J, Brent R, Wiltshire R, Trent J, Vogelstein B, Kinzler KW (1995) APC Binds to the Novel Protein EB1. *Cancer Research* **55:** 2972-2977

Su L-K, Qi Y (2001) Characterization of Human MAPRE Genes and Their Proteins. *Genomics* **71:** 142-149

Teixido-Travesa N, Roig J, Luders J (2012) The where, when and how of microtubule nucleation - one ring to rule them all. *Journal of Cell Science* **125:** 4445-4456

Thibaut J, Merieux Y, Rigal D, Gillet G (2011) A novel assay for the detection of anti-human platelet antigen antibodies (HPA-1a) based on peptide aptamer technology. *Haematologica* **97:** 696-704

Tirnauer JS, Bierer BE (2000) Eb1 Proteins Regulate Microtubule Dynamics, Cell Polarity, and Chromosome Stability. *The Journal of Cell Biology* **149:** 761-766

Tirnauer JS, Canman JC, Salmon ED, Mitchison TJ (2002) EB1 targets to kinetochores with attached, polymerizing microtubules. *Molecular Biology of the Cell* **13:** 4308-4316

Turnbull WB, Daranas AH (2003) On the Value of c: Can Low Affinity Systems Be Studied by Isothermal Titration Calorimetry? *Journal of the American Chemical Society* **125:** 14859-14866

Tuszynski JA, Carpenter EJ, Huzil JT, Malinski W, Luchko T, Luduena RF (2006) The evolution of the structure of tubulin and its potential consequences for the role and function of microtubules in cells and embryos. *The International Journal of Developmental Biology* **50:** 341-358

Uekita T, Itoh Y, Yana I, Ohno H, Seiki M (2001) Cytoplasmic tail–dependent internalization of membrane-type 1 matrix metalloproteinase is important for its invasion-promoting activity. *The Journal of Cell Biology* **155:** 1345-1356

van der Vaart B, Manatschal C, Grigoriev I, Olieric V, Gouveia SM, Bjelic S, Demmers J, Vorobjev I, Hoogenraad CC, Steinmetz MO, Akhmanova A (2011) SLAIN2 links microtubule plus end-tracking proteins and controls microtubule growth in interphase. *The Journal of Cell Biology* **193:** 1083-1099

Vitre B, Coquelle FM, Heichette C, Garnier C, Chretien D, Arnal I (2008) EB1 regulates microtubule dynamics and tubulin sheet closure in vitro. *Nat Cell Biol* **10:** 415-421

Wang PJ, Huffaker TC (1997) Stu2p: A Microtubule-Binding Protein that Is an Essential Component of the Yeast Spindle Pole Body. *The Journal of Cell Biology* **139:** 1271-1280

Warbrick E (2006) A functional analysis of PCNA-binding peptides derived from protein sequence, interaction screening and rational design. *Oncogene* **25:** 2850-2859

Warbrick E, Lane DP, Glover DM, Cox LS (1995) A small peptide inhibitor of DNA replication defines the site of interaction between the cyclin-dependent kinase inhibitor p21WAF1 and proliferating cell nuclear antigen. *Current Biology* **5:** 275-282

Waterman-Storer CM, Salmon ED (1997) Microtubule dynamics: Treadmilling comes around again. *Current biology : CB* **7:** R369-R372

Weisbrich A, Honnappa S, Jaussi R, Okhrimenko O, Frey D, Jelesarov I, Akhmanova A, Steinmetz MO (2007) Structure-function relationship of CAP-Gly domains. *Nature Structural & Molecular Biology* **14:** 959-967

Wells WA (2005) Microtubules get a name. *The Journal of Cell Biology* **168:** 852-853

Wickramasinghe RD, Ferrigno P, Roghi C (2010) Peptide aptamers as new tools to modulate clathrin-mediated internalisation — inhibition of MT1-MMP internalisation. *BMC Cell Biology* **11:** 58

Widlund PO, Stear JH, Pozniakovsky A, Zanic M, Reber S, Brouhard GJ, Hyman AA, Howard J (2011) XMAP215 polymerase activity is built by combining multiple tubulin-binding TOG domains and a basic lattice-binding region. *Proceedings of the National Academy of Sciences* **108:** 2741-2746

Woodman R, Yeh JTH, Laurenson S, Ferrigno PK (2005) Design and Validation of a Neutral Protein Scaffold for the Presentation of Peptide Aptamers. *Journal of Molecular Biology* **352:** 1118-1133

Woods KL, Theiler R, Mühlemann M, Segiser A, Huber S, Ansari HR, Pain A, Dobbelaere DAE (2013) Recruitment of EB1, a Master Regulator of Microtubule Dynamics, to the Surface of the Theileria annulata Schizont. *PLoS Pathog* **9:** e1003346

Wu J, Park JP, Dooley K, Cropek DM, West AC, Banta S (2011) Rapid Development of New Protein Biosensors Utilizing Peptides Obtained via Phage Display. *PLoS ONE* **6:** e24948

Yeh JTH, Binari R, Gocha T, Dasgupta R, Perrimon N (2013) PAPTi: A Peptide Aptamer Interference Toolkit for Perturbation of Protein-Protein Interaction Networks. *Scientific Reports* **3**

Zanic M, Widlund PO, Hyman AA, Howard J (2013) Synergy between XMAP215 and EB1 increases microtubule growth rates to physiological levels. *Nat Cell Biol* **advance online publication**

Zhang T, Zaal KJM, Sheridan J, Mehta A, Gundersen GG, Ralston E (2009) Microtubule plus-end binding protein EB1 is necessary for muscle cell differentiation, elongation and fusion. *Journal of Cell Science* **122:** 1401-1409

Zimniak T, Stengl K, Mechtler K, Westermann S (2009) Phosphoregulation of the budding yeast EB1 homologue Bim1p by Aurora/Ipl1p. *The Journal of Cell Biology* **186:** 379-391